CIVIL ENGINEER

2022

Yearly Technical Magazine

Department of Civil Engineering

Department of Civil Engineering

SAINTGITS College of Engineering

Kottukulam Hills, Pathamuttom P.O

Kottayam, Kerala - 686532

email: mail@saintgits.org

Ph: 0481 - 2436170,2436169

>> CONTENTS

CIVIL ENGINEER

CONTACTS

Department of Civil Engineering
SAINTGITS College of Engineering
Kottukulam Hills
Pathamuttom P O, Kottayam
Email:mail@saintgits.org,Ph:0481-2430349,
2436169, 2436170.

HOD's Message 2

About Department 3

Programme Objectives 4

Technical Papers 5

- NUMERICAL STUDY ON WEB OPENINGS IN CASTELLATED BEAMS
- PERFORMANCE EVALUATION OF PROPOSED CONTAINER TERMINAL AT VIZHINJAM PORT
- DAMAGE IDENTIFICATION BASED ON CHANGE IN STIFFNESS USING PARTICLE SWARM OPTIMIZATION
- REJUVENATION OF RAP BINDERS USING WASTE OIL
- ANALYSIS OF SHEET PILE WALL SUBJECTED TO PITTING CORROSION
- FEASIBILITY STUDY OF FLYOVER AT CHAGANASSERY BYPASS
- DETERMINATION OF SOIL PROPERTIES, FLOOD HEIGHT AND PREPARATION OF FLOOD INUNDATION MAP USING GIS
- STUDY ON THE UTILIZATION OF SHAPE MEMORY ALLOY IN CIVIL STRUCTURES

>> HOD's Message

I am happy to learn that the Department of Civil Engineering SAINTGITS College of Engineering is coming out with a technical magazine published by Civil Engineering faculty. I take this opportunity to congratulate the chief editor for bringing out this magazine as per schedule, which in itself is an achievement considering the effort and time required. I would like to thank all editorial team members for providing students a platform for technical thoughts and knowledge expansion. I express my considerable appreciation to all the authors of the articles in this magazine. I express my gratitude to all for their involvement, encouragement, support and guidance.

Prof. Dr. Reebu Z Koshy
Head of Department

ABOUT DEPARTMENT

DEPARTMENT OF CIVIL ENGINEERING

Vision

Emerge as a centre of excellence in Civil Engineering education

.

Mission

Develop Civil Engineers with commendable knowledge, innovative ideas and leadership qualities, who can appropriate technology and contribute efficiently to the industry and research

PROGRAMME EDUCATIONAL OBJECTIVES (PEOS)

PEO1: To prepare graduates to satisfy the requirements of their employers for professional practice in Civil Engineering thereby serving the needs of society and profession.

PEO2: To prepare graduates to take up post graduate studies/research.

PEO3: To prepare graduates for professional advancement and business leadership.

PROGRAMME OUTCOMES (PO)

1. **Engineering Knowledge**: Apply the knowledge of mathematics, science, engineering fundamentals, and an engineering specialization to the solution of complex engineering problems.

2. **Problem Analysis**: Identify, formulate, review research literature, and analyse complex engineering problems reaching substantiated conclusions using first principles of mathematics, natural sciences and engineering sciences.

3. **Design/Development of Solutions**: Design solutions for complex engineering problems and design system components or processes that meet the specified needs with appropriate consideration for the public health and safety, and the cultural, societal, and environmental considerations.

4. **Conduct Investigations of Complex Problems**: Use research-based knowledge and research methods including design of experiments, analysis and interpretation of data, and synthesis of the information to provide valid conclusions.

5. **Modern Tool Usage**: Create, select, and apply appropriate techniques, resources, and modern engineering and IT tools including prediction and modelling to complex activities with an understanding of the limitations.

6. **The Engineer and Society**: Apply reasoning informed by the contextual knowledge to assess societal, health, safety, legal and cultural issues and the consequent responsibilities relevant to the professional engineering practice.

7. **Environment and Sustainability**: Understand the impact of the professional engineering solutions in societal and environmental contexts, and demonstrate the knowledge of, and need for sustainable development.

8. **Ethics**: Apply ethical principles and commit to professional ethics and responsibilities and norms of the engineering practice.

9. **Individual and Team Work**: Function effectively as an individual, and as a member or leader in diverse teams, and in multidisciplinary settings.

10. **Communication**: Communicate effectively on complex engineering activities with the engineering community and with society at large, such as, being able to comprehend and write effective reports and design documentation, make effective presentations, and give and receive clear instructions.

11. **Project Management and Finance**: Demonstrate knowledge and understanding of the engineering and management principles and apply these to one's own work, as a member and leader in a team, to manage projects and in multidisciplinary environments.

12. **Life-long Learning**: Recognize the need for, and have the preparation and ability to engage in independent and lifelong learning in the broadest context of technological change.

NUMERICAL STUDY ON WEB OPENINGS IN CASTELLATED BEAMS

Renju Reghukumar[1], Er. M Gayathri Devi[2]

[1] *PG Student, Department of Civil Engineering, Saintgits College of Engineering*

[2]*Assistant Professor, Department of Civil Engineering, Saintgits College of Engineering*

Abstract: *Castellated steel beams (CSB) have been employed extensively in steel structure buildings now a days. There is a common practice of adopting the depth of web openings up to 80% depth of the section. Due to this large depth of web openings there is a large reductionin the stiffness of the beams. Stiffeners are provided around the openings in the castellated beam to have a good structural performance. Thickness of stiffeners provided is 20mm. Inthis work, a nonlinear numerical analysis is carried out to explore the structural performance of castellated beams with and without stiffener around the edge of openings on strength capacity. Analysis of castellated steel beams is carried out by providing stiffeners in various cut off such as circular, square, hexagonal, octagonal and triangular. Results of analysis are compared to have the adequate section with increase in strength in each case*

Keywords*: Castellated steel beams, Stiffeners, Numerical analysis, Various cut off, Strength capacity*

Introduction:

Castellated beam is a beam that has a regular and repeating pattern of hexagonal holes. It is created by cutting the pattern lengthwise across two different halves, offsetting, and then welding them together to create a single expanded beam as shown in Fig. 1.

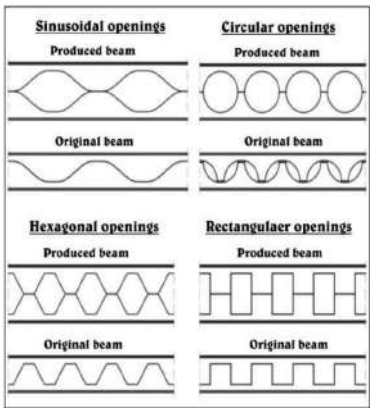

Fig. 1 Castellated beam

These beams have been used in various construction projects since the second half of the twentieth century. There has alsobeen something of a c-beam renaissance in recent years as engineers have discovered the many versatile uses of these beams in the construction of various construction projects. However, castellated beams still have their own advantages that make many architects and engineers prefer them. For instance, even after all these years, castellated beams offer a desirable weight to strength ratio at a very affordable cost. They have also been the standard for so long that they are easy for any installers and electricians to work with. C-beams have also become a major part of the architectural aesthetic in America and throughout the world. Using them in construction virtually guarantees that yourfinal building will look classy and elegant. These c-beams have a number of modern

applications. Far from being yesterday's technology, they still provide the backbone for much of the major architecture you will see in any given city. Due to continuous efforts of theresearch community there is an advancement in construction technology. These efforts lead to the emergence of several new structural elements like the open web beams, castellated beams, beams with corrugated web, use of slotted angle sections and many more. Castellated beams with different web openings are shown in Fig. 2.

Fig. 2 Different web openings

The many researchers have been studying continuously the close behaviour of such structural elements and provide design guidelines for analysis and design. Castellated or cellular beam is also called as perforated beams which are widespread essential parts in steel structures. Many researchers have been performed numerical andexperimental investigation with the intention to study theresponse of castellated beams to the different loading.

Literature Review:

Mohebkhaha A and Showkatib H (2005) studied of the effect of lateral braces on inelastic buckling has not been made especially for castellated beams, and it is not known whether the limiting stiffness for elastic buckling can be applied to castellated beams that buckle inelastically. This paper develops a three dimensional (3-D) finite element model using a finite- element program and uses it to investigate the effect of elastic lateral bracing stiffness on the inelastic flexural–torsional buckling of simply supported castellated beams with an elastic lateral restraint under pure bending. It was found that for inelastic castellated beams, the effect of bracing initially is increased to some extent as the lateral unbraced length increases and then decreased until the beam behaves as an elastic beam. In other words, the effect of bracing depends not only on the stiffness of the restraint but also on the modified slenderness of thebeam. Also, the results show that Winter'ssimplified method to determine full brace requirements cannot be applied to inelastic castellated beams. Zirakian T and Showkati H (2006) Tests of six full-scale castellated beams are described, in which the experimental investigation of distortional buckling was the focus of interest. In addition to the test strengths, the accurate critical loads of the beams have been obtained using some extrapolation techniques, and ultimately a comparison has been made between the obtained test loads and some theoretical predictions. Gandomi et al. (2011) studied a robust variant of genetic programming, namely gene expression programming (GEP), is utilized to build a prediction model for the load capacity of

castellated steel beams. The proposed model relates the load capacity to the geometrical and mechanical properties of the castellated beams. The model is developed based on a reliable database obtained from theliterature. To verify the applicability of the derived model, it is employed to estimate the load capacity of parts of the test results that were not included in the modelling process. The external validation of the model was further verified using several statistical criteria recommended by researchers. A multiple least squares regression analysis is performed 6 to benchmark the GEP-based model. A sensitivity analysis is further carried out to determine the contributions of the parameters affecting the load capacity. Theresults indicate that the proposed model is effectively capable of evaluating the failure load of the castellated beams. The GEP-based design equation is remarkably straightforwardand useful for pre-design applications. Ehab Ellobody (2011) investigates the behaviour of normal and high strength castellated steel beams under combined lateral torsional and distortional buckling modes. An efficient nonlinear 3D finite element model has been developed for the analysis of the beams. The initialgeometric imperfection and material nonlinearities were carefully considered inthe analysis. The nonlinear finite element model was verified against tests on castellated beams having different lengths and different cross sections. Failure loads and interaction of buckling modes aswell as load–lateral deflection curves of castellated steel beams were investigated in this study. An extensive parametric study was carried out using the finite element model to study the effects of the change in cross-section geometries, beam length and steel strength on the strength and buckling behaviour of castellated steel beams. The parametric study has shown that the presence of web distortionalbuckling causes a considerable decrease inthe failure load of slender castellated steel beams. It is also shown that the use of high strength steel offers a considerableincrease in the failure loads of less slender castellated steel beams. The failure loads predicted from the finite element model were compared with that predicted from Australian Standards for steel beams under lateral torsional buckling. It is shown that the specification predictions are generally conservative for normal strength castellated steel beams failing by lateraltorsional buckling, unconservative for castellated steel beams failing by web distortional buckling and quite conservative for high strength castellated steel beamsfailing by lateral torsional buckling. Showkati et al. (2012) The economical and structural advantages of these elements have prompted many researchers to investigate the failure behaviour of such structures. Despite numerous reported researches on the buckling stability of castellated beams, no experimental study is found on lateral–torsional buckling of these elements with elastic bracing. In thispaper,

the experimental study of nine full- scale castellated beams is 7 reported with the aim of investigation of the performance as well as effect of elastic bracing on the buckling stability of these structural elements. In addition to the presentation of the experimental observations and findings, the current test results are compared with the results of other reported experimental, analytical and numerical studies. Ultimately, the experimental findings and results are evaluated by considering the AISC 360–05 code requirements and predictions. Soltani et al. (2012) A numerical model is developed to predict the behaviour of castellated beams with hexagonal and octagonal openings up to failure. The numerical model takes into account both material and geometric nonlinearities. To initiate buckling, an initial small out-of-plane geometric imperfection, obtained from aneigenvalues buckling analysis, was imposed to the model. Results of experimental data obtained from previous works have shown that the model is ableto predict, with good accuracy, the ultimate load and to some extent the modeof failure. A parametric study is then realized to assess the cross-section classification given in the Annex N and to compare between the ultimate load behaviour of castellated beams with hexagonal and octagonal openings when subjected to flexure and shear force. The numerical results have been compared with those obtained with the design method presented in ENV1993-1-1 Annex

N. Wang et al. (2014) Large deflectionbehaviours of the restrained castellated steel beam in a fire are investigated using the finite element method. Studied CSBs adopted a newly proposed fillet corner polygonal web opening shape. The capability of the finite element model is validated against verified numerical results on solid web restrained steel beamsat elevated temperatures in a fire. Studied parameters of the castellated steel beaminclude the expansion ratio, the webopening dimension, the web opening shape, the arrangement of the web opening and the elastic axial restraint to the beam. The evolution of the end reaction force, the middle span deflection, and bendingmoments at critical sections of the CSB with the elevation of temperatures are presented. For the axial stiffness of a CSB is smaller thanthat of the original solid web steel beam, the compression force due to the restrained thermal elongation in a CSB in a fire is lower than that in the solid web beam. And the CSB goes into the catenary action phase at a lower temperature compared with the solid web steel beam. The web opening 8 dimension, theweb opening shape and the arrangement of web opening have very little influences on thecatenary action behaviours of the restrained castellated steel beam in a fire. Wang et al. (2016) Shear buckling behaviours of web-post in a Castellated Steel Beam with hexagonal web openings under vertical shear were investigated using finite element method. Through treating the upper part of the web- post as a free body under horizontal shear force, whose

shear buckling strength can be calculated by the thin plate shear buckling theory, design equations for the vertical shear buckling strength of the web-post were proposed. Parameters that affected the verticalshear buckling strength of the web-post were studied, which were the opening height to web thickness ratio h0/tw, the web-post width to web thickness ratio e/tw, the web height of Tee section above the opening to the web thickness hf/tw, the web thickness tw and the incline angle of the opening edge α. After obtaining the vertical shear buckling strength of a CSB through finite element model, the shear buckling coefficient k can be obtained through inverse analysis. Research results showed that k decreased nonlinearly with the increase in e/tw and hf/tw and it increased linearly with theincrease in α and h0/tw. Practical calculating method for k was proposed based on parameter analysis results. The vertical shear buckling strength of the web-post calculated using the proposed shear buckling coefficient k agreed well with that obtained from the finite element simulation. For the proposed method was based on the elastic buckling of the web- post, it overestimated the shear buckling strength when the web-post buckled in theelastic–plastic state. Hassan Abedi Sarvestani (2017) In this article, behaviourof ten beam specimens, including five hexagonal castellated beams and five typical wide flange beams, in the post-tensioned semi-rigid beam-to-column steel connections of moment-resisting frames has been analysed theoretically and numerically by well-known finite element software (ABAQUS 6.11-PR3) under the earthquake simulated by cyclic loading up to 4.4 % lateral drift. Hexagonal castellated beams provide lower weight and higher bending strength in comparison with typical wide flange beams in post-tensioned semi rigid steel connections. The results of finite element analysis verified against experiment have proved that the theoretical method based on the previous researches accurately predicts the behaviour of hexagonal castellated beams in the post-tensioned 9 connections. All beam specimens did not suffer from the flange buckling and web shear buckling under the standard cyclic loading up to 4 % lateral drift; likewise, hexagonal castellated beams in the post-tensioned connections showed adequate strength against web post failure and vierendeel mechanism up until 4% drift. In order to investigate the ultimate failure modesof the specimens, they have also been subjected to an added half cycle loading up to 4.4 % lateral drift beyond the standard loading. The further drifts have leaded to the web-post buckling in most specimens with hexagonal castellated beams and flange buckling in all specimens with wide flange beams. In addition, the parametric study is suggested as a further investigation to comprehensively understand the behaviour of hexagonal castellated beams in the PT connections and it is required to reach more general conclusions. Dafafea et al. (2018) The presence of large openings in the web generates

specific mechanical behaviour in comparison with that of solid web beams and leads quite often to the reinforcement of the opening by welding stiffeners. An experimental program based on thirteen steel beams with a single rectangular web opening is performed. It aims to evaluate the influence of the openings reinforced or not by stiffeners on the behaviour of the beam loaded in shear and bending. The stiffeners are used to increase theresistance of the openings. Different solutions are compared using various positions and lengths of stiffeners in the longitudinal and vertical directions. The comparisons are based on the failure load, the stiffness and the strain distribution. The experimental results and observations show the efficiency and the limits of the different studied solutions of stiffening. It has been observed that long horizontal stiffeners were the best stiffening solution. Furthermore, the use of double or single sided stiffeners showed that in both cases, they improve significantly the ultimate carrying capacity of the beam as long as the anchorage length is sufficient. The results can be used as a basis to develop numerical and analytical models. Nayak. C and Morkhade. S (2019) presents anextensive parametric study on the steel beam with corrugated web having openings in the web. The objective of the present study is to observe the structural performance of this special type of beam towards the strength capacities. In the parametric study 60 models of steel beams with trapezoidally corrugated web with opening has been analysed by finite element analysis using 10 ANSYS v12. The variables in the present study are angle of corrugation, thickness of web and diameter of opening. The angle of corrugation, web thickness and diameter of web openingsconsidered in the study are 0°, 30°, 45° and 3
mm, 4 mm, 5 mm and 0.5, 0.6, 0.75 times the overall depth of beam, respectively. The parametric study shows that lesser the angle of web corrugation, the more increase in the load carrying capacity is obtained. Ultimate strength capacity of 30° corrugated web beam with different diameter of opening such as 0.5D, 0.6 D, and 0.75 D is found to be 15.2 %,
14.83 %, 9.72 %, which is more than the beam with plain web. The height to thickness (h/tw) ratio considered in the study are 30, 37.5, 40, 50, and 66.67, respectively. The height to thickness (h/tw) ratio is found to be the main parameter influencing the buckling behaviour of steel beam with corrugated web. Thabhawee H.A and Alhasan A.A (2019) focused on improving the behaviour of thecastellated beam with octagonal openings using steel ring stiffener and adjusting the bestdimension and distribution for the stiffeners. All the models of specimens have been fabricated from a parent I section (IPE 140). The models have been modelled and analysed using finite element software ANSYS (version 15). The analysis results showed that reinforcing octagonal castellated beams by adding steel ring stiffeners

around octagonal web opening was very active way to increase the ultimate load for long span, where the ultimate load of reinforced octagonal castellated beam increased up to (286 %) compared with parent I-section beam.Economically, the percentage of additional steel material which used to expansion and reinforce the castellated beams (spacer plate and steel ring stiffeners) was (36 %) when compared with the weight of parent I-section beam. While the allowable load at deflection (L/180) was (260 %) compared to the allowable load of parent section at the same deflection. The gained benefit was increasing the ultimate and allowable load of reinforced octagonal castellated beams by (186 %) and (160 %) respectively by using additional steel material only (36 %)from the weight of parent I- section, which the additional steel material consisted from the spacer plates and steel rings. Also, the results indicate that thebest dimensions for the ring were when thickness equal to the web thickness of theparent section and the width equal to the half of the parent section flange width. 11 Gupt L.M and Morkhade S (2020) explains the state of the art of behaviourof Steel Castellated Beams. The present research status of behaviour of castellated beams is not mature and need much through study compared to beams without openings in the web. The existence of various shapes of openings such as circular, hexagonal, rectangular, octagonal and oval etc. in beams web add some additional failure modes namely; lateral- torsional buckling of web posts, web post buckling due to shear force, formation of four plastic hinges around the corners of openings, rupture of welded of joints in the castellated beams over a conventional steel beams. A review of experimental and analytical work carried out on castellated steel beams has beenpresented. The paper also focuses on the influence of various parameters such as types of openings, size of openings, spacing of the openings, aspect ratio, various numbers of openings and strengthening on the behaviour of steel beams with web openings. Liu et al. (2020) presented numerical investigations on the behaviour of a Bolted Castellated Steel Beam (BCSB) with octagonal web openings. Instead of welding the upper and the lower Tee-sections of a Castellated Steel Beam (CSB) together in the factory, they were connected using high strength bolts at the construction site. Thus, the upper and the lower Tee-sections can be transported separately, especially being convenient for a castellated steel beam with great sectionheight. The residual stresses in the web-post induced by welding could also be avoided.The shear buckling behaviour of the web-post in a BCSB with octagonal openings was studied using a verified finite element model. The buckling mode and the buckling strength of the web post in a BCSB were compared with those of a traditional Welded Castellated Steel Beam (WCSB). Research

results showed that web-posts in a BCSB withoctagonal web openings had as good structural performance as those in a WCSB. Studied parameters of the BCSB included the bolt diameter, the width-to-thickness ratio of the web-post and the bolt layout. To increase the buckling strength of the web-post, a BCSB using stiffened connection plate was proposed. The Strut Model for predicting the buckling strength of the web-post in a traditional WCSB was employed for calculating that in a BCSB. Comparisons of buckling strengths obtained by Strut Model predictions and finite element simulations showed that the Strut Model could be used to predict the web-post buckling strength of a BCSB. 12 Morkhade et al. (2020) examined the effect large depth of web openings and found that there is drastic reduction in the stiffness of the beams. The castellated beam becomes structurally more capable by providing the stiffeners. Therefore in this research work, a nonlinear numerical analysis is carried out so as to observe the effectiveness of stiffeners. From the results obtained it is found that robustness of castellated beams enhances by 44 % as compared to conventional steel I beam. The average increase in strength of castellated steel beams by provision of stiffeners is 36 % over unreinforced openings. The web buckling failure can be prevented by using stiffeners. The predominant failure mode is found to be Vierendeel mechanism for both reinforced and unreinforced web openings. Hosseinpour M and Sharifi Y (2021) examined the effects of web distortion on the buckling behaviour of castellated steel beams. To this purpose, a series of nonlinear finite element (FE) models was constructed and well verified against an experimental work on the distortional buckling of castellated beams; both material nonlinearities and initial geometric imperfections were carefully applied to the models. Next, an extensive parametric study was performed using the finite element models to investigate the effects of beam length, steel grade and cross-section dimensions on the ultimate buckling load and buckling modes of castellated steel beams. The results showed that the use of low grade steel and thick flanges makes an economical design in the castellated steel beams. Moreover, it is concluded that lateral- distortional buckling (LDB) mode is more common in the castellated beams with intermediated overall slenderness, thick flanges and slender web. Finally, the ultimate loads obtained from finite element analysis (FEA) were compared with the results predicted by AS4100, EC3 and AISC codes. It was concluded that all three Specifications provide unsafe estimates for most specimens in this study.

Objective:

Following are the objectives carried:

1. To conduct nonlinear numerical analysis

on different web openings in castellatedbeams with stiffeners

2. To find the percentage of increase in strength in each opening
3. To find the stress concentration in each opening
4. To find the strain value in each opening

Castellated beams used in construction are highly effective structural elements found in long span floor and roof systems. Their high flexibility, reducedweight and great aesthetics make themoptimal picks for low-cost solutions. Castellated beams are made from standardhot rolled I – H – U sections with different web openings. Different typesof stiffenersare provided in castellated beams as each type performs in different way in enhancing the structural performance. Stiffened Castellated Steel Beams (SCSB) with different web openings are analysed.

Study of this work is limited to:

1. FEA using ANSYS software
2. Steel section of ISMB200
3. Web openings - circular, square, hexagonal, octagonal, triangular
4. Stiffeners of thickness = 20 mm
5. Imperfection of L/1000 included for geometrical nonlinearity

Methodology:

The beam model is validated with Morkhade *et. al*., 2020. The castellated steel beam has been fabricated from ISMB200 section. The span of CSB is 1850 mm. The numerical analysis has been done by using ANSYS software version 18.1. The standard material properties of steel considered in the analysis yield strength σ_y =250 N/mm^2, ultimate strength σ_u = 410 N/mm2 , modulus of elasticity E = 210 GPa, strain hardening modulus ET = 5000 N/mm^2 and Poisson's ratio μ = 0.30.

Modelling of CSB

After validating the numerical model, a thorough investigation has been performed with the purpose to analyse the structural behaviour of reinforced castellated beams. Thecastellated steel beams CSB300 are prepared from ISMB200 parent section. The reinforcement is provided around the openings. Thickness of stiffeners is taken equal to 20 mm. No lateral support was provided to the beams. The material as well as geometrical nonlinearity is taken into consideration of finite element models. An initial imperfection of L/1000 has been included to account for geometrical nonlinearity. Castellated beam with web openings of circular, hexagonal, octagonal, square and triangular are analysed without stiffeners and with stiffeners. Thickness of stiffeners used is 20 mm. Area of opening is

taken from the experiments result from the journal Morkhade et. al., 2020. The beam is fixed at 2 ends and loaded with point load at centre.

CSB without stiffeners

The geometric model for castellated beam with circular, hexagonal, octagonal, square and triangular web openings are shown in Fig. 3, Fig.

4, Fig 5, Fig. 6 and Fig. 7respectively.

Fig. 3 Geometric model of CSB with circular opening

Fig. 4 Geometric model of CSB with hexagonal opening

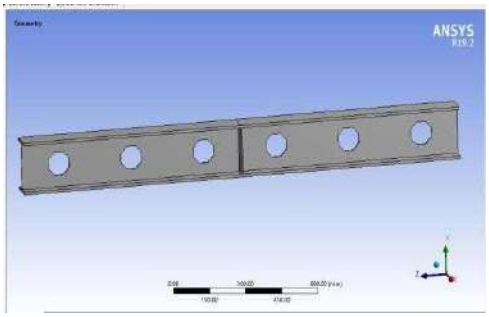

Fig. 5 Geometric model of CSB with octagonal opening

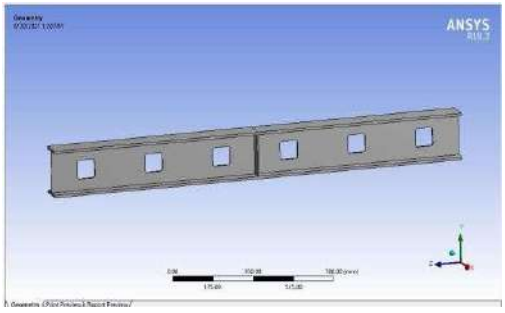

Fig. 6 Geometric model of CSB withsquare opening

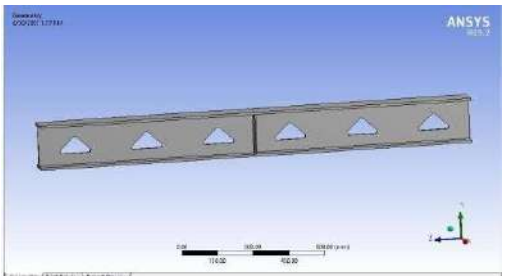

Fig. 7 Geometric model of CSB withtriangular opening

CSB with stiffeners

Stiffeners provided are of steel sections of diameter 20 mm around the edge of each opening in all the castellated beams with different web openings. The geometric model for castellated beam with circular, hexagonal,

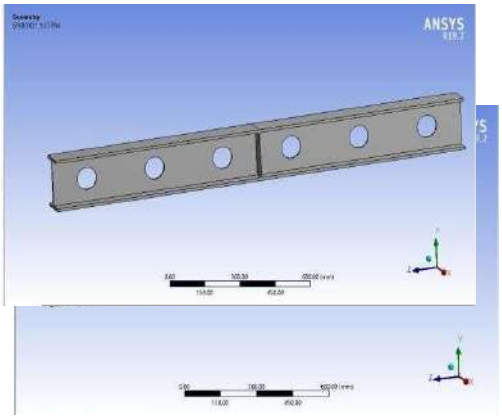

octagonal, square and triangular web openings provided with stiffeners around each opening are shown in Fig. 8, Fig. 9, Fig 10, Fig. 11 and Fig. 12 respectively.

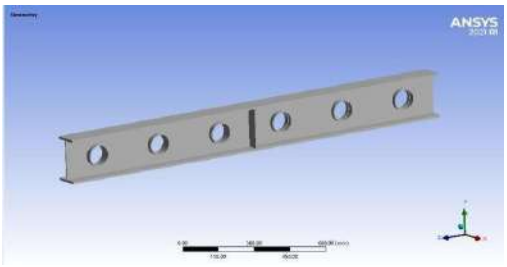

Fig. 8 Geometric model of SCSB with circular opening

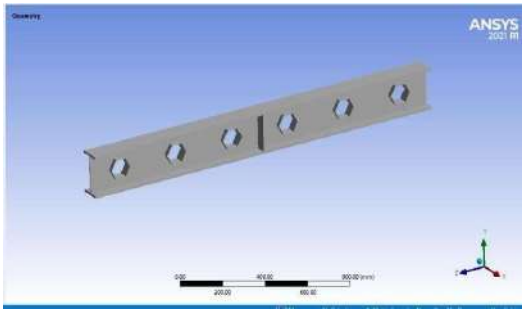

Fig. 9 Geometric model of SCSB with hexagonal opening

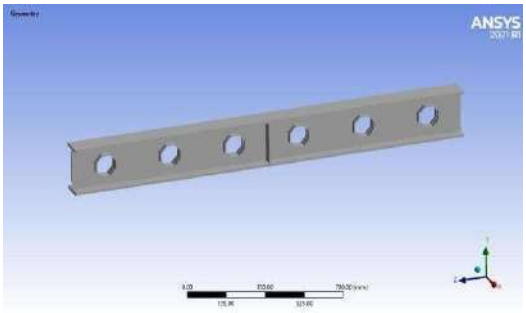

Fig. 10 Geometric model of SCSB with octagonal opening

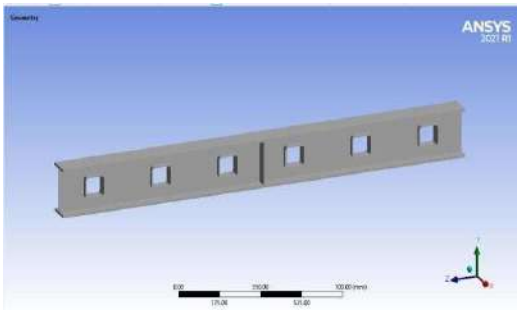

Fig. 11 Geometric model of SCSB with square opening

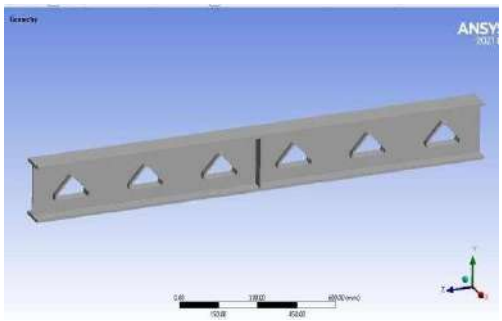

Fig. 12 Geometric model of SCSB with triangular opening

Results and discussion

After confirmation of correctness of the results attained from numerical analysis, an extensive investigation has been carried out. Theinvestigation consists of analysis of castellated steel beams with and without stiffeners around the openings. The parametric study reveals that castellated steel beams found to be very effectiveas a structural solution as compared to the conventional solid web beams. But on the contrary, the unreinforced web openings are not always an economical solution. Provision of reinforcement around the web openings proves to be an excellent solution for enhancing the strength capacity of castellated beams.

CSB without stiffeners

Circular web opening

The total deformation, stress and strain are shown in Fig. 13(a), Fig. 13(b), Fig. 13(c) respectively. The total deformation is 140.67 mm, stress is 243.65 MPa, strain is 0.0023144 mm/mm.

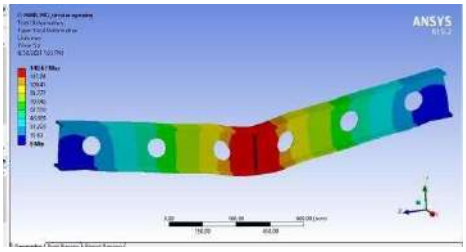

Fig. 13(a) Total deformation of CSB with circular opening

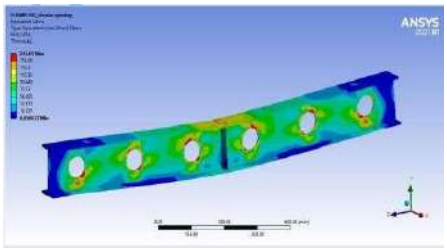

Fig. 13(b) Stress of CSB with circular opening

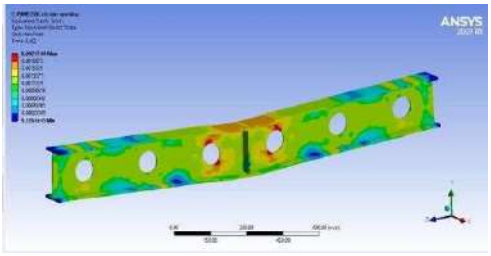

Fig. 13(c) Strain of CSB with circular opening

Heaxagonal web opening

The total deformation, stress and strain of CSB are shown in Fig. 14(a), Fig. 14(b), Fig. 14(c) respectively. The total deformation is 126.44 mm, stress is 233.55 MPa, strain is 0.0021826 mm/mm.

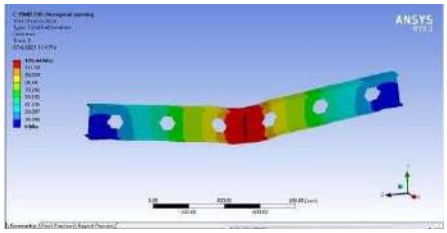

Fig. 14(a) Total deformation of CSB with hexagonal opening

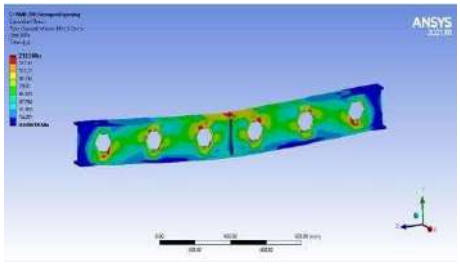

Fig. 14(b) Stress of CSB with hexagonal opening

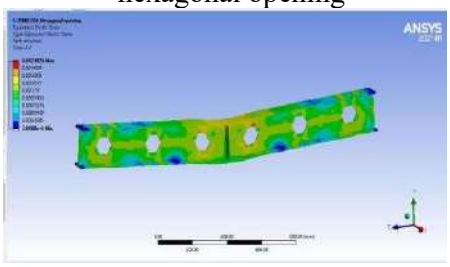

Fig. 14(c) Stain of CSB with hexagonal opening

Octagonal web opening

The total deformation, stress and strain of CSB are shown in Fig. 15(a), Fig. 15(b), Fig. 15(c) respectively. The total deformation is 124.64011 mm, stress is 234.71 MPa, strain is 0.0020293 mm/mm.

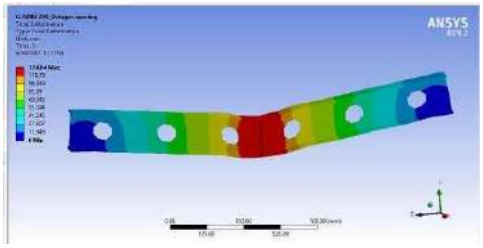

Fig. 15(a) Total deformation of CSB with octagonal opening

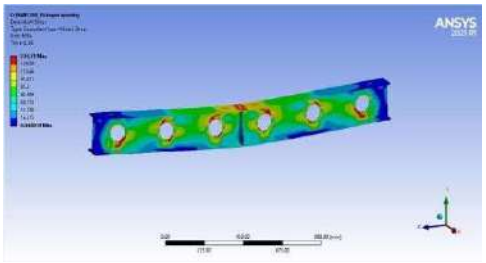

Fig. 15(b) Stress of CSB with octagonal opening

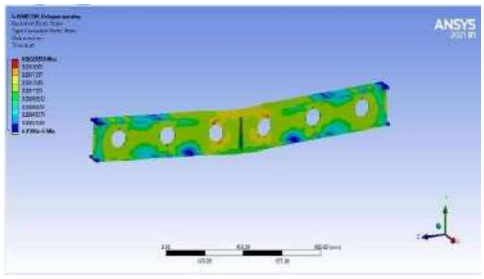

Fig. 15(c) Strain of CSB with octagonal opening

Square web opening

The total deformation, stress and strain of CSB are shown in Fig. 16(a), Fig. 16(b), Fig. 16(c) respectively. The total deformation is 138.6700 mm, stress is 241.71 MPa, strain is 0.0021496 mm/mm.

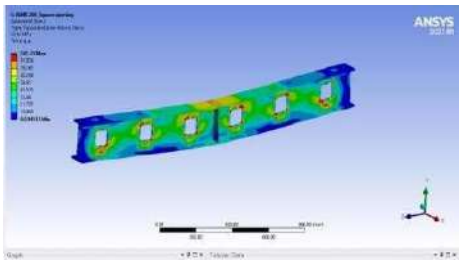

Fig. 16(a) Total deformation of CSB with square opening

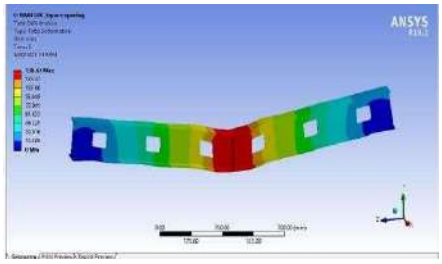

Fig. 16(b) Stress of CSB with square opening

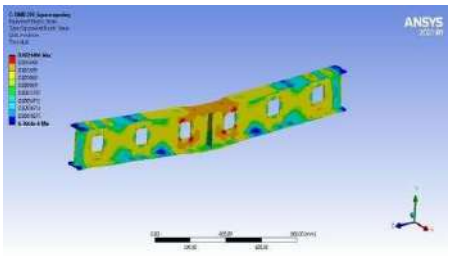

Fig. 16(c) Strain of CSB with square opening

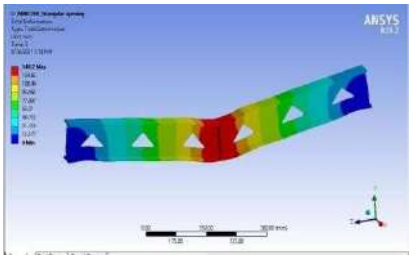

Fig. 17(a) Total deformation of CSB with triangular opening

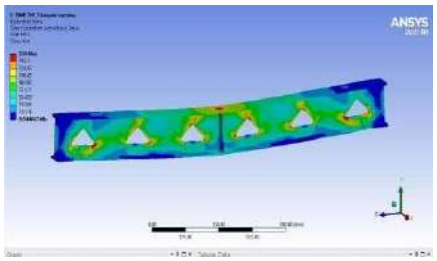

Fig. 17(b) Stress of CSB with triangular opening

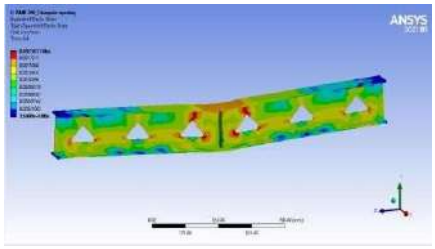

Fig. 17(c) Strain of CSB with triangular opening

Triangular web opening

The total deformation, stress and strain of CSB are shown in Fig. 17(a), Fig. 17(b), Fig. 17(c) respectively. The total deformation is 140.2100 mm, stress is 234.0 MPa, strain is 0.0023051 mm/mm.

CSB with stiffeners

Circular web opening

The total deformation, stress and strain are shown in Fig. 19(a), Fig. 19(b), Fig. 19(c) respectively. The total deformation is 153.9900 mm, stress is 247.2 MPa, strain is 0.0020293 mm/mm.

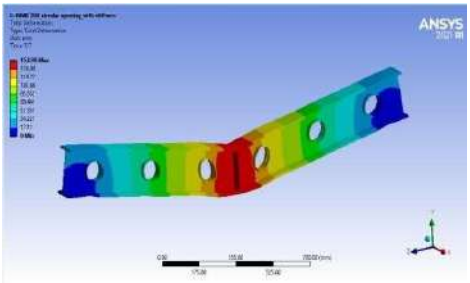

Fig. 19(a) Total deformation of SCSB circular opening

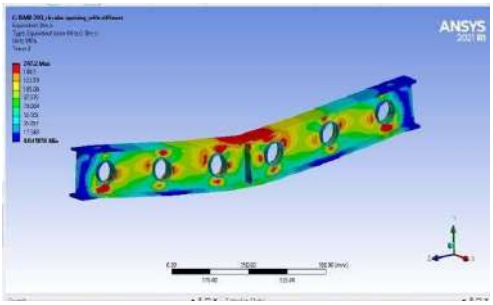

Fig. 19(b) Stress of SCSB circular opening

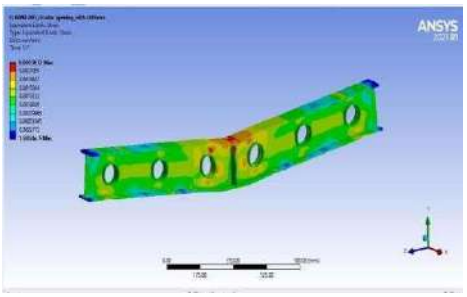

Fig. 19(c) Strain of SCSB circular opening

Hexagonal web opening

The total deformation, stress and strain are shown in Fig. 20(a), Fig. 20(b), Fig. 20(c) respectively. The total deformation is 150.0200 mm, stress is 240.51 MPa, strain is 0.0021841 mm/mm.

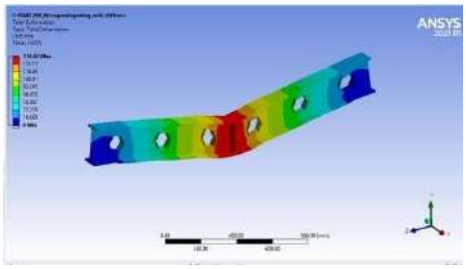

Fig. 20(a) Total deformation of SCSB hexagonal opening

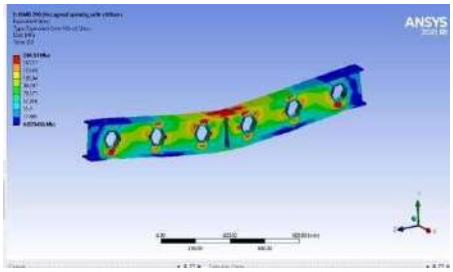

Fig. 20(b) Stress of SCSB hexagonal opening

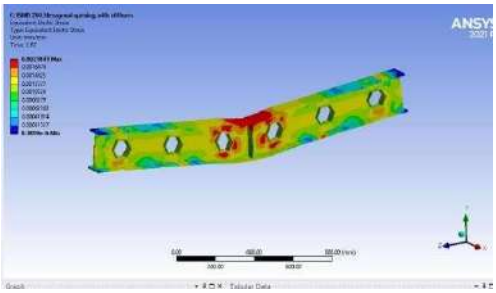

Fig. 20(c) Strain of SCSB hexagonal opening

Octagonal web opening

The total deformation, stress and strain are shown in Fig. 21(a), Fig. 21(b), Fig. 21(c) respectively. The total deformation is 138.4100 mm, stress is 237.03 MPa, strain is 0.0021386 mm/mm.

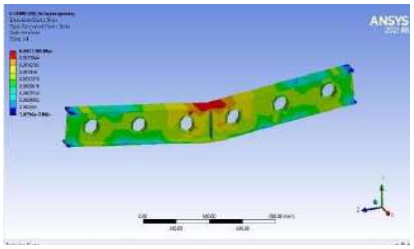

Fig. 21(a) Total deformation of SCSB octagonal opening

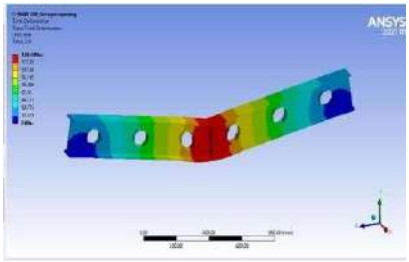

Fig. 21(b) Stress of SCSB octagonal opening

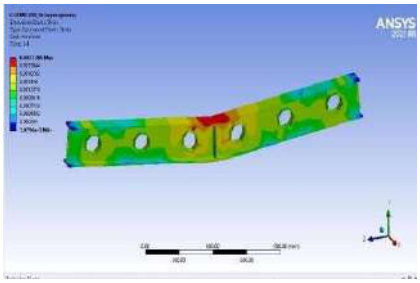

Fig. 21(c) Strain of SCSB octagonal opening

Square web opening

The total deformation, stress and strain are shown in Fig. 22(a), Fig. 22(b), Fig. 22(c) respectively. The total deformation is 164.67 mm, stress is 243.79 MPa, strain is 0.0023256 mm/mm

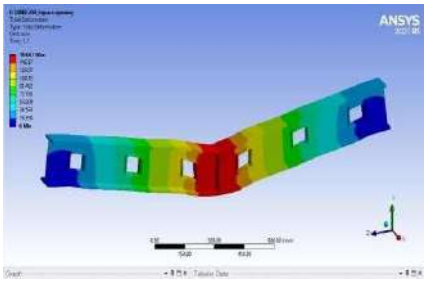

Fig. 22(a) Total deformation of SCSB square opening

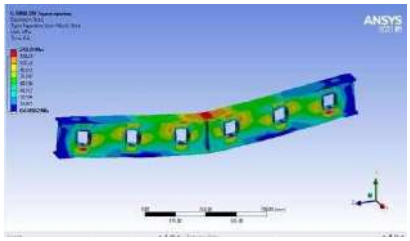

Fig. 22(a) Stress of SCSB square opening

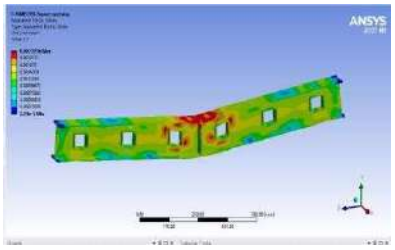

Fig. 22(b) Stress of SCSB square opening

Triangular web opening

The total deformation, stress and strain are shown in Fig. 23(a), Fig. 23(b) and Fig. 23(c) respectively. The total deformation is 146.0700 mm, stress is 245.35 MPa, strain is 0.0023481 mm/mm.

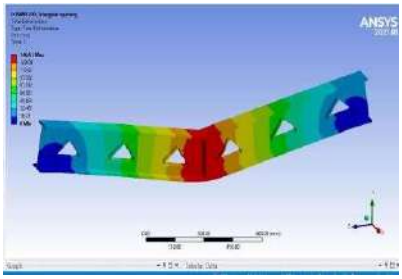

Fig. 23(a) Total deformation of SCSB triangular opening

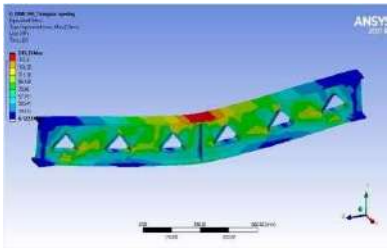

Fig. 23(b) Stress of SCSB triangular opening

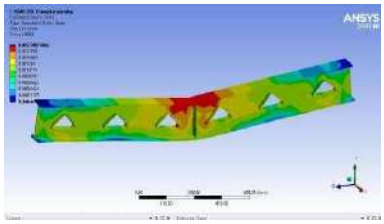

Fig. 23(c) Strain of SCSB triangular opening

Discussions:

Stiffeners increases ultimate load carrying capacity, decreases the total deformation, decreases the stress concentration and decreases the equivalent strain. Castellated beam with triangular opening provided with stiffeners has high ultimate load carrying capacity of 305 kN. And it has the low deformation, low stress concentration and low strain value at ultimate load of 146.07 mm, 240.3 MPa, 0.0023481 mm/mm respectively. Fig. 24 & Fig. 25 shows Load – Deformation graph of CSB & SCSB with triangularweb opening respectively.

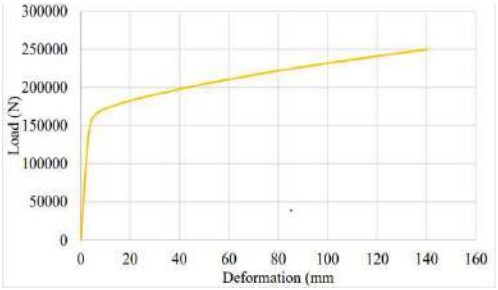

Fig. 24 Load – Deformation graph of CSB with triangular opening

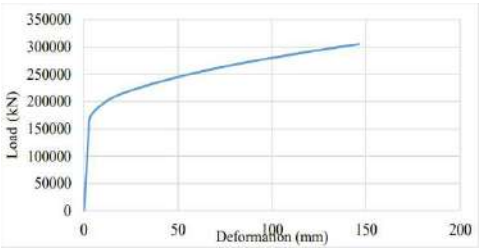

Fig. 25 Load – Deformation graph of SCSB with triangular opening

Conclusions:

In this work the nonlinear numerical analysis of castellated steel beams with and without stiffeners around the edge of web openings has been studied. The castellated steel beams CSB300 used in the analysis have been prepared from

plain ISMB200.

1. The strength is increased by the provision of stiffeners around openings when compared to CSB without stiffeners around the openings.
2. The increase in ultimate load by the provision of stiffeners around the openings is 11.47% over CSB without stiffeners around the openings.
3. The decrease in total deformation by the provision of stiffeners around the openings is 37.9 % over CSB without stiffeners around the openings.
4. The decrease in stress by the provision of stiffeners around the openings is 4.62 % over CSB without stiffeners around the openings.
5. The decrease in strain by the provision of stiffeners around the openings is 1.83 % over CSB without stiffeners around the openings.
6. Castellated beam with triangular opening provided with stiffeners has high ultimate load carrying capacity of 305 kN.
7. It has the low deformation of 146.07 mm at ultimate load of 350 kN.
8. It has the low stress concentration of 240.3 MPa at ultimate load of 350 kN.
9. It has the low strain value of 0.0023481 mm/mm at ultimate load of 350 kN.
10. By provision of stiffeners around the openings web buckling failure can be prevented.
11. Total volume of the steel remain same in all the cases as the areaof the openings is same in different web opening is used.

References:

1. **Bo Dafafea, T. A., Durif, S., Bouchaïr, A., Fournely, E. (2018),** Experimental study of beams with stiffened large web openings, *Journal of Constructional Steel Research-Elsevier,* Vol 154, pp 149 -160
2. **Ellobody, E.** (2011), Interaction of buckling modes in castellated steel beams, *Journal of Constructional Steel-Elsevier*, Vol 67, Issue5 , pp 824 – 825
3. **Frans, R., Parung, H., Sandy, D., Tonappa, S. (2016),** Numericalmodelling of hexagonal castellated beam under monotonic loading, *Sustainable civil engineeringstructures and construction materials- Elsevier, Procedia Engineering, Vol 171, pp* 781 - 788
4. **Gandomia, A. H., Tabatabaeib, S. M., Moradianc, M. H., Radfard, A., Alavi, A. H., (2011),** A new predictionmodel for the load capacity of castellated steel beams, *Journal of Constructional Steel Research-Elsevier, Vol 67, Issue 7, pp 1096 -1105*
5. **Hosseinpour, M., Sharifi, Y. (2021),** Finite element modelling of castellated steel beams under lateral-distortional buckling mode, *Structures - Elsevier, Vol 29, pp 1507- 1521*
6. **Mohebkhaha, A., Showkatib, H.**

(2005), Bracing requirements for inelastic castellated beams, *Journal of Constructional Steel Research- Elsevier, Vol* 61 pp 1373
- 1386

7. **Morkhade, S., Gupta, L.M. (2020),** Behaviour Of Castellated Steel Beams State Of The Art View, *Electronic Journal Of Structural Engineering- Research Gate, Vol* 19, pp 39 - 48
8. **Morkhade, S., Lokhande, R.S., Gund, U.D., Divate, A.B., Deosarkar, S.S., Chavan, M.U. (2020),** Structural Behaviour of Castellated Steel Beams With Reinforced Web Openings, *Asian Journal Of Civil Engineering- Research Gate,* Vol 21, pp 1067 – 1078
9. **Nayak, C., Morkhade, S. (2019),**Study of effect of web openings on the strength capacities of steel beam with trapezoidal corrugated web, *Asian Journal of Civil Engineering- research Gate, Vol 20, pp 1089 - 1099*
10. **Sarvestani, A.H. (2017),** Cyclic behaviour of hexagonal castellated beams in steel moment-resisting frames with post-tensioned connections, *Structures- Elsevier, Vol 11, pp 121 - 134*
11. **Soltania, M. R., Bouchaïrb A., Mimoune, M. (2012),** Nonlinear FE analysis of the ultimate behaviour of steel castellated beams, *Journal of Constructional Steel Research- Elsevier, Vol 70, pp 101 - 114*
12. **Showkatia, H., Ghazijahanib, G. T., Nooric, A., Zirakian, T. (2012),** Experiments on elastically braced castellated beams, *Journal of Constructional Steel Research- Elsevier, Vol 77, pp 163 - 172*
13. **Thabhawee, H.A., Alhasan, A.A. (2019),** Reinforcing the Octagonal Web Openings Of Castellated Beam By Steel Ring, *Al-qadisiyah Journal For Engineering Sciences- research Gate,* DOI:10.30772/Qjes.V12i1.581
14. **Wang, P., Guo, K., Liu, M., Zhang, L. (2016),** Shear buckling strengths of web-posts in a castellated steel beam with hexagonal web openings, *Journal of Constructional Steel Research-Elsevier,* Vol 121, pp 173 - 184
15. **Wang, P., Ma, Q., Wang, X. (2014),** Numerical studies on large deflection behaviours of restrained castellatedsteel beams in a fire, *Journal of Constructional Steel Research, Vol 100,pp 136 - 145*
16. **Wang, P., Ma, Q., Wang, X. (2014),** Investigation on Vierendeelmechanism failure of castellated steel beams with fillet corner web openings, *Engineering structures-Elsevier*, *Vol74, pp 44 - 51*
17. **Wang, P., Wang, X., Ma, N., (2014),** Vertical shear buckling capacity of web-posts in castellated steel beams with fillet corner hexagonal web openings, *Engineering structures-Elsevier, Vol 75, pp 315 - 326*
18. **Zirakian, T., Showkati, H. (2006),** Distortional buckling of castellated beams, *Journal of Constructional Steel Research-Elsevier*, Vol 62, pp 863–871.

PERFORMANCE EVALUATION OF PROPOSED CONTAINER TERMINAL AT VIZHINJAM PORT

Reema Thomas[1], Er. Amey Abraham[2]

[1] *PG Student, Department of Civil Engineering, Saintgits College of Engineering*

[2]*Assistant Professor, Department of Civil Engineering, Saintgits College of Engineering*

Abstract: *A berth is a designated location in a port or harbour used for mooring vessels when they are not at sea. A berth offers a vertical front that enables safe and secure mooring and can facilitateunloading or loading of cargo or people from vessels. For all buildings that were plannedanddetailed using IS standards, ductility has become a problem. Existing building's seismic qualification has been crucial in these scenarios. The weak structures are finally strengthenedas a result of seismic qualification. This is accomplished by performing pushover analysis and evaluating the structure's performance using Capacity spectrum approach. A non-linear analysismethod called "Pushover analysis" can be used to estimate a structure's strength capacity beyondthe elastic limit and up to ultimate strength. This method also predicts potential weak areas in thestructure by keeping track of the sequence of damages of each andevery member in structure. This paper illustrates the evaluation of performance of proposed container terminal at Vizhinjamport which was designed using IS code. Weaker areas of thestructure are identified and tuning ofsuch elements is done.*

Keywords*: Container berth, Capacity spectrum approach, Pushover Analysis, Seismic qualification, Vizhinjam Port*

Introduction:

When ships are not at sea, they are moored in a specific area of a port or harbourcalled a berth. Berths provide a vertical front that allows safe and secure mooring that can facilitate the unloading or loading of cargo or people from vessels. A container berth is any berth at a state port or pier that has been designated by the State for preferential usage by ships that predominantly load or unload shippingdevices. Near a quay, jetty, or floating dock is where most berths are located. Berth is either general/specific to types of vessels that use them. Berth sizes range from 5 to 10 metres for small boats in marinas to more than 400 metres for larger tankers. Numerous factors, such as the soil features in the area where the berth will be located, will affect its planning and design. All basic datas were adopted from Vizhinjam International Seaport which were supposed to be used in the project such as environmental data.

All berth components must be properly planned for both current needs and anticipated future demands.

Literature Review:

Carbonari *et al.,* (2019) studied that stretchable dolphin with marine fenders breasting are widely employed in jetties belonging to offshore oil platforms, andtheir design is performance-based. The suggested design process, which is basedon the kinetic energy approach, makes the assumption that both the dolphin's displacement and the fender's performance will be as anticipated. It also enablesthe evaluation of the flexible system's stiffness, which is necessary to achieve the desired energy absorption capacity. This is because the space between the mooring point of the breasting system and the oil terminal is often reserved for logistical and operational needs. Applications show how the suggested strategy works and how the dolphin-fender interaction contributes to withstanding berthing operations, enabling the creation of a flexible berthing structure even in the case of relatively small vessels. Kannan *et al.,* (2020) studied about the two alternative techniques for doing seismic analysis of a cargo berth. The linear static analysis was done using the IS 1893 codes, and the results were used to determine the structure's seismic coefficient, base shear, and natural time period. The second analytical technique is a nonlinear static pushover technique that makes use of SAP 2000 to simulatethe cargo berth. The pushover curve, or base displacement vs. base shear, is discovered. The pushover curve, or base displacement vs. base shear, is discovered. Utilizing both the outcomes of the traditional cargo berth design, performance-based seismic analysis can be tailored to satisfy performance and cost-effectiveness requirements. Ortiz *et al.,* (2020) examined capacity management problem at a container terminal using an optimization-based decision support system (DSS). In order tobalance supply (equipment assignment) and demand (truck arrivals), the capacity management problem at a container port must be solved while raising productivity and customer service metrics. The DSS is created in cooperation with an industrial partner to support them in their operational decision-making when determining the appointment quotas. Given the accessibility of yard resources to tackle a related optimization problem that balances the supply and demand of moves in the yard, the underlying strategy uses a tabu search metaheuristic algorithm. The DSS is adaptable and lets you configure and read from external files for a number of factors. Real-world data were used in the experimental instances to gauge the system's effectiveness. Perumalswamy *et al.,* (2021) conducted experimental study in cohesion less soil. The berthing structures are built

with diaphragm wall tied with piles. The soil quality, width, and slope created after dredging all affect where the diaphragm wall should be placed—either in front of or behind the berthing structure. If the soil is very soft clay or very loose sand, the pipe sheet pile wall can be utilized in place of the diaphragm wall due to its great bending strength and ease of construction. For various dredge levels, two layouts with pipe sheetpile walls in the front or in the back connected to two rows of pile are studied. According to the findings, a configuration with a pipe sheet pile wall in the fronthas twice the capacity of one with a wall in the back. Kumar *et al.,* (2021) studied on berthing structure in backwaters along westerncoast of India. The main causes of coastal structure deterioration are chloride-induced or carbonation-induced. Using non-destructive test measures and testedmodels, an effort is made to comprehend how climate change affects the quickly degrading of structures. Both of these processes are reliant on variables such as temperature, relative humidity, CO_2 concentration, rainfall, etc., which alter as the climate changes. According to the study, the deterioration of the berthing structure is a result of climate change. Due to the natural ageing processes, it is discovered that the concentration of chlorides and the carbonation are higher than that. Guo *et al.,* (2021) proposed a berth allocation problem (BAP) with ship handlingtime uncertainty by considering the influence of weather. In order to handle BAP, a two-stage optimization approach that concentrates on evaluating vessel handling time under various weather situations is created. Calculating the vessel handling times in stage I while taking the impact of the weather into consideration. A mixed-integer programming (MIP) model is presented in stageII as a means of solving the BAP based on the vessel handling times discoveredin stage I. Liu *et al.,* (2021) studied the berthing control problem for automatic ships by using a virtual guide system based on heuristic dynamic programming (HDP) method. The berthing control problem can first be changed into a tracking control problem with the addition of an automatic virtual guidance system, which can then be changed again into an optimal regulation problem. Second, the optimal regulation control problem of the marine surface ship with an unknown ship model is solved using the HDP approach. In order to confirm the viability of the suggested control scheme, simulations are conducted on an autonomous model ship and the HDP approach is compared with the back stepping control. Ghasemof *et al.,* (2022) studied about the performance-based design of buildings using FEMA P-58 methodology. Three office buildings were optimized for original cost and yearly

maintenance costs. Different performance measurements are used to compare design choices. Investigated is the role thosevarious components play in the cost of building repairs. The optimization processis carried out for three sample office buildings with steel moment frames of three,six, and nine stories using the well-known multi-objective optimization method known as NSGA-II. Ghasemof *et al.,* (2022) investigated the effects of various demand parameters used in steel moment frame building's best performance-based design. The effect of demand parameters on the optimal PBD of steel MRFs was investigated. FEMA P-58 was used to assess losses within a multi-objective optimization problem. Three steel MRF buildings are optimized for initial cost and annual repair cost. Monte Carlo analysis was performed to consider variations in the uncertain factors. Story drift ratio is more effective than other demand parameters in earthquake losses.

Objective:

The objectives of the project are

1. To design a proposed container terminal at Vizhinjam port using IS codes
2. To conduct seismic performance evaluation of the terminal
3. To identify weak points in the berthing structure through pushover analysisand tune the elements of the structure subsequently

Methodology:

Loads coming in container berth was taken from IS codes and environmental data regarding Vizhinjam International Seaport was taken from project report. After collection of data container berth is designed with an approximate pan area of 800m×53.673m which is supported on pile foundation. Analysis is done usingSTAAD Pro. Design based on IS code is optimized by performance based. Weak points in the berthing structure are identified and subsequent tuning of elements.

Components of Berthing Structure:

Various parts of berth structure are pile, pile cap, beams and slab

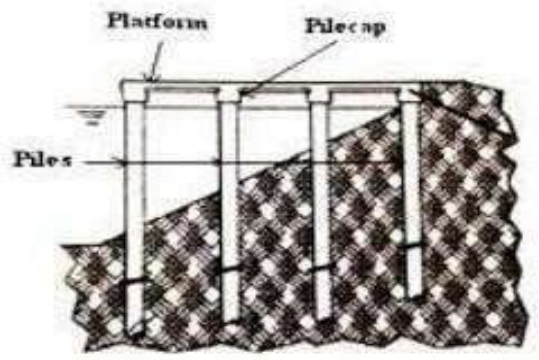

Fig. 1 Components of berthing structure

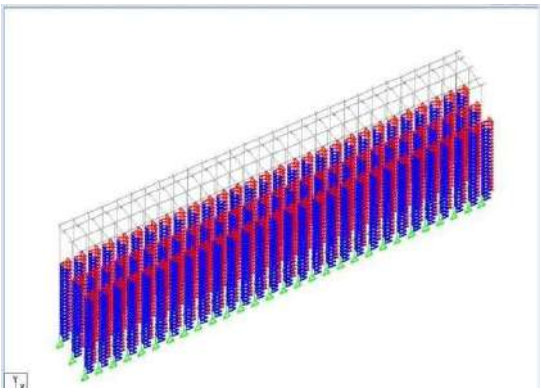

Fig. 2 STAAD model of berthing structure

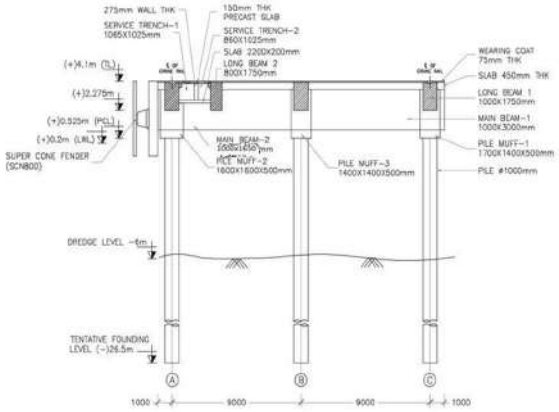

Fig. 3 Dimensions of berthing structure

Geometry of Berthing Structure:

Slab panel size: 800m × 53.675m

Size of longitudinal beam: 1.75m×1m, 1.75m×0.8m

Size of transverse beam: 3m×1m, 1.65m×1m

Depth of beams: 1.2m

Diameter of pile: 1m

Length of vessel: 400m

Dredge level: 6m

Span: 9m

Load Calculations:

Dead Load (IS 875- 1987 Part 1)

Dead load can be calculated by using the following steps

Slab Weight= $0.45\times25=11.25kN/m^2$

Transverse beam=$3\times1\times25=75kN/m$

Longitudinal beam=$1.75\times1\times25=43.75kN/m$

Pile= $((\pi\times1^{2)}/4)\times25= 50.26kN/m$

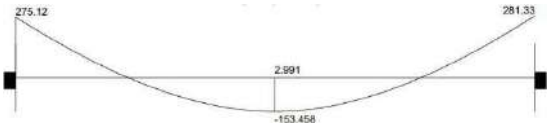

Fig. 4 Shear force diagram of dead load

Live Load (IS 4651(Part III)-1974)

For a container terminal normally, uniform vertical live load is taken as 3 to 5 T/m^2.Here assuming a live load of $50kN/m^2$

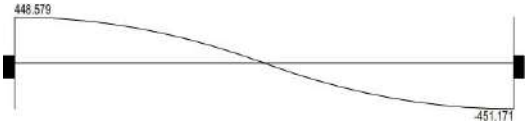

Fig. 5 Shear force diagram of live load

Berthing Load (IS 4651(Part III)-1974)

Berthing energy can be calculated using the formula

$$E= ((W_DV^2)/2g)\ (C_m)(C_e)(C_s)$$

Where,

W_D= Displacement tonnage =39600T

V=Velocity of Vessel in m/s= 0.2m/s

g= Acceleration due to gravity =$9.81m/s^2$

C_e=eccentricity coefficient= 0.393

C_m= mass coefficient= 1.087

C_s=softness coefficient= 0.95

E= 32.764T.m

Mooring Load (IS 4651(Part III)-1974)

Mooring load can be calculated using the formula

$$F=C_wA_wP$$

Where,

C_w=Shape factor=1.3 to 1.6

A_w= Wind age area in m^2

A_w= 1.175Lp (D_M-D_L) =1692m^2

V_z=56.728m/s

P= 0.06V_Z^2=193.08kg/m^2

F=4485.25kN

Fig. 6 Shear force diagram of Berthing load

Fig. 7 Shear force diagram of Mooring load

Current load (IS 4651(Part III)-1974, BS 6349 Part I Section 5)

Current load can be calculated using formula

$$F= (Wv^2)/2g$$

Where

w=Unit weight of water=1.025 tones/m^3

V= Velocity of current= 1.5m/s

g= Acceleration due to gravity =9.81m/s^2

F=4496.4Kn

Earth Pressure (IS 4651(Part III)-1974)

Earth pressure can be calculated using formula

$$P_a=k\gamma h$$

Where

k=Coefficient of earth pressure

φ= angle of internal friction of soil=30°

k=0.333

γ=unit weight of soil=17.5Kn/m^3

h=height of structure=26.5m

P_a=153.03Kn/m^3

Wind load (IS 875-Part III-1987)

Wind load can be calculated using formula

$$V_z=V_b\times k_1\times k_2\times k_3$$

Where

V_b=Basic wind speed=50.025m/s

k_1= Probability factor=1.08

k_2=Terrain, height and structure size factor=1.05

k_3=Topography factor=1

V_z=56.728m/s

P= 0.06V^2=193.08kg/m^2

Seismic Load (IS 1893-Part 1)

Design seismic base shear

$$V_B= A_h\times W$$

Where

A_h= (z/2) (s_a/g) (I/R)

A_h=horizontal seismic coefficient

W=seismic weight of structure

Z=zone factor= 0.16

I=Importance factor= 1.5

R=response reduction factor= 3

S_a/g= 2.5

A_h= 0.1019

W=Seismic weight of structure= 45986.35Kn

V_B= 4686.009Kn

Design lateral force= 27.5Kn/m

Vehicle Load

Following vehicular loads are considered

1. IRC Class 70R Tracked vehicle
2. IRC Class 70R Wheeled vehicle
3. IRC Class AA Tracked vehicle
4. IRC Class AA Wheeled vehicle
5. IRC Class A Train of vehicles

Wave force (IS 4651(Part III)-1974)

Wave force can be calculated using formula

$$F_{DM} = (1/2) \times C_D \times \rho \times D \times H^2$$

Where,

F_{DM}=Total drag force

C_D=Drag coefficient=2

ρ=mass density of sea water=1020kg/m^2

D=diameter of pile=1m

H=Wave height=1.6m

F_{DM}=251.205Kn/m^2

Temperature load (IS 456:2000)

A temperature load of 20Kn/m^2 is taken for the analysis

Performance Evaluation:

Designing structures for predictable performance under initially anticipated loads is known as performance-based design. It aims to offer a fair level of certainty that a design will meet that performance level. Producing structures with predictable seismic performance is the goal of performance-based design. Pushover analysis is a static method for calculating seismic structural deformation that employs a simplified non-linear methodology. It aids in illustrating the most likely method of eventual failure as well as the progression of failure in buildings. This method can forecast structural weak places by monitoring the progression of damage to each component of the building. A non-linear computer model is used for pushover analysis.

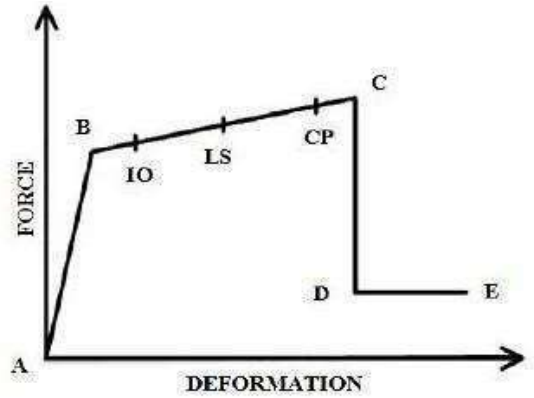

Fig. 8 General Pushover Curve

The load-deformation curve of the base shear force v/s the horizontal roof displacement of the building, also known as the capacity curve or pushover curve, illustrates the nonlinear behaviour of the structure. Pushover curve allows for the determination of the structure's performance point at various stages.

Model of Berthing structure:

Figure shows the model of berthing structure.

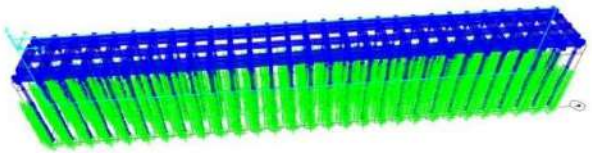

Fig. 9 SAP model in 3d view

Analysis of the structure (SAP2000)

Berth structure is analysed using SAP2000 software by conducting pushover analysis. In the first step gravity load analysis is done.

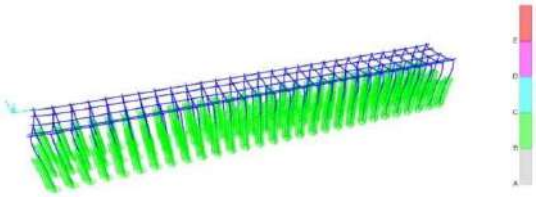

Fig. 10 Dead load Deformation

Formation of Hinge (Pushover Analysis 1)

Seismic load of 27 kN is applied on the structure and number of steps is increased. On reaching 27th step, a hinge which is in Life Safety (LS) zone is formed**.** On increasing number of steps, number of hinges also increases. From 28th step onwards the hinge which is in the Collapse prevention zone (CP) startsforming. Tuning of elements are done which are on the CP zone. Pushover curve is also obtained from the analysis.

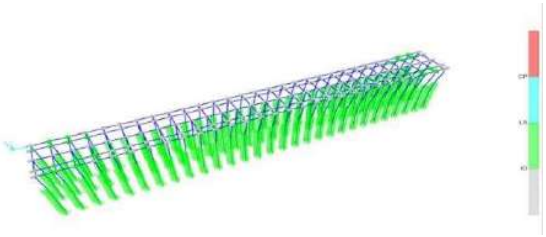

Fig.11 Hinge formation at column

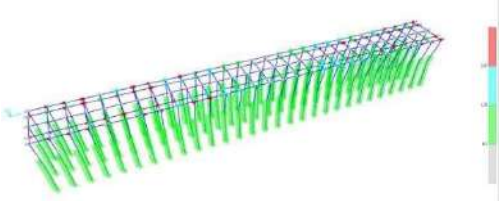

Fig. 12 Hinge formation of beams 27th step

From 27th step onwards hinges which are beyond acceptable limit, starts forming. Number of hinges within acceptable limit decreased and number of hinges beyond acceptable limit increased.

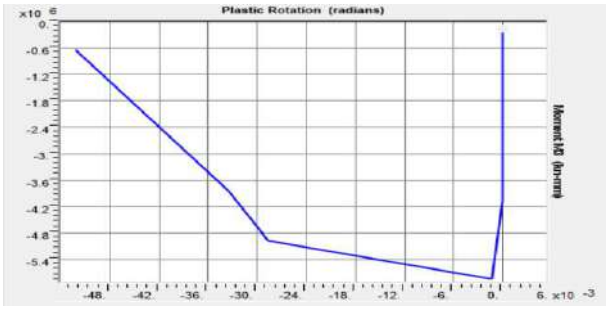

Fig. 13 Pushover Curve of beams at 28th step

Tuning of beams is done by increasing dimensions of beams which are in IO-LS, LS-CP, CP-C, C-D, D-E and >E zones.

Pushover Analysis 2

st

1 stage of tuning is done by increasing the dimensions of beams 110, 112 and 129 and column 113.

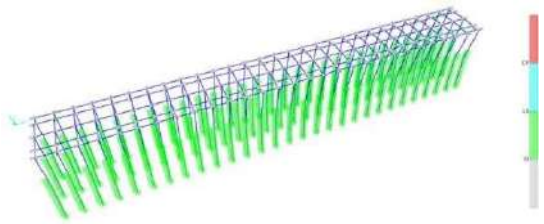

Fig. 14 Hinge formation at column 113

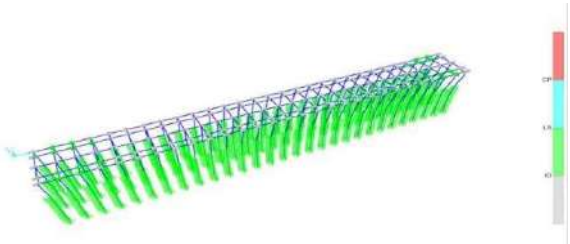

Fig. 15 Hinge formation of beams at 25th step

From 25th step onwards hinges which are beyond acceptable limit, starts forming.On 27th step the hinges which are beyond the acceptable limit is of greater number.

Pushover Analysis 3

Second stage of tuning is done by increasing the dimensions of beams and columns

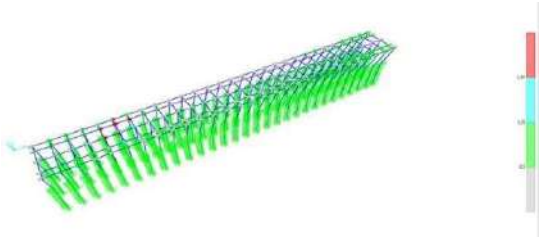

Fig. 16 Second stage tuning of column 113

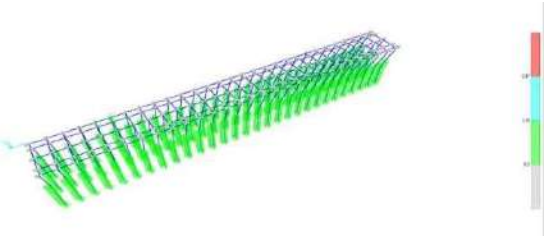

Fig. 17 Hinge formation of beams -10th step

From 10th step onwards hinges which are beyond acceptable limit, starts forming. On 20th step the hinges which are beyond the acceptable limit is of greater number.

Pushover Analysis 4

From 13th step onwards hinges which are beyond the acceptable limit, starts forming.

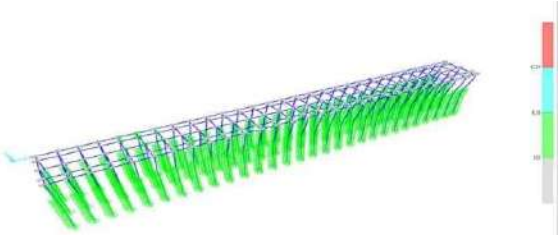

Fig. 18 Hinge formation of beams at 13th step

Pushover Analysis 5

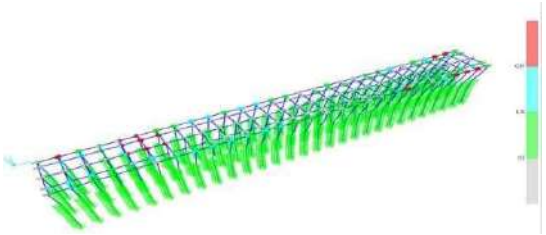

Fig. 19 Hinge formation of beams at 17th step

From 16th step onwards hinges which are beyond acceptable limit, starts forming. On 17th step the hinges which are beyond the acceptable limit is of greater number.

Conclusion:

Pushover analysis is a non-linear analysis technique used to calculate a structure's strength capacity from its ultimate strength in the post-elastic region up to its strength capacity beyond its elastic limit. It might be useful to show how progressive failure in structures actually happens and to pinpointthe final failure mode. By tracking the order of damages to each and every member of the structure, this system can also identify possible weak points in the structure.

1. Design of certain beams and columns of the berthing structure done using IS code is not adequate for withstanding seismic load and henceit requires tuning
2. Since transverse beams fall within the acceptable limit i.e. A-B and B-IO range, there is no need for tuning

References:

1. **Auyeung, A., Alice, S Dikshant** (2019) Performance based design of bridge piers under vehicle collision, *Engineering Structures,* 191, 752-765
2. **Carbonari, A Giulia** (2019) A performance-based approach for the design of coupled dolphin fender berthing structures, *Marine Structures,* 64, 78-91
3. **Guo, W Jun, Z Jianfeng** (2021) Berth Allocation problem with uncertain vessel handling times considering weather conditions, *Computers and Industrial Engineering*,158, 107417
4. **Ghasemof, M Masoud, M Reza (**2022) Multi objective optimization for probabilistic performance-based design of buildings using FEMA P-58 methodology, *Engineering Structures,*Volume 254, 113856
5. **Ghasemof, M Masoud, M Reza** (2022) Effect of demand parameters in the performance based multi-objectiveoptimum design of steel moment frame buildings, *Soil Dynamics and Earthquake Engineering,* Volume 153, 107075
6. **Jalilkhani, G Seyed, D Masood** (2020) Multimode adaptive pushover analysis procedure for estimating the seismic demands of RC moment resisting frames, *Engineering Structures*, 213, 110528
7. **Jiang, N Hesham** (2021) Improved pushover method for seismic analysis of shallow buried underground rectangularframe structure, *Soil Dynamics an Earthquake Engineering*, 140, 106363
8. **Kumar, S A Sannasiraj, M Kantharaj** (2021) Effect of climate change in the deterioration of a berthing structure in a tropical environment, *Journal of the Institution of Engineers Series A*, June 2021, 697-703
9. **Liu, L Tieshan, S Qihe** (2021) Virtual guide automatic berthing control of marine ships based on heuristic dynamic programming iteration method, *Neurocomputing*, 437, 289-299
10. **Maria, G Nicola, C Giovanni** (2021)Two step automated procedure based on adaptive limit and pushover analysis for the seismic assessment of masonry structures, *Computers & Structures*, 252,106561
11. **Ortiz, C Norberto** (2020) A decisionsupport system for a capacity management problem at a container terminal, *International Journal of Production Economics,*222, 107502

DAMAGE IDENTIFICATION BASED ON CHANGE IN STIFFNESS USING PARTICLE SWARM OPTIMIZATION

Deepthy Susan Mathew[1], Er. Sneha M. Varghese[2]

[1] *UG Student, Department of Civil Engineering, Saintgits College of Engineering*

[2]*Assistant Professor, Department of Civil Engineering, Saintgits College of Engineering*

Abstract: *Micro-damages may occur during the service life of a structure. It is difficult for direct visual identification. These micro-damages will accumulate and lead to failure of the structure. Hence damage identification is of great significance. In this study location and severity of crack is identified. Wavelet transform is used to find the location and particle swarm optimization is used to find the severity of a crack. Damage in the beam is initiated by using a transfixion crack and the method of element stiffness reduction is used to simulate damage severity. ANSYS workbench and MATLAB are the softwares employed in order to obtain the results. Damage identification method is done on a fixed and a cantilever beam andthe results are compared. To know whether this method is applicable when crack location is changed, a fixed beam is analysed with a different crack location.*

Keywords*: Crack, Damage Identification, Location of Crack, Severity of Crack*

Introduction:

During the service life of a structure, micro-damages may occur, which aredifficult for direct visual identification. These micro-damages will accumulate andeventually lead to structure failure or collapse. Structural damage identification can evaluate whether the working state of a structure is safe and also provide a technical basis for structural reinforcement measures. Therefore, the structural damage identification and life prediction are of great significance and importance. The basic theory of damage identification is based on the vibration response which states that the damage causes changes in physical properties, such as stiffness, damping, and mass. Also, damage affects the modal characteristics, i.e., modal damping, mode shape, and natural frequency. Therefore, damage can be identified by analyzing changes in the structural vibration characteristics. The uniform crack is defined as having a height that does not change along the thickness direction of the beam, and the non- uniform crack is defined as having a height that changes along the thickness dimension of the beam. The uniform crack in beam structures is a crack with equal height transfixion along the thickness direction,and the non-uniform crack in beam structures is semielliptical crack along the thickness direction. In this project transfixion crack, which is a uniform crackis used to represent the damage in beams. A technique based on wavelet transform combined with the particle swarm optimization algorithm is used for finding the damage location and severity in the structure. The structural strain mode iscalculated by using the structural modaldata in ANSYS, and

the waveletcoefficient diagram is obtained by wavelettransform of the strain mode in MATLAB. The structural damage location can bedetermined from the wavelet co-efficient diagram. Then MATLAB is employed torun PSO to obtain the damage severity ofthe structure.

Literature Review:

Lonkar *et al.* (2011), proposed that there is significant change in vibration responses of cracked structures when the crack depth is significant in comparison to the depth ofthe structure. This fact enables the identification of cracks in structure fromtheir vibration response data. However, when crack is relatively small, it is difficultto identify the presence of crack by only observation of vibration response data. A crack in beam reduces its dynamic stiffness. Consequently, its characteristics, such as natural frequencies and mode shape would change. Such changes depend on crack size and location. In this paper, the wavelet transform is applied to detect localized damage based on simulated dynamic response data from finite element analysis. Free vibration finite element analysis of a cracked cantilever beam is performed. The MATLAB code is generated to introduce crack at location and in specified size. The modal responses of cracked beam were obtained and analyzed using

Wavelet transform and curvature mode shapes.The wavelet transform detected the location of single as well as multiple cracks introduced by code. The algorithm was proposed to determine crack size using wavelet coefficientsand damage curvature plots. Vosoughi (2014), presented a developed hybrid method for crack identification of beams. Based on the Euler-Bernouli beam theory and concepts of fracture mechanics, governing equation of the cracked beams was reformulated. Finite element (FE) method was used to discretise the equation in space domain. After transferring the equations from time domain to frequency domain, frequencies and mode shapes of the beam were obtained. Efficiency of the governed equation for free vibration analysis of the beams was shown by comparing the results with those available in literature and via ANSYS software. The used equation yields to move the influence of cracks from the stiffness matrix to the mass matrix. For crack identification measured data were produced by applying random error to the calculated frequencies and mode shapes. An objective function was prepared as root mean square error between measured and calculated data. To minimizethe function, hybrid genetic algorithms (GAs) and particle swarm optimization (PSO) technique were introduced. Zhang *et al.* (2015), presented a comprehensive investigation of Particle Swarm Optimisation. Advances with PSO, including its modifications (including quantum-behaved PSO, bare-bones PSO, chaotic PSO, and fuzzy PSO), population topology (as fully connected, von Neumann, ring, star, random, etc.), hybridization (with genetic algorithm, simulated annealing, Tabu search, artificialimmune system, ant colony algorithm, artificial bee colony, differential evolution, harmonic search, and biogeography-based optimization), extensions (to multi-objective, constrained, discrete, and binary optimization), theoretical analysis (parameter selection and tuning, and convergence analysis), and parallel implementation (in multicore, multiprocessor, GPU, and cloud computingforms) were discussed. A survey on applications of PSO to the eight fields suchas, electrical and electronic engineering, automation control systems, communication theory, operations research, mechanical engineering, fuel and energy, medicine, chemistry, and biology were also presented. Chatterjee *et al.* (2016), proposed a particle swarm optimization-based approach to train the neural network (NN). The PSO is employed to find a weight vector with minimum root-mean-square error (RMSE) for the NN. The proposed(NN-PSO) classifier is capable to tackle the problem of predicting structural failure of multistoried reinforced concrete buildings by detecting the failure possibility of the multistoried RC building structure in the future. A database of 150 multistoried buildings RC structures was employed in the experimental results. The PSO algorithm was involved to select the optimal weights for the NN classifier. Fifteen features

have been extracted from the structural design, while ninefeatures have been opted to perform the classification process. The NN-PSO performance was evaluated by different standard performance measure metrics. The experimental results established the dominanceof the proposed model for detecting the structural status of a multistoried RC building structure. Patel *et al.* (2016), discussed about the feasibility of using output-only model-free wavelet-based techniques for damage identification of a six storied scaled reinforced concrete (RC) building. The vibration signals at different floor levels of the RC building were acquired using wireless accelerometers. The vibration measurements were carried out for different cases i.e., bare frame and varying mass at different floors. The signal discontinuity of the acceleration response ofRC building was extracted using complex continuous Gaussian wavelet transformation and it was analysed. The proposed methodology was easy and simple to use. Changes in the behaviour of wavelet transform coefficients at different scales (corresponding to different frequency) were observed and used to locate the level at which mass was added. The results showed that the wavelet transform based approach is capable of identifying the location of change of building's physical properties with increased accuracy. Alam (2016), discussed about the algorithm for classical particle swarm optimization (PSO). Also, its codes in MATLAB environment were presented. The effectiveness of the algorithm was analysedwith the help of an example of three variable optimization problem. The convergence characteristic of the algorithmwas discussed. The algorithm is guided by personal experience (Pbest), overallexperience (Gbest) and the present movement of the particles to decide their next positions in the search space. The codes discussed were generalized for solving any optimization problem with inequality constraints of any size. Khatir *et al.* (2017), presented a technique for the detection and localization of an open crack in beam-like structures using experimentally measured natural frequencies and the particle swarm optimization (PSO) method. For this technique variation in local flexibility near the crack was considered. The natural frequencies of a cracked beam were determined experimentally and numerically using the finite element method. The MATLAB algorithm was used to estimate the location and severity of a crack by minimizing the differences between measured and calculated frequencies. The change in the natural frequencies of the structure due to the presence of a crack was used as an objective function. A numerical study using simulated data of a cantilever beam and a 2-D frame structure were presented. Furthermore, this approach was validated using vibration experiments on a free–free laboratory beam.Fu *et al.* (2018), proposed a method for the stiffness estimation of cracked beams based on the stress distributions. The presence of crack causes non-linear stress distributions along the sections of a beam, which

change the neutral axis of the sections and further affect the stiffness of the beam. Regions of the beam where stresses are affected by the crack were first analysed, and according to the distance to the crack different non-linear stress distributions were modelled for those regions. The inertia moments of section were evaluated by substituting these stress distributions into the internal force equilibrium of the section. The finite element technique was adopted to estimate the stiffness of the cracked beam. The estimated stiffness was used to predict the displacements of simply supported beams with a crack The results showed that both static and vibrational displacements were accurately predicted. Nadjafi *et al.* (2019), proposed a method for damage identification based on modal flexibility curvature (MFC) and particle swarm optimization (PSO) algorithm. Modal flexibility curvature was calculated using central difference approximation, based on entries of the modal flexibility matrix. Two beam-like structures under different damage scenariosare studied. The aim of the study was to develop an effective vibration-based method for damage localization and quantification in beam-like structures by means of the modal data. The change in stiffness can be simulated by decreasingone of the parameters that havecontribution in the stiffness of the beam- like elements, such as the modulus of elasticity (E), cross sectional area (A), moment of inertia (I), etc. Guo *et al.* (2020), proposed a method to identify damage based on the wavelet transform and improved particle swarm optimization (WIPSO) algorithm. First, the singularity of wavelet coefficients is used to identify the structural damage location, and then,the improved particle swarm optimization (IPSO) algorithm is used to calculate the damage severity. The ability of wavelet coefficients to identify the location of the structural damage under different noise levels is studied. To evaluate the performance of IPSO, the standard particle swarm optimization algorithm, the genetic algorithm (GA), and the bat algorithm (BA) are also considered. The results show that WIPSO can effectively and accurately identify the structural damage location and severity. To verify the effectiveness of the proposed method, an experiment wasconducted on a beam with fixed support. This also showed that this method can be used for damage identification. Guo *et al.* (2021),studied about the non-uniform microcrack identification in beams. In this study, the non- uniform crack is modelled as a semi-elliptical crack. Damage location and damage severityof the structure is identified using wavelet transform and intelligent algorithms in MATLAB. The intelligent algorithms used for the identification of damage severity are particle swarm optimization (PSO) and genetic algorithm (GA). The results show that the wavelet-particle swarm optimization (WPSO) and the wavelet-genetic algorithm (WGA) can accurately and efficiently identify thestructural semi-elliptical damage location and severity. To study the effectiveness of the method, an experimental

investigation was carried out on a fixed beam.

Objectives:

Damage mitigation is one of major concernsthese days. This can be achieved by early damage identification. The objectives of the work include

1. To find the location and severity of acrack
2. Compare the results of fixed andcantilever beam
3. Analyze the beam with a different crack location

Methodology:

The model of the beam with damage is modelled in ANSYS Workbench. Modal analysis is done on the beam to obtain the displacement modes. Then wavelet toolbox in MATLAB is used to get the wavelet co-efficient graph which gives the damage location. Then Particle Swarm Optimization (PSO) algorithm is employed which gives the damage severity. The methodology of the workis as follows.

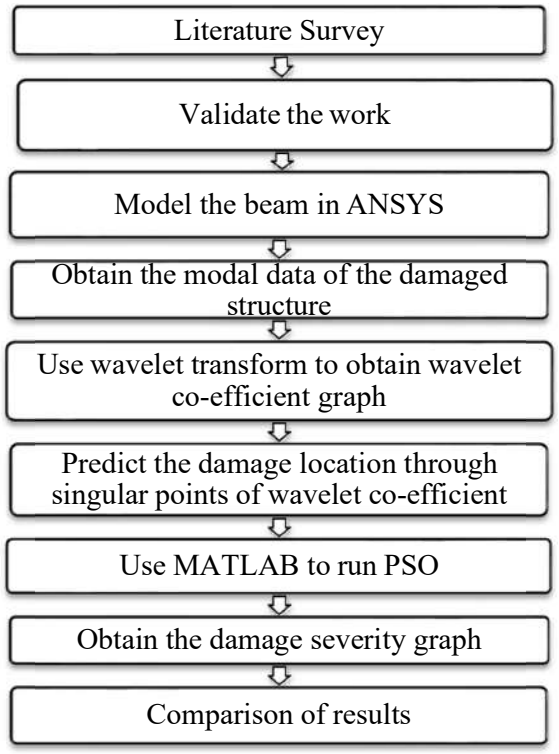

Analysis on a Different End Conditionand Crack Location

Analysis on Cantilever Beam

To know whether this method of damage identification is applicable to beams withdifferent end conditions a cantilever beam was analysed. The damage location was at 4^{th}, 25^{th} and 38^{th} element and damage severities were 4%, 10% and 20% respectively. The damage form in the cantilever beam was set as atransfixion crack along the thickness direction. The section size of the beam was b × h = 60 ×80 mm and the material parameters of the beam are shown in Table 1.

Table 1 Model details of cantilever beam

PROPERTY	VALUE
Support Conditio n	Both ends fixed
Span	1118 mm
Breadth	60 mm
Height	80 mm
Density	7800 kg/m^3
Poisson's ratio	0.3
E	$2.1 \times 10^{11}\ N/m^2$
Number of elements	43

The finite element model of the cantilever beamis divided into 43 elements with an element size of 26 mm. The damaged elements and damage severity of the cantilever beam are shown inTable 2. The model of the damaged beam in ANSYS is shown in Fig 1.

Table 2 Damage Depth and Severity ofCantilever Beam

Damaged element	Severity (%)	Damage depth (mm)
12	4	1.1
25	20	5.7
38	10	2.8

Modal analysis was done to obtain the displacement modes. The displacement modes of beam obtained from ANSYS is shown in Fig 2(a) to Fig 2(f).

MATLAB was employed to take the second derivative of the structural displacement mode to obtain the strain mode. Then, the wavelettoolbox in MATLAB is used to select the DB wavelet to transform the strain modal data, and the wavelet coefficient graph was obtained. PSO algorithm was used to obtain the severityof the damage

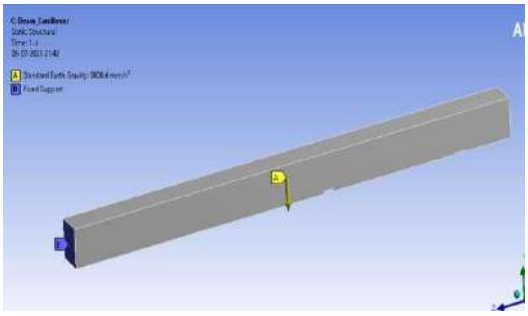

Fig 1 Model of cantilever beam in ANSYS

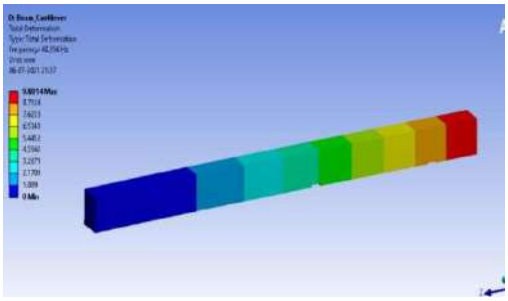

Fig 2(a) Total Deformation 1 of Cantilever Beam

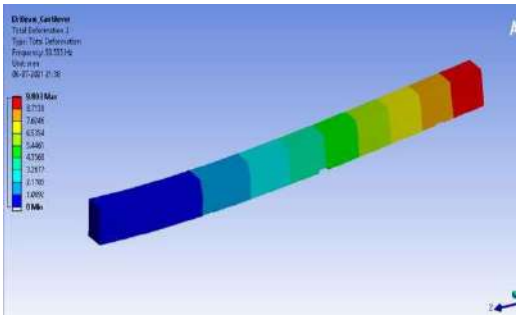

Fig 2(b) Total Deformation 2 of Cantilever Beam

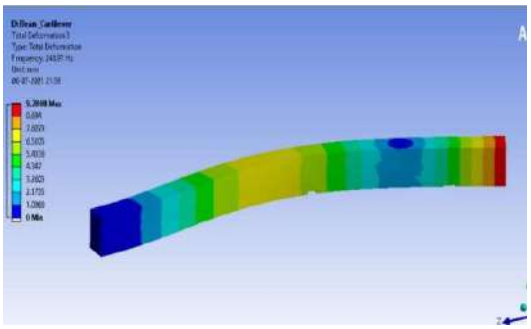

Fig 2(c) Total Deformation 3 of Cantilever Beam

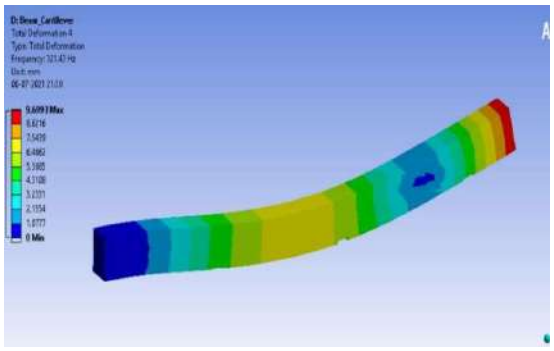

Fig 2(d) Total deformation 4 of a Cantilever Beam

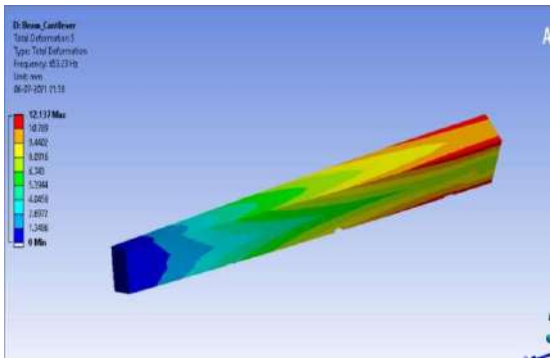

Fig 2(e) Total Deformation 5 of CantileverBeam

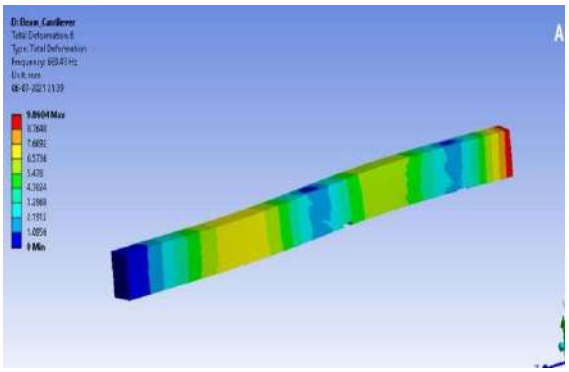

Fig 2(f) Total Deformation 6 of Cantilever Beam

.

Results and Discussion of Cantilever Beam

Fig 3 shows the wavelet co-efficient graph obtained from MATLAB using the wavelet toolbox.

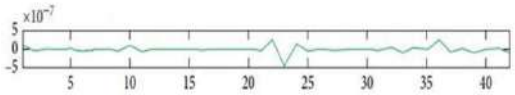

Fig 3 Wavelet Co-efficient Graph of Cantilever Beam

The graph shows peaks at the points 10, 23 and 36. It is because the strain mode data calculated by the second-order derivation of the displacement mode with MATLAB will be reduced by two. Therefore, points 10, 23, and 36 in the wavelet coefficient diagram actually correspond to elements 12, 25, and 38 in the fixed beam structure model. There will be mutations around the damage location that are affected by the damage, butthe maximum value point of the modulus corresponds to the damage location. Therefore, the damage in the fixed beam occurs in elements 12, 25, and 38, which is consistent with the damage element setting of the finite element model of the cantilever beam.

The damage severity graph obtained afterusing

the PSO algorithm is shown in Fig 1. The severity graph shows damage severities of 4%, 10% and 20%, which was the given damage itself.

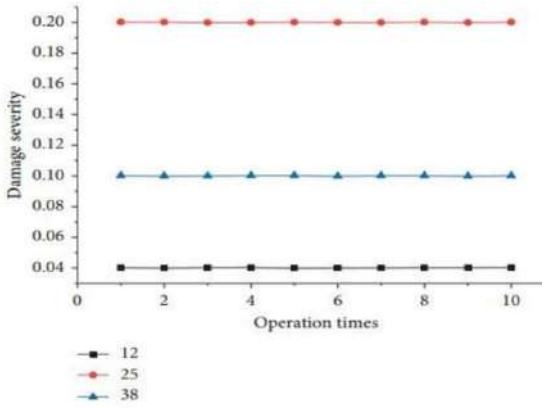

Fig 4 Damage Severity Graph of CantileverBeam

Analysis on Fixed Beam with Different Crack Location

To know whether this method is applicable to beams having a different crack location a fixed beam was analyzed with a different damage location. The damage was given at a distanceof L/3 m from both ends. Elements 14 and 29 were given a damage severity of 10% and 20%. The damage form was set as a transfixion crack along the thickness direction. The section size of the beam was b × h = 60 × 80 mm and the material parameters of the beam are shown in Table 3.

The finite element model of the fixed beam is divided into 43 elements with an element size of 26 mm. The damaged elements and damage severity of the fixed beam are shown in Table 4. The model of the damaged beam in ANSYS is shown in Fig 3.

Table 3 Model Details of Fixed Beam withCrack at L/3 Distance

PROPERTY	VALUE
Support Condition	Both ends fixed
Span	1118 mm
Breadth	60 mm
Height	80 mm
Density	7800 kg/m^3
Poisson's ratio	0.3
E	2.1×10^{11} N/m^2
Number of elements	43

Table 4 Damage severity and Depth of Fixed Beam with Crack at L/3 Distance

Damaged Element	Severity (%)	Damage Depth (mm)
14	10	2.8
29	20	5.7

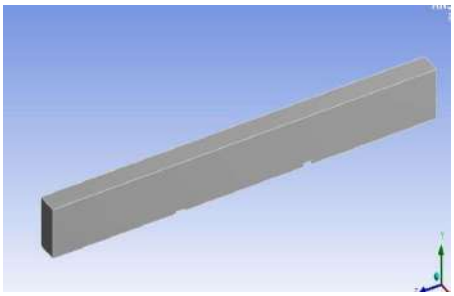

Fig 3 Model of Fixed Beam with Crack atL/3 Distance in ANSYS

Modal analysis was done on the beam to obtain the displacement modes. The displacement modes of beam obtained from ANSYS is shown in Fig 3(a) to Fig 3(f).

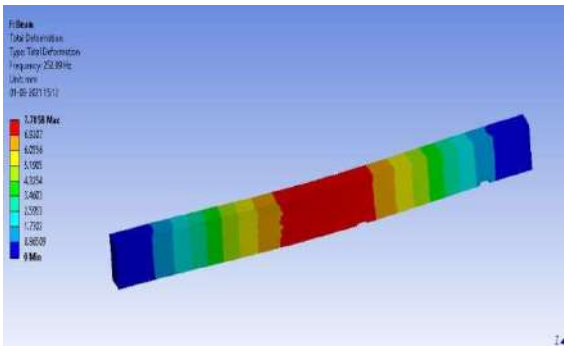

Fig 3(a) Total Deformation 1 of Fixed Beamwith Crack at L/3 Distance

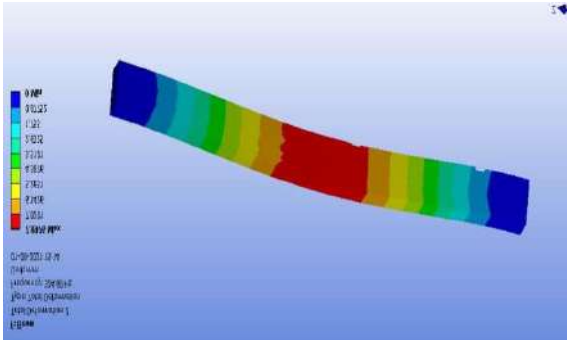

Fig 3(b) Total Deformation 2 of Fixed Beamwith Crack at L/3 Distance

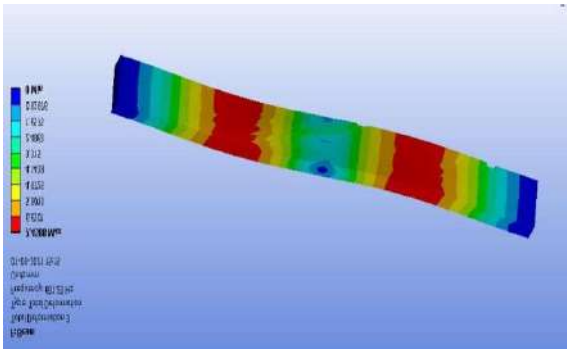

Fig 3(c) Total Deformation 3 of Fixed Beamwith Crack at L/3 Distance

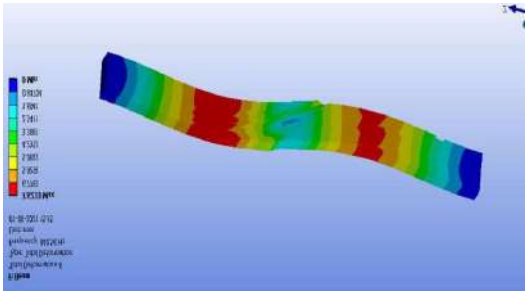

Fig 3(d) Total Deformation 4 of Fixed Beamwith Crack at L/3 Distance

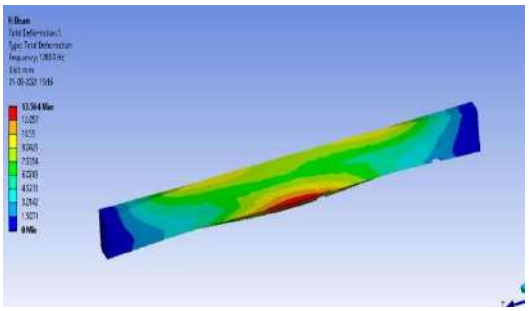

Fig 3(e) Total Deformation 5 of Fixed Beamwith Crack at L/3 Distance

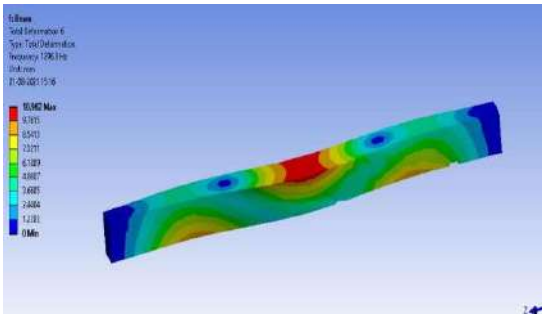

Fig 3(f) Total Deformation 6 of Fixed Beamwith Crack at L/3 Distance

MATLAB was employed to take the second derivative of the structural displacement mode to obtain the strain mode. Then, the wavelet toolbox in MATLAB is used to select the DB wavelet to transform the strainmodal data, and the wavelet coefficient graph was obtained. PSO algorithm was used to obtain the severity of the damage.

Results and Discussion of Beam withCrack at L/3 Distance

Fig 4 shows the wavelet co-efficient graph obtained from MATLAB after employing the wavelet toolbox.

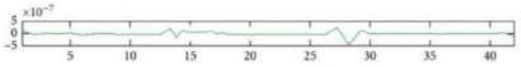

Fig 4 Wavelet Co-efficient Graph of Fixed Beam with Crack at L/3 Distance

The graph shows peaks at the points 12 and 27. It is because the strain mode data calculated by the second-order derivation of the displacement mode with MATLAB will be reduced by two. Therefore, points 12 and 27 in the wavelet coefficient diagram actually correspond to elements 14 and 29 in the fixed beam structure model. There will be mutations around the damage location that are affected by the damage, but the maximum value point of the modulus corresponds to the damage location. Therefore, the damage in the fixed beam occurs in elements 14 and 29, which is consistent with the damage element setting of the finite elementmodel of the fixed beam. Fig 5 represents the damage severity graph after employing PSO.

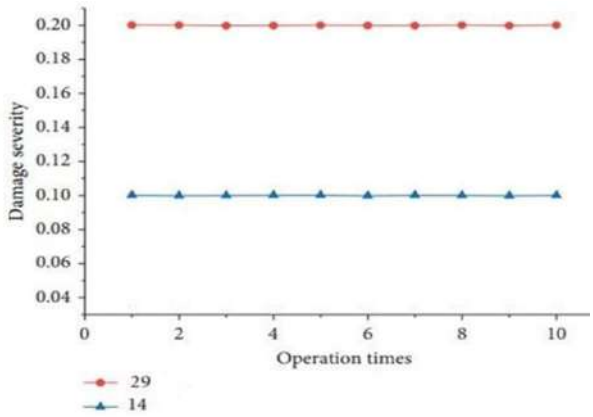

Fig 5 Damage Severity Graph of Fixed Beam with Crack at L/3 Distance

Damage severity graphs shows 10% and 20% severities which were the severities of the given crack.

Comparisons of Results of Beams with Different End Condition and Crack Location

By comparing the results obtained, it is clear that the damage location and severity are same for fixed and cantilever beams. The damage location was at points 12, 25 and 38. The damage severity was 4%, 10% and 20%.The damage location and severity obtained are exactly which was provided. This means this method of damage identification can be applied to beams with different endconditions.

The result obtained for the fixed beam with crack at L/3 distance from both ends also showed satisfactory results. The damage was given at 14th and 29th element and the damage severities were 10% and 20%. The results also showed the same values. Thegraph shows peaks at the points 12 and 27. It is because the strain mode data calculated by the second-order derivation of the displacement mode with MATLAB will be reduced by two. Therefore, points 12 and 27 in the wavelet

coefficient diagram actually correspond to elements 14 and 29 in the fixed beam structure model. There will be mutations around the damage location that are affected by the damage, but the maximum value point of the modulus corresponds to the damage location. Therefore, the damage in the fixed beamoccurs in elements 14 and 29, which is consistent with the damage element setting of the finite element model of the fixed beam. Hence this method is also applicable when damage location is changed.

Conclusions:

A combination of wavelet transform method and particle swarm optimization algorithm was used for damage identification. Location of damage was found using wavelet co-efficientgraph and severity was found using PSO. To know whether the method proposed was applicable to beams with different end conditions, a fixed and a cantilever beam was compared which were having the same location and severity. To check whether this method holds good for beams with different crack location a fixed beam was analyzed which had the cracks at a distance of L/3 distance from both ends.

The following conclusions were made after analyzing the results.

- The damage location and severity obtained for both fixed and cantileverbeams were same, which shows that the proposed method was effective in analyzing beams with different end conditions.
- The results obtained after analyzing the fixed beam with crack at L/3 distance from both ends showed accurate values. Hence the proposed method is applicable even when crack location is changed.
- Wavelet transform and particle swarm optimization algorithm are effective in damage identification.

References:

1. **Guo, J., D. Guan and Y. Pan (2021),** "*Research on Damage Identification of Nonuniform Microcrack in Beam Structures*", Hindawi-Advances in Civil Engineering
2. **Guo, J., D. Guan, and J. Zhao (2020),** ***"Structural Damage Identification Based on the Wavelet Transform and Improved Particle Swarm Optimization Algorithm"***, Hindawi-Advances in Civil Engineering
3. **Nadjafi, S., G. Amiri, A. Z. Hosseinzadeh and S. Razzaghi (2019),** "*An Effective Approach for Damage Identification in Beam-Like Structures Based on Modal Flexibility Curvature and ParticleSwarm Optimization",* Journal of Rehabilitation in Civil Engineering
4. **C., Y. Wang and D. Tong (2018),** "*Stiffness Estimation of Cracked Beams Based on Nonlinear Stress Distributions Near the Crack*", Hindawi – Mathematical Problems in Engineering
5. **Khatir, S., K. Dekemele, M. Loccufier, T. Khatir and M. A.Wahab (2017),** "*Crack identification method in beam-like structures using changes in experimentally measured frequencies and Particle Swarm Optimization*", Comptes RendusMecanique
6. **Chatterjee, S., S. Sarkar, S. Hore, N. Dey, A. S. Ashour and V. E. Balas (2016),**

"*Particle swarm optimization trained neural network for structural failure prediction of multistoried RC buildings*", Neural Computing and Applications

7. **Patela, S., A. P. Chourasiaa, S. K. Panigrahia, J. Parashar, N. Parvezb and M. Kumar (2016),** "*Damage Identification of RC Structures using Wavelet Transformation*", Procedia Engineering
8. **Zhang, Y., S. Wang and G. Ji (2015),** "*A Comprehensive Survey on Particle Swarm Optimization Algorithm and Its Applications*", Hindawi - Mathematical Problems in Engineering
9. **Vosoughi, A. (2014),** "*A developed hybrid method for crack identification of beams*", Smart Structures and Systems
10. **Lonkar, A., Srivastava R. K (2011),** **"***Crack Detection in Structure Using Wavelet Transform and Higher Order Differentiated Mode Shapes"*, International Journal of Mechanical Engineering

REJUVENATION OF RAP BINDERS USING WASTE OIL

Aiswarya K H[1], Aswathi G Nair[1], Fathima Abdur Rahman[1], Hrudya V[1], Er. Jithin Kurian Andrews[2]

[1] *UG Student, Department of Civil Engineering, Saintgits College of Engineering*

[2]*Associate Professor, Department of Civil Engineering, Saintgits College of Engineering*

Abstract: *The shortage and the subsequent increase in the cost of virgin aggregates necessitatethe use of Reclaimed Asphalt Pavement (RAP) in pavement construction. One among the manychallenges in using RAP in large proportions is the greater stiffness of the mix, which occurs due to the aging of bitumen. Since RAP is an aged material, rejuvenators can be used in order to enhance the properties. A commonly used rejuvenator is an asphalt emulsion that is not mucheconomical. This study evaluates the viability of partially replacing asphalt emulsions with waste cooking oil. The selection of the optimum amount of waste oil, as a rejuvenator can leadto efficient use of resources and help towards more sustainable construction. The optimum amount of waste oil to be used was determined based on the cohesive strength and rutting potential of the RAP modified waste oil rejuvenated base layers by performing the Indirect Tensile Strength (ITS) Test and wheel tracker test. The results indicate that the adding more than 1% of Waste Cooking Oil is not recommended since it decreases the cohesive strength andincreases the rut depth much more than desired. Thus, the possibility of replacing asphalt emulsion partially with waste cooking oil tends to be possible only in small traces satisfying thestrength and durability.*

Keywords*: Rejuvenators, Asphalt emulsions, Waste cooking oil, Indirect Tensile Strength, Rutdepth*

Introduction:

The recent series of landslide disasters in Kerala has been widely attributed to the unscientific excavations in numerous illegal quarries, which have changed the landscape and made the hills on which they are located unstable. The subsequent intervention by the Kerala High Court in shutting down many of these quarries made headlines for days. This caused a shortage of Virgin Aggregates (VA), whose main source is quarries. Herein lies the relevance of using recycled materials for road construction. Recycled Asphalt Pavement (RAP) refers to the removed or reprocessed pavement materials containing asphalt and aggregates. RAP is extracted by an Asphalt Pavement Milling Machine. RAP can be provided as the base material in road construction as a sustainable solution. Using 100% RAP for road construction is not feasible as it has a high potential for creep and permanent deformation. RAP can be blended with VA, stabilized by cement and flay ash confined by geocell, etc. 50-60% RAP is the optimum amount since using above 60% reduces the overall strength, but less than50% will not provide an economic advantage. Oxidation in RAP, which causes the ageing of bitumen, leads to increasing brittleness and stiffness, making roads prone to cracking. Asphalt rejuvenation is the process of restoring the chemical properties that have been deteriorating since the laying of asphalt. To rejuvenate aged bitumen, asphalt emulsion is used, which improves the tensile strength and resistance to a water attack. But asphalt emulsion is no longer cost-effective, due to it being a petroleum product. Replacing it with other materials also helps minimize reliance on non-renewable resources.

Among the various organic-based rejuvenators, waste oil is commonly proposed. Waste oil contains light oil components analogous to those of virgin bitumen and it has been proposed as a sustainable product for improving the recycling of aged asphalt (Zahoor et al., 2021). This study aims to determine the optimum amount of Waste Cooking Oil (WCO) to be used in rejuvenating RAP, which is ascertained based on parameters of strength and rutting potential.

Due to increased environmental awareness and limited resources, researchers are seeking new methods and technologies to ensure sustainability, efficiency and less emission of greenhouse gases in the asphalt industry. In recent years, reutilization of materials has been on the forefront of new technologies. RAP, which is aged pavement is reclaimed to be used over. It can relieve the manic use of natural resources and as a matter of course cause less damage to our environment. The use of RAP could reduce energy consumption, mineral usage, relevant pollution, and

costs.

Since RAP is an aged material, it cannot be directly added without enhancing its properties. The most important characteristic of aged bitumen is the lack of oily components. Rejuvenator enhances the moisture content and cracking resistance in RAP. The most common rejuvenator is asphalt emulsion. But its increasing cost and the need to switch to eco-friendlier materials bring in the need of replacing asphalt emulsion with organic rejuvenators. Even though WCO is commonly proposed, its efficiency as a rejuvenator is highly debated. The study proposes to investigate the performance of WCO as rejuvenator and if it is capable of fully replacing asphalt emulsion. If not, the optimum amount of WCO to partially replace asphalt emulsion is to be determined.

The project emphasizes to study the effects of Waste Cooking Oil (WCO) as partial replacement for asphalt emulsion as rejuvenator for Reclaimed Asphalt Pavement (RAP) based on cohesive strength and rutting potential. Indirect Tensile Strength (ITS) Test was done to evaluate the cohesive strength and Wheel Tracker Test was done to evaluate the rutting potential of the samples. 50% RAP and 50% Virgin Aggregates (VA) are used for the samples to be tested. The emulsion content for standard modified base layers is fixed at 3% and the oil content as replacement for emulsion is varied at 1%, 2% and 3%.

Literature Review:

Dokandari *et al.* (2017) revealed that on addition of rejuvenators as oily additives, the properties of RAP binder could be enhanced. Oil content was varied from 1 to 7%, and found that 5.4% of Waste Engine Oil (WEO) by weight of binder and 5.1% of Waste Vegetable Oil (WVO) by weight of binder have been found adequate based on penetration values. Binder penetration, softening point values and viscosity of binder could be modified by optimum WEO and WVO contents. Rejuvenated RAP mixtures were found to be less brittle and more durable than non-rejuvenated RAP mixtures. Aging indices of rejuvenated mixtures were improved compared to non-rejuvenated mixtures.

Suo *et al.* (2020) evaluated the rheological properties, high temperature and fatigue performance of the recovered bitumen which was rejuvenated with wastecooking corn and soyabean oil as rejuvenators. The oil content was varied from 0 to 10%. Study revealed that 6-8% vegetable oil could be used for rejuvenation. According to the results of penetration test, softening point test and ductility test, the fundamental physical properties of vegetable oil-based recovered asphalt have stronger recovery ability. At the same time, the workability of vegetable oil-based rejuvenator can effectively reduce the recycling

temperature.

Zahoor *et al.* (2020) made a comprehensive review and revealed that addition of waste cooking oil to asphalt binder improves fatigue and thermal cracking properties of mix, but at the expense of rutting resistance. Addition of waste cooking oil in asphalt mixtures reduce the rutting resistance while improving bitumen fatigue and resistance to thermal cracking. This study revealed that the efficiency of rejuvenation process is significantly affected by the acid value of WCO. This paper emphasizes the efficiency enhancement of asphalt binder using WCO as a rejuvenator, also exploring the possibility of utilizing it with RAP.

Kamariya. U *et al.* (2018) studied the relevance of using RAP in the construction of bituminous pavements and also the advantages and disadvantages of different RAP processing methods. RAP is one of the most recycled materials in the world. By using RAP in flexible pavement construction, problem of disposal of RAP wastes can be solved. It also helps in substantial saving of cost and natural resources.

Mahankale. S. S *et al.* (2016) studied the vitality of using RAP for the construction of bituminous pavement. Using RAP is advantageous as RAP mixes can yield results equal or even higher than fresh mixes. Chances of reflective cracking are found to be less with recycled mixes. Using RAP reduces the cost of project marginally as it reduces the use of virgin aggregates and binder from natural nonrenewable resources. Optimal percentage of RAP depends on the composition of reclaimed bituminous material and type of layer in which it is to be used.

Rafiq. W et al. (2020) made a study to evaluate the effect of moisture damage on asphalt pavements. The evaluation was done using Wheel tracker to find out the rutting performance on mixes containing high percentage of RAP. Samples were made by varying the percentage of RAP i.e., 30%, 50% and 100%. The results showed that the asphalt mixes containing RAP has less rut depth as compared to the control mix and hence showed better anti-rutting properties and moisture stability. Studies were also conducted to evaluate the stripping performance of the mixes containing RAP and hence concluded that RAP mixtures were greatly dependent on the interaction between the binder and aggregates.

Past studies revealed that samples made using 100% RAP showed low strengthand a high potential for permanent deformation. The low strength of RAP is due to ageing. Oxidation is the main factor that causes ageing of bitumen leading to an increase in brittleness and stiffness, which makes roads more prone to cracking. Asphalt rejuvenation is the process of restoring the chemical

properties that have been deteriorating since the laying of asphalt. Asphalt emulsion 6 can be used to improve the tensile strength and resistance to water attack by rejuvenating the aged bitumen, but since asphalt emulsion is a petroleum product it is no longer cost-effective. Waste vegetable oil rejuvenators can effectively reduce the viscosity and stiffness of aged bitumen. It can improve both the fatigue resistance and low-temperature crack resistance. Waste oil contains light oil components analogous to those of the virgin bitumen and it has been proposed as a sustainable product for improving recycling of aged asphalt.

Objective:

The objectives of the study are:

1. Evaluation of cohesive strength of RAP modified base layers using ITS test
2. Evaluation of rutting potential of RAP modified base layers using wheel tracker test
3. Optimization of waste cooking oil in the rejuvenation of RAP

This work emphasizes studying the effects of WCO as a rejuvenator in RAP modified base layers based on the parameters of cohesive strength and rutting potential by the means of ITS test and wheel tracker test, respectively.

Methodology:

For the determination of optimum WCO content for the rejuvenation of RAP different tests was carried out to characterize the WCO as well as RAP and to analyse the cohesive strength and the rutting potential. The characterization of was performed using the acid value test. The Residual Bitumen Binder test was performed in order to determine the bitumen content of the RAP mixture. The cohesive strength is the strength of bonding between the particles or surfaces that make up the RAP material. The Indirect Tensile Strength of the RAP was determined using the Indirect Tensile Strength Test. The accumulation of permanent deformation of subgrade is known as rutting. The rut depth of the RAP samples rejuvenated with WCO was evaluated using the wheel tracker test.

As WCO includes many constituents, acid value test is performed to identify its degree of acidity. The acid value is determined by titrating the WCO dissolved in alcoholic medium with alcoholic potassium hydroxide having 0.1 normality. A sample of 2 g WCO is poured into 200 ml conical flask and mixed with 50 ml of isopropyl alcohol, which is an organic dissolvent is used as the solvent. Approximately 4 to 5 drops of phenolphthalein are added to the above mixture as an indicator and is mixed thoroughly. The sample to be titrated and the indicator is shown in Fig. 3.1.

Fig. 3.1 WCO and Phenolphthalein

The mixture is titrated against potassium hydroxide till the color changes from colorless to light pink. The volume ofaqueous potassium hydroxide corresponding to this stage is noted as V. The acid value number indicates the level of rancidity as well as acidity of the WCO used for the test.

The acid value is calculated using theformula,

$Acid\ value = V\ x\ N\ xMW$

where, N is the normality of the potassium hydroxide

M is the molecular weight of potassium hydroxide

W is the weight of WCO

Fig. 3.2 Titration of oil sample against KOH

The acid value is the amount of titrating base, expressed as mg of potassium hydroxide, required to neutralize all the acidic constituents of one gram of the vegetable oil. This is an indication of free fatty acids present in the vegetable oils. As the acid value increases, the content of free fatty acids will also increase. The increase in free fatty acids creates more free radicals in the oil which in turn improves its capability to react with oxygen to form undesirable 9

products like aldehydes and ketones. These products reduce the oxidative stability. Hence the free fatty acids should be as low as possible for a good lubricant. The acid value was evaluated as per ASTM D974**.**

For the purpose of this study, RAP is characterized using Residual Bitumen Binder Test. The test is done using the apparatus Centrifugal Extractor. It is also called as a centrifugal contactor or annual centrifugal contactor, uses the rotation of the rotor inside a centrifuge. It is used for the determination of bitumen percentage in bituminous mixtures. As RAP is a recycled material, it is a heterogenous mix of aggregates of different sizes, cement, emulsion and bitumen. Characterization is done to assess the amount of bitumen binder present in this mix. 500 g of RAP is weighed and placed in a container into

which 700 g of benzene is added. Benzene does not react with the constituents of RAP. It is therefore used for easy extraction of bitumen. The mixture is left undisturbed for a period of 30 to 60 minutes, after which it is placed in Centrifuge Extractor is shown in Fig. 3.3, in which the process is done.

Fig. 3.3 RAP-Benzene mixture placed in Centrifuge Extractor

After extraction, the bitumen is drained and the remaining constituents are left in the apparatus, which is later dried, and weighed. Fig. 3.4 shows the constituents of RAP that got extracted.

Fig. 3.4 Constituents of RAP after extraction

In order to evaluate the cohesive strength of RAP modified base layers, samples are made by varying the WCO content and their ITS value is found. The content of emulsion and WCO in the samples are varied as 2% emulsion – 1% WCO, 1% emulsion – 2% WCO, and 0% emulsion – 3% WCO. The results obtained from these samples are compared against standard samples – 50% RAP – 50% VA (3% emulsion) and 100% VA (3% emulsion). The samples are tested in ITS machine is shown in Fig. 3.5under dry condition. Standard Test Method for ITS of bituminous mixtures was based on ASTM D6931-12.

Fig. 3.5 Indirect Tensile Strength Apparatus

The aggregates are sieved according to the gradation in IRC 37 Annexure 9 (2012) and TG2 (August 2020). A total of 10 samples were prepared for this test – 2 samples of each variety. The Optimum Fluid Content (OFC) for 100% VA samples were fixed at 7% and that for 50% RAP – 50% VA samples are fixed at 6.5%. The amount of VA and RAP required are calculated based on the gradation given in IRC 37 –Annexure 9

(2012) and TG2 (August 2020), as shown in Fig. 3.6.

Table IX-1 Gradation of RAP Mixes

Sieve Size,mm	Per Cent Passing
45	100
37.5	87-100
26.6	77-100
19	66-99
13.2	67-87
4.74	33-50
2.36	25-47
0.60	12-27
0.3	8-21
0.075	2-9

Fig. 3.6 Gradation of Rap mixes as per IRC 37 – Annexure 9

Different steps involved in testing are sieving, mixing, compacting, extracting, oven curing for 72 hours and testing of each sample. Mixing is the process by which components like emulsion, water, aggregates and cement are thoroughly mixed together in a pan before transferring it into the mould. Mixing ensures proper bonding of components of mix. After transferring the mix into a mould, it is compacted by giving 50 blows on each face of the mould. By compaction, air is expelled out and makes the mix compact. After compaction, samples are left undisturbed for air cooling and are extracted from mould with the help on an extractor and transferred to oven. Oven drying removes moisture content from the samples. They are kept in the oven for 3 days at 40oC. Samples were prepared based on MORTH Specification. The different seive sizes used in sample preparation are 20 mm, 13.2 mm, 4.75 mm, 2.36 mm, 600 µm, 300 µm, 75µm and pan. The weight of each aggregate taken are mentioned in Table 3.1.

Table 3.1 Weight of Aggregates for ITS Test **Seive size**

Seive size	Percentage retained	Weight of aggregates in kg
20 mm	17.5	0.21
13.2 mm	5.5	0.066
4.75 mm	35.5	0.426
2.36 mm	5.5	0.066
600 µm	16.5	0.198
300 µm	5	0.06
75 µm	9	0.108
Pan	5.5	0.066
Total weight		1.2

The quantity of emulsion, oil, VA of different sizes, RAP, water and cement are calculated as required and they are mixed – initially, dry mixed and then wet mixed. They are thoroughly mixed in a pan before being transferred to the mould. The ITS mould used is shown in Fig. 3.7 that is cylindrical in shape with a diameter of 105 mm and a height of 70 mm. After transferring the mix to the mould, it is compacted by giving 50 blows on either face using a Marshall Compactor as shown in Fig. 3.8.

Fig. 3.7 ITS Mould

Fig. 3.8 Marshall Compactor

After compacting, the samples are air cooled for a period of 24 hours. After air cooling, the samples are extracted from the mould using an extractor, after which the samples are oven-dried at 40°C for a period of 72 hours. The ITS samples prepared and the extraction of sample using the extractor is shown in the Fig. 3.9 and Fig. 3.10, respectively.

Fig. 3.9 Prepared ITS Samples

Fig. 3.10 ITS Sample Extraction

The ITS samples are then tested in the ITS machine, and the ITS values are determined.

The size of the mould used for wheel tracker test was 300 mm x 150 mm x 100 mm. In order to find the mass of VA, RAP, emulsion, oil, cement and water in wheel tracker test, the density of each mix for different samples of ITS test was determined, for which, during ITS sample preparation, after the compaction using Marshall compactor, the dimensions ofthe sample are measured, and its weight was noted. The density of each sample is calculated by the formula,

$$Density = MassVolume$$

After determining the density of the samples, the mass of materials for each sample for wheel tracker test is calculated, such that the density of a type of sample for both ITS testing and wheel tracker testing is the same. After calculating the mass of VA, RAP, emulsion, oil, cement and water for a sample as shown in the

table.

Table 3.2 Materials for Wheel Tracker Mould

Sample	Mass (kg)	Density (kg)	Aggregates (kg)	Emulsion (kg)	Water (kg)	Cement (kg)	Oil (kg)
50 RAP 3% emulsion	9.6837	2151.95	9.5	0.283	0.3389	0.094	0
50 RAP 2% emulsion 1% oil	9.6833	2214.32	9.4	0.188	0.338	0.0938	0.0938
50 RAP 1% emulsion 2% oil	9.9644	2151.85	9.6	0.0962	0.3488	0.0962	0.19234
50 RAP 3% oil	9.9644	2214.32	9.6	0	0.34875	0.0958	0.287

The required quantities of VA, RAP, emulsion, oil, cement and water for each of the sample is taken and the materials are thoroughly mixed – first by dry mixing and followed by wet mixing. The mixture is placed in the mould and compacted.

Fig. 3.11 Mould containing prepared Wheel Tracker Sample

Hand compaction is done initially, followed by compaction using Compression Testing Machine (CTM). Compaction is intended to reduce air void content, optimize the granular skeleton and increase materials density. This sample is oven dried for a period of 72 hours. Mould containing the sample and the oven dried sample kept in wheel tracker for testing is shown below.

Fig. 3.12 Sample in Wheel Tracker for testing

The wheel tracking test (WTT) is an important tool to define asphalt mixture rutting performance. The wheel tracking device was placed in a chamber to allow maintaining the sample at the different test temperatures required. The test temperature used here is 40 degrees Celsius. Prepared each sample is subjected to 20000 cycles and corresponding rut depth is noted.

Wheel Tracking is used to access the resistance to rutting of emulsified aggregate mixes under different test conditions. After filling the mould, it is compressed using compression testing machine and is leveled. Then various tests like Immersion and Non-Immersion test are carried out. This machine contains two specimens in which one specimen is tested at a time by tracking wheels fitted with

pneumatic tyre under specified conditions of load, speed and temperature.

The development of rut profile is monitored at specified intervals during the test. The test procedures and conditions are controlled and data acquired using Wheel Rut Tester Software running on a host computer via high-speed digital interface with a USB controlled system. Fig 3.13 shows Wheel Rut Tester Software.

Fig. 3.13 Wheel Rut Tester Software Source: Instruction Manual of GEOTRAN Industrial

Results and discussions:

Characterization of WCO: After performing the titration of WCO against KOH, the acid value is calculated using the formula, $Acid\ value = V\ x\ N\ xMW$

Where, N is the normality of the potassium hydroxide

M is the molecular weight of potassium hydroxide

W is the weight of WCO

V is the volume of KOH

Table 4.1 Acid Values of WCO

Trial no.	Acid value (mg KOH)
1.	198
2.	187
3.	185

Average Acid Value = 190 mg KOH

The WCO used was highly rancid. The high acid value makes it unhealthy to be used as a dietary oil. Vegetable oil having acid value less than 0.6 mg KOH/g is considered safe for consumption by FAO/WHO.

Characterization of RAP: By performing Residual Bitumen Binder test the residual bitumen content was obtained by:

Table 4.2 Residual Bitumen Binder Test Result

Description	Weight (g)
RAP before extraction	500
RAP after extraction	476
Residual Bitumen	24

Residual Bitumen Content

$= 500 - 476500$ x 100 = 4.8 %

RAP used in this study is base course material. It is aged and contains residual bitumen content of 4.8% of its weight.

Indirect Tensile Strength Test: Indirect Tensile strength test was performed to evaluate cohesive strength of samples. Dial Gauge readings are calibrated using a multiplication factor of 28.25 for readings less than 88.5. For obtaining the Indirect Tensile Strength value of each sample

value of F is obtained that is substituted in the following equation:

βsz = 2. $Fmax\pi.h.d$ N/mm2

F max = Load (N)

h = depth of ITS Mould in mm

d = diameter of ITS mould in mm

Table 4.3 Values of samples with compaction of 50 blows

ITS SAMPLE	Load (N)	ITS (kPa)
100% VA 3% emulsion	2316.5	207.7
50% RAP 3% emulsion	1977.5	177.3
50% RAP 2% emulsion, 1% oil	960.5	86.1
50% RAP 1% emulsion, 2% oil	649.75	58.25
50% RAP 3% emulsion, 3% oil	141.25	12.66

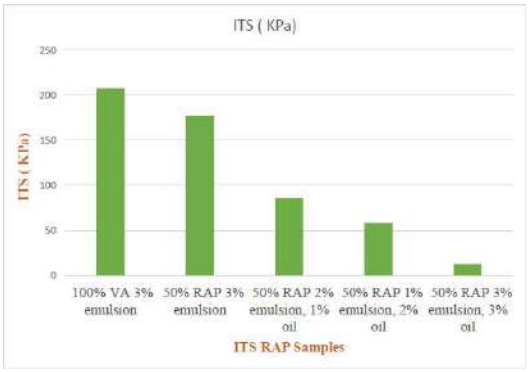

Fig. 4.1 Results of ITS test

From the obtained values it is evident that as the percentage of oil increases ITS strength value decreases for the RAP samples that are rejuvenated with oil. In case of standard RAP sample it has much higher ITS strength value. Highest ITS strength value is obtained for the sample with 100% VA.

Wheel Tracker Test: The rutting potential of the samples were analysed using the wheel tracker test. The obtained values of rut depth of each sample are as follows:

Table 4.4 Values obtained from the wheel tracker

Slab Specimen	Number of Passes	Rut Depth
100% VA 3% emulsion	20000	8.6
50% RAP 3% emulsion	20000	10.34
50% RAP 1% oil 2% emulsion	20000	13.01
50% RAP 2% oil 1% emulsion	4000	20.11
50% RAP 3% oil	2728	20.1

As per researches rut depth between 6 and 10 mm is considered as small level rutting, rut depth between 10 and 15mm is defined as medium level rutting. Maximum allowable rut depth is considered as20mm.

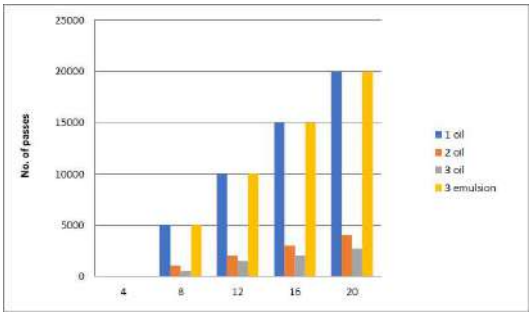

Fig. 4.2 Results of Wheel Tracker test

Therefore, from the values obtained it is clear that standard RAP sample and VA sample having smaller rut depth value is more resistant to rutting whereas the oil samples have comparatively higher rutting potential. RAP sample having 2% emulsion and 1% oil have much lesser value than other oil sample and is has moderate rutting value. 2% oil and 1% emulsion slab sample and 3% oil sample with zero emulsion content slab sample failed at 4000 and 2728 wheel passes whereas for 1% oil and 2% emulsion sample reached 20000 cycles with a rut

depth of 13.1mm. Thus, as the percentage of oil increases in the RAP sample the rut depth also increases.

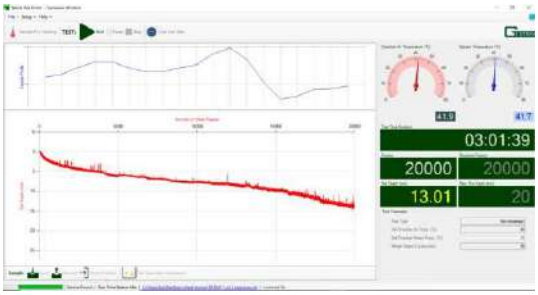

Fig. 4.3 Wheel Rut Tester Software result of 50% RAP sample with 1% oil and 2% emulsion

Fig. 4.3 shows the test result of 50% RAP slab sample with 1% oil and 2% emulsion. Test conditions were set as 40O C, maximum cycles 20,000 and maximum rut depth as 20mm.

Conclusions:

In recent years shortage and price of virgin aggregates have escalated considerably and its extraction of raw materials on a much larger scale which in turn caused dangerous environmental issues. Using RAP helps to mitigate the problems associated with shortage of aggregates. Addition of WCO in small percentage as a rejuvenator could be economical and also helps to reduce health and environmental hazards caused by reuse of oil. Dokandari et al. (2017) stated that optimum amount of WCO that could be used was 5.1% and Suo et al. (2020) concluded that 6% to 8% vegetable oil can be used for rejuvenation. But based on performance test conducted, following conclusions were developed from this study:

- The acid value of the Waste Cooking Oil was found to be 190 mg KOH, indicating that the WCO used is highly rancid.
- The RAP used in this study was base course material having a residual bitumen content of 4.8% of its weight.
- As percentage of oil increases, ITS strength of RAP rejuvenated with waste oil decreases and sample prepared using 100% virgin aggregate obtained highest ITS value.
- After performing Wheel Tracker Test, RAP samples rejuvenated using 2% emulsion and 1% oil, the rut depth obtained was 13.01mm which was much lesser value than RAP samples rejuvenated with 2% and 3% WCO with rut depth of 20mm.
- Rut depth was found to increase with the increase in oil content.
- Based on strength and rutting potential of RAP samples rejuvenated with WCO, not more than 1% of oil could be used as partial replacement of emulsion.

References:

1. **Z. Suo, H. Chen , Q. Yan, Y. Tan , X. Li** and **A. Zhang** (2021) Laboratory Performance Evaluation on the Recovering of Aged Bitumen With Vegetable Oil Rejuvenator, *Frontiers in Materials,* Vol. 8

2. **M. Zahoor, S. Nizamuddin, S. Madapusi** and **F. Giustozzi** (2020) Sustainable asphalt rejuvenation using waste cooking oil: A comprehensive review, *Journal of Cleaner Production*, Vol. 278

3. **P. A. Dokandari, D. Kaya, B. Sengoz** and **A. Topal** (2017) Implementing Waste Oils with Reclaimed Asphalt Pavement, *Proceedings of the 2nd World Congress on Civil, Structural, and Environmental Engineering* (CSEE'17), Vol. 142

4. **W. Rafiq, M. B. Napiah, M. H. Sutanato, W. S. Alaloul, Z. N. B. Zabri, M. I. Khan** and **M. A Musarat** (2020) "Investigation on Hamburg Wheel –Tracking Device Stripping Performance Properties of Recycled Hot-Mix Asphalt Mixtures*"*, *Materials 2020,* 13(21),10.3390/ma13214704.2020

5. **U. Kamariya, L. B. Zala** and **A. A. Amin** (2018) Utilization of Reclaimed Asphalt Pavement (RAP), *International Research Journal of Engineering and Technology*, 3077-3083

6. **S. S. Mahankale, R. S. Patel, V. *A.* Patil, A. A. Dalvi** and **K. U. Saraf** (2016) Use of RAP Material in Bituminous Pavement, *International Conference on Emerging Trends in Engineering and Management Research*

7. Tentative Guidelines for the Design of Flexible Pavement-IRC 37, 2012

8. Technical Guidelines 2 –TG2

ANALYSIS OF SHEET PILE WALL SUBJECTED TO PITTING CORROSION

Gopika P[1], Er. M. Gayathri Devi[2]

[1] *PG Student, Department of Civil Engineering, Saintgits College of Engineering*

[2]*Assistant Professor, Department of Civil Engineering, Saintgits College of Engineering*

Abstract: *Corrosion of steel structures in the marine environment is a major problem. Among thesepitting is considered to be more dangerous than uniform corrosion damages because it is more difficult to detect, predict and design. This study mainly focuses on pitting corrosion of sheet pile wall and how it affects the structural performance of sheet pile. A case study of Carnarvon Fascine wall is studied and characteristics of pitting corrosion of that sheet pile wall was taken for analysis.A literature survey is carried out to find the trend of corrosion pit depth, pattern and size. From the literature survey, parameters such as pit depth and pattern of pitting corrosion are fixed. The corrosion is represented as circular cut in the steel sheet pile wall. Corrosion at one side of the sheet pile is studied. A geometry is modelled in Solid Works and imported to ANSYS workbench for the analysis. Ultimate load of each model is found out. A comparative study on three models is carried out and find the difference in ultimate load, deformation, Von-Mises stress and equivalent strain.*

Keywords*: Pitting corrosion, Pit depth, Pattern of Pitting corrosion, Steel sheet pile wall*

Introduction:

Corrosion of steel structures in the marine environment is a major problem. The deterioration of this kind of structures is costly and difficult to predict both when designing new structures and when estimating the remaining service life timefor existing structures. The Shire of Carnarvon has recently completed several projects to revitalise the Carnarvon Fascine and the Town Centre. A major componentof this work was the redevelopment of the foreshore along the Carnarvon Fascine including the installation of a new steel sheet pile wall to provide coastal protection to the development. Since construction, the wall has experienced significant corrosion of the steel sheet piles, which has raised concerns overthe durability of the structure. It is not clear the exact dates that the wall was installed, however from the information provided it appears that the majority of the wall was installed around mid to late 2013. Based on the measured sectionloss the typical corrosion rates were around 0.25to 0.75 mm/yr. However, for the localised pitting that has resulting in holes in the sheetpile wall the corrosion rates are in the order of 2to 3 mm/yr. Corrosion can occur on both facesof the sheet pile wall being the landside and the waterside. Each side of the wall has a different

exposure environment which can affect the rate of corrosion. The corrosion rates specified above do not distinguish between the front and rear of the wall and are therefore a combined corrosion rate including corrosion on both the front and rear of the wall. They repaired the sections by cleaning back the existing sheet pile to bare metal to enable welding of the new steel to the existing sheet pile, installed a new plate of steel over the thin section of sheet pile to strengthen the structure, reinstating the paint coating over the repaired section to prevent further corrosion.It is proposed that pitting (and crevice corrosion) plays an important role in the overall corrosion process, but that longer term pitting behaviour is considerably more complex than usually considered.

This study focuses on assessing or evaluating the influence of corrosion on the design strength of one section of sheet. This study only focuses on analysis of a section of sheet piles subjected to corrosion on the waterside.

Literature Review:

Nakai *et al.* (2006) conducted a series of tests on structural models which consist of web, shell and face plates to investigate the effect of pitting corrosion on strength of web plates subjected to patch loading. In these tests, artificial pitting was made on theweb plates and two equal concentrated loadshave been applied vertically at the one third points of simply supported models. It was found that web crippling behaviour is strongly affected by the pit distribution on the web plates. Turnbull *et al.* (2010) conducted a finite element (FE) analysis to evaluate the stress and strain distribution associated with a singlecorrosion pit in a cylindrical steel specimen stressed remotely in tension. A key observation was the localisation of plastic strain to the pit walls (just below the surface of the specimen). Simulation of a growing pit in a static stressfield indicated corresponding plastic strain rates that were commensurate with values associated with stress corrosion cracking. This observation introduces a wholly new concept in understanding of the evolution of stress corrosion cracks from pits and correlates with recent X-ray tomography measurements. Incontrast, for these high stress conditions the stress is maximised towards the crack base away from the shoulder. However, at low applied stresses and for FE solutions assuming only elastic deformation the stress is maximised at the pit shoulder, just below the pit mouth. It appears that plasticity causes the stress to re- distribute towards the pit base. Results shown that plastic strain is localised on the pit wall below the pit mouth rather than at pit base. Paulo Osório and Ton Vrouwenvelder (2011) studied the failure probability of marine steel sheet pile structures with special consideration of the corrosion impact. The relation between the probability distribution of corrosion and equivalent thickness reduction is non-linear and

dependent on the profile. The pattern of the relation between the coefficient of variation CoV and the reliability index β (that indicates the level of safety), is such that it forms a kind of platform along lower values of CoV and also a sudden decrease occurs after a certain value of CoV that depends on the mean value of the distribution. Robert E Melchers and Robert J Jeffrey (2013) studied the accelerated low water corrosion (ALWC) of steel piling in harbours. They found that elevated levels of dissolved inorganic nitrogen in sea and brackish waters is responsible for microbiologically influenced corrosion of steel piling below the low water tide level. Small changes in metal composition have a significant effect on the severity of ALWC. Corrosion are more frequent near the corners or folds of the Z and to a lesser extent of the U profiles The results support the previous inference that the vertical differential corrosion of steel piling in seawater (ALWC) largely is the result of microbiologically influenced corrosion (MIC). The localized perforation that is the long-term outcome of ALWC is consistent with localised differences in metal composition and grain-structure. WallH and Wadso L (2013) investigated the indicative values for the corrosion rate of steel sheet piles on the Swedish west coast. Corrosion rates (mm/year) can be used both when designing new structures by oversizing the steel thickness and when estimating the bearing capacity of existing sheet pile structures. Earlier investigations on the corrosion rates along the Swedish east coast with salinity from about 0.2% to 0.8% are still used today as guidelines for the corrosion rate of all steel structures in the Swedish maritime environment even though the salinity on the west coast can be as high as 3.0%. The age of the three inspected sheet pile structures ranged from 36 to 51 years. The dimensions of the original sheet pile sections are known. One of the quay structures is located along a river. The salinity at all wharfs varied from low values at the surface to approximately 2% at the bottom (also in the river outflow). The measured average corrosion rates were in the same order as the design values in the European code. Melchers *et al.* (2014) studied localized corrosion of steel sheet piling. His results are perforation by long-term corrosion of sheet pile profiles will occur earlier in the webs when the webs are thinner than the flanges. The centerline segregation zone can corrode faster than the remaining parts of the webs of both sheet pile profiles. In an advanced state, typically after many years exposure, this vertically oriented differential corrosion along the pile length causes localized perforation of the pile wall thickness. Such perforation and loss of pile wall thickness can have a significant effect on the structural capacity of the sheet piling. It has caused serious concern about the risks to marine infrastructure and the economic implications for its management. About 30% of commercially

available U-profile pile sections have webs (pans) somewhat thinner than the remaining parts of the pile. Zve *et al.* (2015) studied the effect of zoning corrosion on the life- time structural reliability of a jacket offshore structure. The probability of failure of the structural system versus the exposure time depends on different structural components. For the earthquake loading scenario, the system's probability of failure is determined by the probability of failure ofa joint in the atmospheric zone, while after aspecific time instance of exposure to corrosion it is governed by the probability offailure of an external diagonal member in the splash zone. The effect of the zoningcorrosion was investigated through the time evolution of the displacements of the structure's joints. For both loadingscenarios, results showed a considerable increase of the structure's displacements dueto the effect of corrosion. This observation reveals that corrosion in terms of uniform thickness loss can affect the global stiffness of the structure considerably with increasing exposure period. Shivangi Saxena and VijayKumar (2017) analysed the sheet pile wall under different loading conditions using FEM. The cantilever sheet pile wall penetrating 18.12 m of sandy soil is safe for the site of our study for the undertaken surcharge. The maximum bending momentis 16.16% lesser in case of water table model as compared to the model without the influence of water table for a penetration depth of 8.58 m. From the analysis, failure is found to occur for the plastic elements extending far beneath the sheet pile tip that may reach the outer boundary of the selected mesh plot. Wang *et al.* (2018) conducted a study to find the ultimate strength assessment of plated steel structure with random pitting corrosion damage. The random pitting damage causes significant degradation to the capacity of loading and deformation in the pitted structure concurrentwith a great variation in the structural strength. The pitting structure collapses due to an amplified local deformation caused by the pitting damage, which induces material plasticity to initiate at the unload edge of the structures and to propagate towards the plate center. The structural failure mode is dominated by a continuous plasticity region linking the pits with higher levels of concentrated stress together. The random pitting corrosion causes a significant strength reduction and variation and even changes structural failure mode. The stiffened panels are thus less sensitive to the change of the pitting distribution than the unstiffened plates. Zhao *et al.* (2018) explained the influence of pitting corrosion on the bending capacity of thin-walled circular tubes. The shape of the corrosion pit considerably affected the bending capacity of TWCT. The reason for the bending capacity reduction was due to the buckling of steel wall at the compression side caused by corrosion pit. The load–displacement curves derived under different conditions. The

influence of width of corrosion pit on bending capacity increased evidently withthe increase in width of corrosion pit. The bending capacity of the TWCT reduced by 5% and 11% when width of corrosion pit was 0.07 m and 0.19 m, respectively. The load–displacement curves corresponding to various thickness of corrosion pit was investigated. Balegh *et al.* (2018) conducted a finite element simulation and predict the mechanical and electrochemical behavior on crevice corrosion in sheet pile steel. It is noticed, the local elastic strain level increases apparently at the opposite face of crevice corrosion as indicated by the red anddark red colors with minor change. The local Von Mises stress level increases apparently, and also it is distributed symmetrically to the center of the crevice, that the highest stress occurs at the crevice center. An increasing depth of corrosion defect results in a concentrated stress at crevice corrosion. When the applied load on the side of geometry corrosion defect is sufficient to cause a plastic deformation at the crevice corrosion. Robert E Melchers (2019) predicted the long-term corrosion of metal alloys in physical infrastructure. Corrosion always occurs as a result of differences, in potential, metal composition, environment, etc. and hence is always non- uniform at some scale**.** The progression of maximum pit depth is very unlikely to follow a power law, it might be satisfactory for the average pit depth as a function of time. The smaller grain sizes theoretically should produce less severe crevice corrosion under the particles, although there was a lower limit, presumably when corrosion becomes dominated by metal grain size and by metal imperfection effects. Yang *et al.* (2019) developed the zonal time-variant corrosion model to assess the seismic collapse capacity of a jacket offshore platform based on the theoretical method and measured data. The pushover and incremental dynamic analysis (IDA) methods are adopted here to calculate the collapse margin ratio (CMR), there serve strength ratio (RSR) and ductility coefficient (μ) that are frequently used for the safety reserve evaluation of a platform. The failure reason and collapse probability of platforms considering different service periods are compared. The most prominent feature of the proposed time-variant zonal corrosion model is to capture potential switch of weaklocation and resulting failure path of corroded jacket offshore platforms although the proposed model needs further calibration by more reliable in-field measured data. As expected, corrosion can definitely cause a reduction in earthquake resistance of a jacket offshore platform, as well as ultimate deformability. The coupled effect between the time-variant vibration properties of the platform and the spectral characteristics of selected motions, the collapse-level spectral acceleration (SA) does not always decrease with increasing corrosion degree. Robert E. Melchers (2020) made a review of trends for corrosion

loss and pit depth in longer-term exposures. For (almost) pure iron and some other ferrous metals in alkaline solutions, pitting commenced very quickly (within days), showing circular or near-circular pits, usually exhibiting shiny bases, that extended only some way into the metal, that is the pits appeared to be limited in depth. Each pitwas associated with a ring of corrosion product around and over the pit mouth and that this region was slightly alkaline. Generally, similar observations have beenmade for field exposure of mild steels in seawater immersion over periods of up to 3–4 years, carried out at Taylors Beach. In oneof the earlier programs, both mass loss (general corrosion) and pit depths were recorded and reported. Particularly for the latter, the maximum pit depth, as well as thenext six deepest pits were reported. It is seenthat the maximum pit depth and the average pit depth are reached quite early and then become almost steady at about 0.25 mm,until $t_a \approx$ 1 year is reached, at which time both trends increase.

Objectives:

Corrosion of offshore structures isinevitable. In an ocean corrosion environment, the strength of a platform is weakened greatly. When simultaneously subjected to earthquakes or other extreme loads, the ultimate bearing capacity of the corroded platform is dramatically reduced, resulting in compounded damage from both corrosion and earthquake. Thus, the influence of corrosion cannot be neglected in the seismic performance investigation of structures. In this study I am going to do an analysis of sheet pile wall in Carnarvon fascine wall.

The objectives of the study are;

1. To find how corrosion pitting affect structural performance of the sheet pile wall
2. Trend analysis of pitting corrosion in steel sheet pile

Methodology:

The methodology of this work includes;

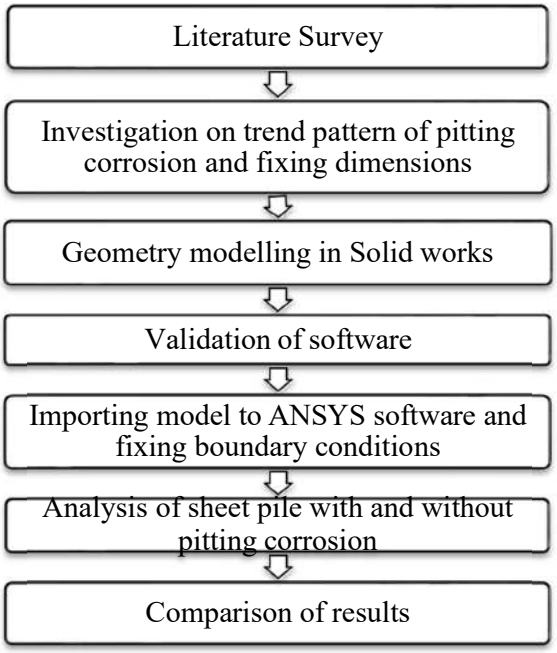

Carnarvon Fascine Wall and Pitting Corrosion Trend Analysis

Carnarvon Fascine Wall

The Shire of Carnarvon has recently completed several projects to revitalise the Carnarvon Fascine and the Town Centre. These projects were funded by the Royalties for Regions program. A major component of this work was the redevelopment of the foreshore along the

Carnarvon Fascine including the installation of a new steel sheet pile wall to provide coastal protection to the development. The aerial view of Carnarvon Fascine wall is shown in Fig 1.

Fig 1 Carnarvon Fascine wall aerial view (Carnarvon Fascine Wall Independent Review, K1488, Report R972 Rev)

The sheet pile wall was installed in two separate stages. The first stage was approximately 90 m at the northern end of the site and the second stage was approximately 700 m extending to the south. Since construction, the wall has experienced significant corrosion of the steel sheet piles, which has raised concerns over thedurability of the structure. To address these concerns the Western Australian State Government, through the Department of Primary Industries and Regional Development (DPIRD) sought an independent structural engineeringassessment of the Royalties for Regions funded wall. The fully constructed sheet pilewall is shown in Fig 2.

Fig 2 Carnarvon Fascine wall (Carnarvon Fascine Wall Independent Review, K1488, Report R972 Rev 1)

This assessment will be used to assist in planning maintenance, future works and informing the community. The currentcondition of the steel sheet pile system based onabove and below water inspection and physical thickness testing. The useful life of the structureif no maintenance is carried out to steel grade S355GP and this is confirmed by the MTS (2015) report showing compliance with the equivalent American steel grade ASTM A328. The specified sheet piles were AZ14-770 to be installed to a minimum depth of -8.5 m AHD. The condition along the length of the wall was fairly uniform with the highest levels of corrosion typically in about a 1.5 m strip covering the intertidal zone. This was evidencedby the rough texture on the front of the wall where steel had been lost. There were a number of holes through the wall which were taped off to enable future patch repairs.

Fig 3 Pitting corrosion and thickness loss in Carnarvon Fascine wall (Carnarvon Fascine Wall Independent Review, K1488, Report R972 Rev 1)

There were 4 holes found in the wall after 4 years. The pit that formed in the wall isshown in Fig 3. The paint coating may also have covered over a number of small holes that are now unable to be detected from a visual inspection.

It is not clear the exact dates that the wall was installed, however from the information provided it appears that the majority of the wall was installed around mid to late 2013. This means that at the time of inspection the wall was around 4 years old. Based on the trend analysis and corrosion depth pattern in Carnarvon fascine wall, pit depth and pit diameter for the fifth year is calculated and is tabulated in table 1.

Table 1 Change in pit dimensions

S1 No.	Year	Pit depth (mm)	Pit diameter (mm)
1	1st	0	0
2	4th	1.75	10
3	5th	2.5	10.75

Trend Pattern Graph

For mild steels immersed for long periods (years) in seawater, pit depth development has been observed to occur in what appear to be steps in pit depth, with early pitting producing plateaus, these plateaus then permitting new pitting. That new pitting then, in turn, produced new, lower corrosion plateaus that, in turn, allowed further, deeper pitting.

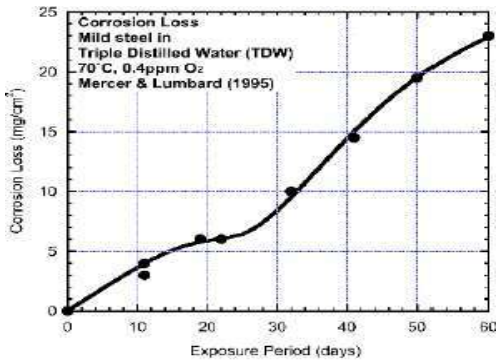

(a)

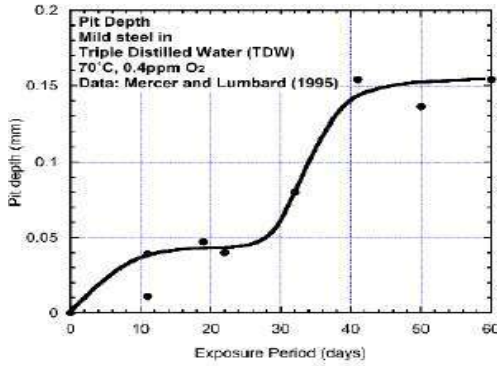

(b)

Fig 4 (a) and (b) Trend of pitting corrosion in terms of pit depth and loss of area (Robert E. Melchers 2020)

A graphical representation of corrosion loss vs. exposure period is shown in fig 4 (a) and pit depth vs exposure period is shown in fig 4 (b). It also shows that pit depth reached a peak value soon after first exposure and that maximum pit depth increased relatively little for some time

thereafter. Comparing with fig 4 (a), fig 4 (b) shows that mass-loss increased roughly in concert with the number of pits per unit area. Interestingly, the upswing in the trend for pit depth and that for mass-loss occur ata very similar time: 25–30 days after first exposure, shown as time t_a on all three plots. It is possible also to read into thatthere is a higher rate of pit formation in the very early period, i.e., in the period 0–10 days.

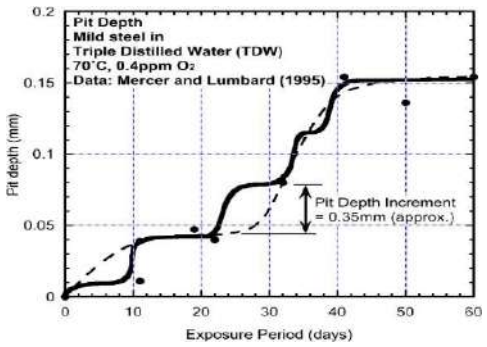

Fig 5 Pit depth data as in Fig 5.4 interpreted as stepped development of the depth of pitting (Robert E. Melchers 2020)

Corrosion Loss in Carnarvon Fascine Wall

The section loss is represented in the following chart. Within the splash zone the average section loss varied from about 1 to 3 mm. The results from the thickness measurements taken on site are summarised in the following charts. Section loss in the sheet pile is shown in fig 6. Wall thickness measurements for different levels on the wall is shown in fig 7. As shown the thinnest sections of steel were found around the high tide line.

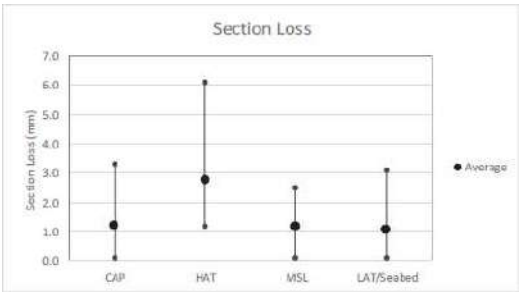

Fig 6 Section loss in Carnarvon fascine wall (Carnarvon Fascine Wall Independent Review, K1488, Report R972 Rev 1)

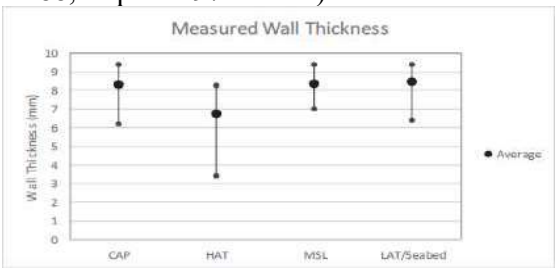

Fig 7 Wall thickness loss in Carnarvon fascine wall (Carnarvon Fascine Wall Independent Review, K1488, Report R972 Rev 1)

Based on the measured section loss the typical corrosion rates were around 0.25 to 0.75 mm/yr. However for the localised pitting that has resulting in holes in the sheet pile wall the corrosion rates are in the order of 2 to 3 mm/yr. Corrosion can occur on both faces of the sheet pile wall being the landside and the waterside. Each side of the wall has a different exposure environment which can affect the rate of corrosion. The corrosion rates specified above do not distinguish between the front and rear of the wall and are therefore a combined corrosion rate including corrosion on both the front and rear of the wall.

Results and Discussions

The three models are analysed in ANSYS Workbench and results for Von- Mises stress, strain and total deformation are found out. A graph is obtained which shows the ultimate load

of these three models. By comparing these results, it shows how badly pitting corrosion affect the structural stability of sheet pile wall.

Model 1: Sheet pile without pitting corrosion

Sheet steel pile wall of Z cross-section same as Carnarvon Fascine wall is modelled in Solid works. This model is imported to ANSYS Workbench as shown in fig 8 and analysis was done. For the analysis, one end of the sheet pile is fixed up to a depth of 4.5 m as per design. The loading and support condition is shown in fig 10.

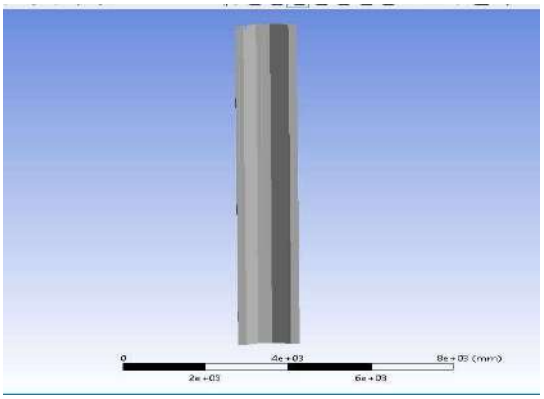

Fig 8 Geometry of sheet pile without pitting corrosion

Load was given to the free end from left. Load is given as displacement towards Y axis and sub steps was turned on and analysis was carried out to find the ultimate load of sheet pile wall. Fine mesh of size 50 mm is used to analyse each models. Meshing diagram of model 1 is shown in fig9.

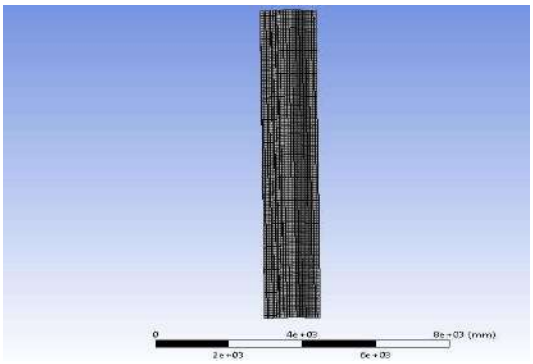

Fig 9 Meshing diagram of Model 1

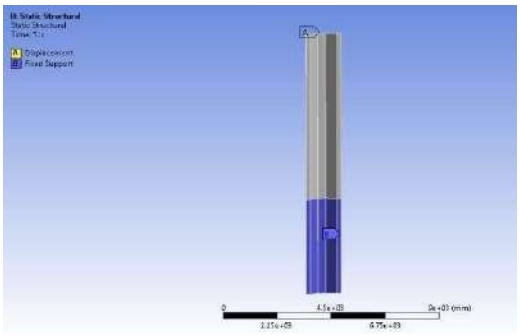

Fig 10 Static Structure of Model 1(with fixed support and loading condition)

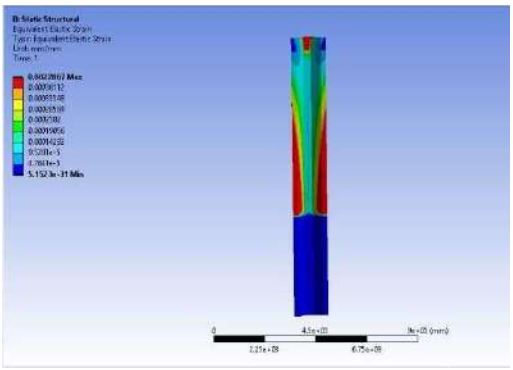

Fig 11 Strain diagram of Model 1

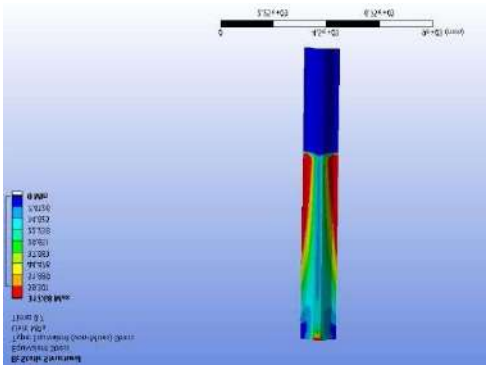

Fig 12 Stress diagram of Model 1

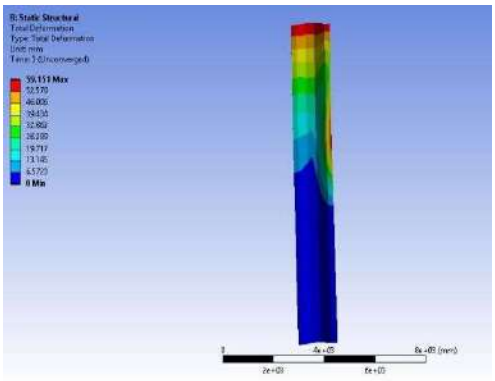

Fig 13 Total deformation diagram of Model 1

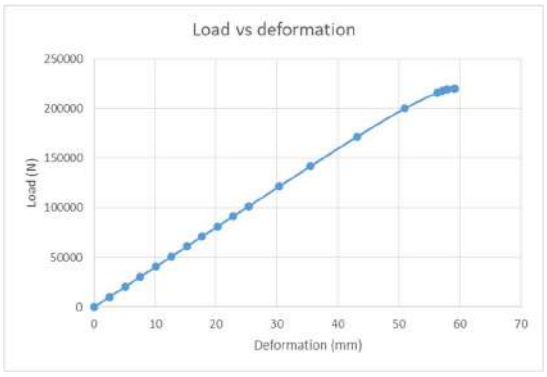

Fig 14 Graph of load against total deformation of Model 1

The equivalent elastic strain and equivalent (Von-Mises) stress is shown in fig 11 and fig 12 respectively. Fig 13 shows the total deformation diagram of sheet pile without pitting corrosion. After the analysis, the ultimate load is obtained as 220 kN, total deformation as 59.151 mm, equivalent stress 317.68 MPa and equivalent elastic strain as 0.0022867.

Model 2: Sheet pile with pitting corrosion (pit diameter of 10 mm)

Model 2 was also modelled in Solid works with pit diameter of 10 mm and pit depth of 1.75 mm. Analysis is carried out andultimate load of sheet pile was computed.

Since pitting corrosion is present we can able to understand about the change in shape of the mesh. The mesh became triangular due to the presence of pitting corrosion. Also in the region near pitting corrosion the mesh is converged. Fig 15 shows the geometry of model 2 which is imported from Solid works. Meshing diagram is shown in fig 16.

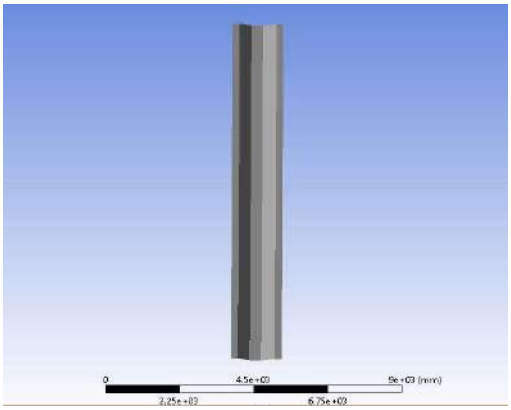

Fig 15 Geometry of sheet pile with pitting corrosion (diameter 10 mm)

Same procedure is followed to find the ultimate load, deformation, equivalent stress and equivalent strain. Fig 17 shows the sheet pile structure with loading and boundary conditions. The equivalent elastic strain and equivalent (Von-Mises) stress is shown in fig 18 and fig 19 respectively. Finally total deformation diagram is represented in fig 20.

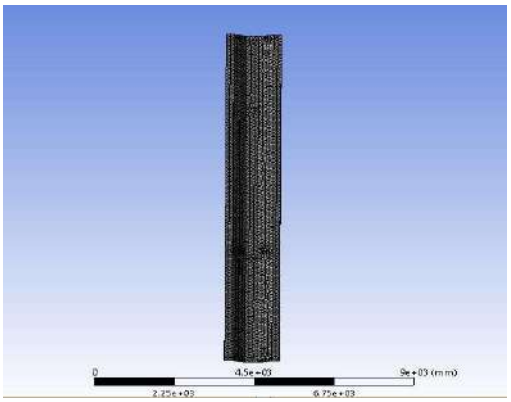

Fig 16 Meshing diagram of Model 2

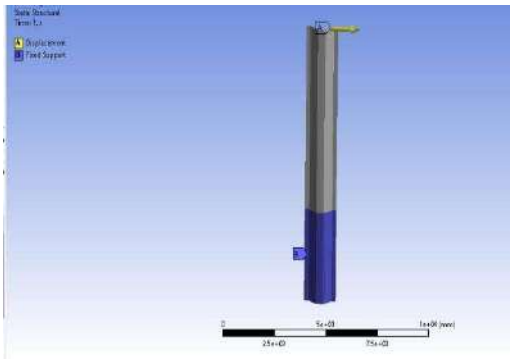

Fig 17 Static Structure of Model 2 (with fixed support and loading condition)

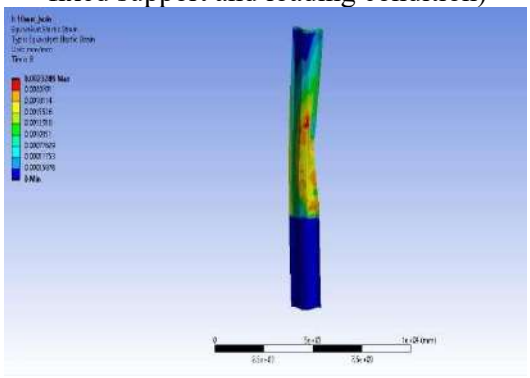

Fig 18 Strain diagram of Model 2

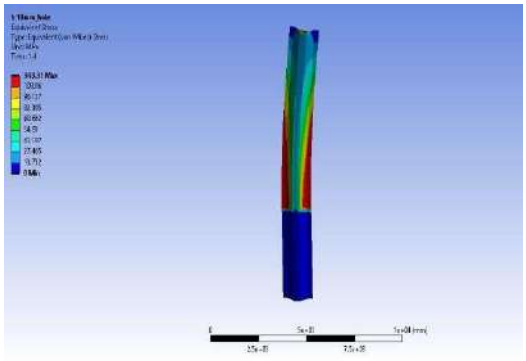

Fig 19 Stress diagram of Model 2

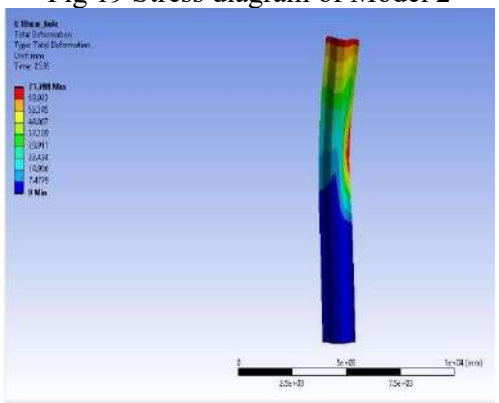

Fig 20 Total deformation diagram of Model 2

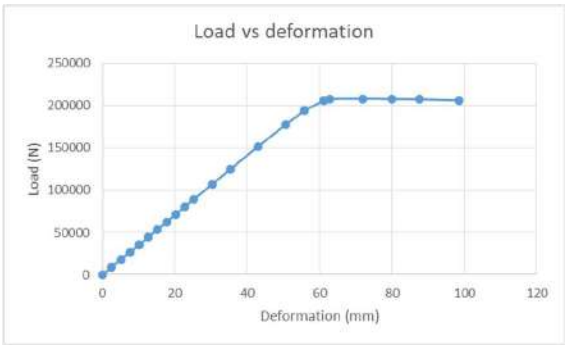

Fig 21 Graph of load against total deformation of Model 2

Graphical representation of load vs total deformation is shown in fig 21. After the analysis, the ultimate load is obtained as 208 kN, total deformation as 71.788 mm, equivalent stress 343.31 MPa and equivalent elastic strain as 0.0023890.

Model 3: Sheet pile with pitting corrosion (pit diameter of 10.75 mm)

Model 3 was also modelled in Solid works with pit diameter of 10.75 mm and pit depth of 2.5 mm. fig 22 shows the geometry of model 3which is imported from Solid works. Same procedure is followed to find the ultimate load, deformation, equivalent stress and equivalent strain. Fig 23 shows the meshing diagram. Fig 24 shows the sheet pile structure with loading and boundary conditions. The equivalent elastic strain and equivalent (Von-Mises) stress is shown in fig 25 and fig 26 respectively. Finally total deformation diagram is represented in fig 27.

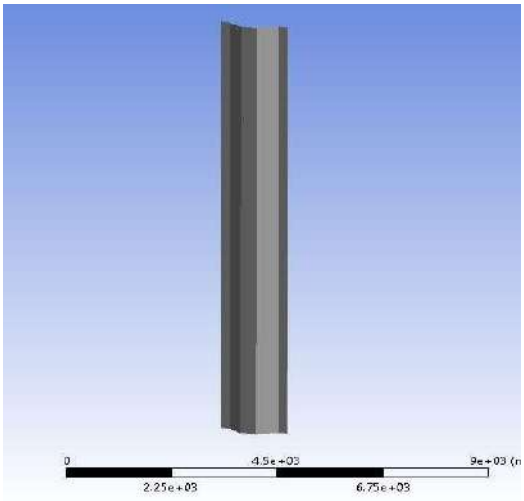

Fig 22 Geometry of sheet pile with pitting corrosion (pit diameter of 10.75 mm)

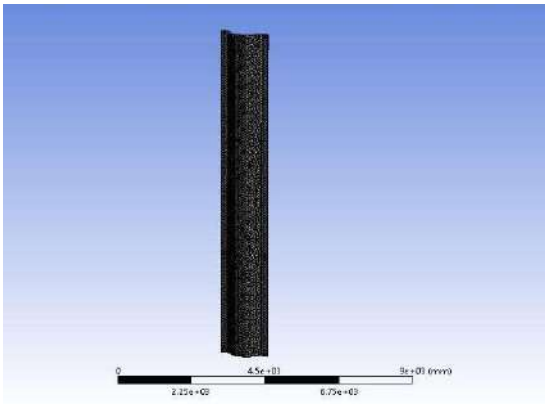

Fig 23 Meshing diagram of Model 3

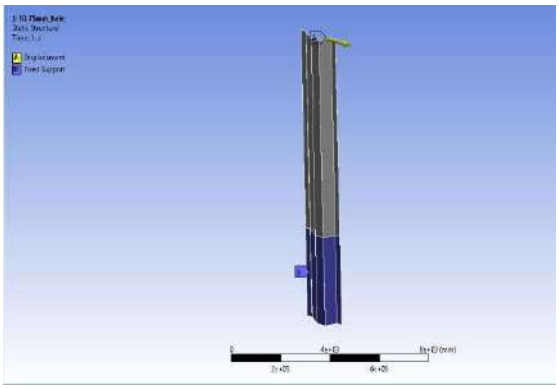

Fig 24 Static Structure of Model 3 (with fixed support and loading condition)

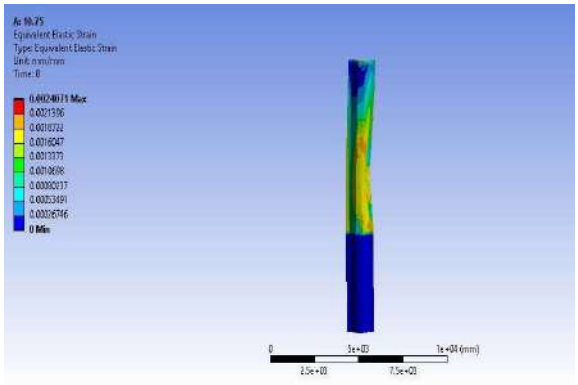

Fig 25 Strain diagram of Model 3

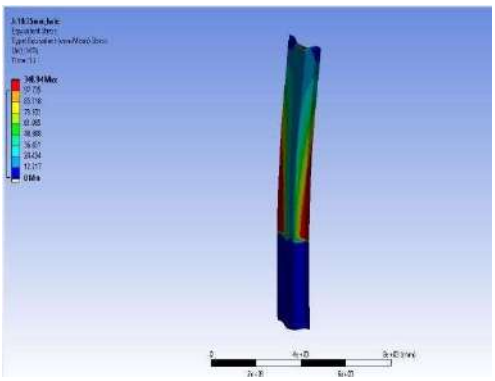

Fig 26 Stress diagram of Model 3

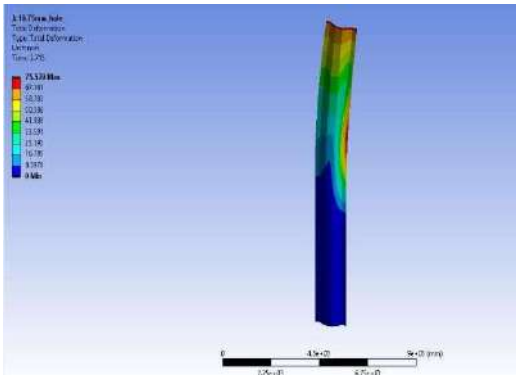

Fig 27 Total deformation diagram of Model 3

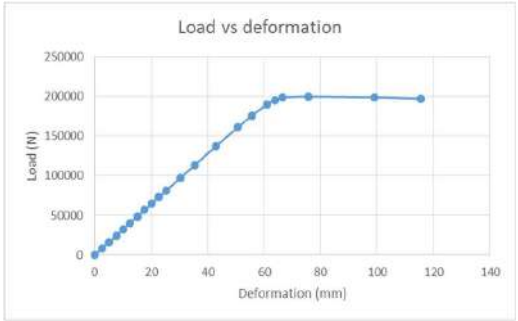

Fig 28 Graph of load against total deformation of Model 3

Graphical representation of load vs total deformation is shown in fig 28. After the analysis, the ultimate load is obtained as 200 kN, total deformation as 75.759 mm, equivalent stress 340.94 MPa and equivalent elastic strain as 0.0024071.

Comparison of Results

Table 2 Comparison of results

Parameter	Without pitting corrosion	With pitting corrosion of diameter 10 mm	With pitting corrosion of diameter 10.75 mm
Ultimate load	220 kN	208 kN	200 kN
Total deformation	59.151 mm	71.778 mm	75.759 mm
Equivalent stress	317. 88 MPa	343.31 MPa	340.94 MPa
Equivalent strain	0.0022867	0.0023890	0.0024071

After running the model, results for maximum stress, strain and deformation was obtained. A comparative study is carried out to find how dangerous pitting corrosion is and the importance of taking remedial measures. The results show that thepresence of pitting corrosion affect the load carrying capacity of the sheet pile. After 4 years, ultimate load is reduced to 5.45%. Total deformation of the structure is increased to 17.59%. Equivalent Von-Mises stress is increased to 7.40%. Equivalent strain is increased to 4.28%.

While analysing trend pattern of pitting corrosion, the dimensions of pitting corrosion is change accordingly and analyse the results. The diameter and depth of pitting corrosion is increased to 0.75 mm based on the trend analysis of pitting corrosion on CarnarvonFascine wall. The difference in results for these 2 models shows the dangerous growth of pittingcorrosion and how it reduce the structural stability of the sheet pile wall. The ultimate loadis reduced to 3.84 % and total deformation value is increased to 5.25%. A small difference in the value in equivalent Von-Mises stress is noticed. It is because, stress depends on load and area. In ANSYS the load is not fixed. Load is given as displacement to find the ultimateload carrying capacity. Since the difference in load is high and difference in area of the two model is comparatively small and this makes a decrease in equivalent Von-Mises stress. Equivalent Von-Mises stress is decreased to 0.69%. Equivalent strain is increased to 0. 75%. **Conclusions:**

This study attempted to evaluate the impact of pitting corrosion on the structural stability of steel sheet pile wall. The result shows that as the pitting corrosion increasing it reduces the structural integrity of the sheet pile wall.

- The structure is subjected to approximately 5% ultimate load reduction by variation of pit diameter and pit depth sizing by 0.75mm
- By analysing the trend pattern, the ultimate load is reduced about 3.84%

- When pitting corrosion is present it increases the stress value and deformation value
- Slight difference shown in the reduction of stress for 10 mm diameter pitting and 10.75 mm diameter pitting is because of the reduction in load carrying capacity of the sheet pile. Since stress is equal to load divided by area
- The useful life of the sheet pile wall is dependent on a number of failure modes. The end of useful life is considered to be when the sheet pile has reached a stage that further deterioration of the structure would lead to loss of service
- So analysis of pitting corrosion based on the trend pattern is a significant study for the calculation of useful life of sheet piles

References:

1. **A. Turnbull, L. Wright** and **L. Crocker** (2010), "New insight into the pit-to-crack transition from finiteelement analysis of the stress and strain distribution around a corrosion pit",*Corrosion Science,* **52**, 1492-1498.
2. **Balegh, B., H. Trouzine,** and **Y. Houmadi** (2018), "Finite element simulation and prediction of mechanical and electrochemical behavior on crevice corrosion in sheet pile steel", *Jordan Journal of Mechanical & IndustrialEngineering*, **12 (1).**
3. **Melchers, R. E.** (2019), "Predicting long- term corrosion of metal alloys in physical infrastructure", *NPJ Materials Degradation*, **3 (1)**, 1–7.
4. **Melchers, R. E.** (2020), "A review of trendsfor corrosion loss and pit depth in longer term exposures", *Corrosion and Materials Degradation*, **1 (1)**, 42–58.
5. **Melchers, R. E.** and **R. J. Jeffrey** (2013), "Accelerated low water corrosion of steelpiling in harbours", *Corrosion engineering, science and technology*, **48 (7)**, 496–505.
6. **Melchers, R. E., R. J. Jeffrey,** and **K. M. Usher** (2014), "Localized corrosion of steel sheet piling", *Corrosion science*, **79**, 139– 147.
7. **Nakai, T., H. Matsushita,** and **N. Yamamoto** (2006), "Effect of pitting corrosion on strength of web platessubjected to patch loading", *Thin-walled structures*, **44 (1)**, 10–19.
8. **Osório, P., C. Odenbreit, S. Van Baars,** and **T. Vrouwenvelder** (2011), "Failure probability of marine steel sheet pile structures with special consideration of the corrosion impact", *In OCEANS 2011 IEEE- Spain. IEEE*, 2011.
9. **Shivangi Saxena** and **Vijay Kumar** (2017), "Analysis of Sheet Pile Wall underDifferent Loading Conditions Using FEM", *Indian Geotechnical Conference 2017 GeoNEst.*
10. **Wall H** and **Wadso L** (2013), "Corrosion rate measurements in steel sheet pile walls

in a marine environment", *Marine Structures*, **33**, 21-32.

11. **Wang, R., R. A. Shenoi,** and **A. Sobey** (2018), "Ultimate strength assessment of plated steel structures with random pitting corrosion damage", *Journal of Constructional Steel Research*, **143**, 331–342.
12. **Yang, Y., Q. Wu, Z. He, Z. Jia,** and **X. Zhang** (2019), "Seismic collapse performance of jacket offshore platforms with time-variant zonal corrosion model", *Applied Ocean Research*, **84**, 268–278.
13. **Zhao, Z., B. Liang, H. Liu,** and **X. Wu** (2018), "Influence of pitting corrosionon the bending capacity of thin-walled circular tubes", *Journal of the Brazilian Society of Mechanical Sciences and Engineering*, **40 (11)**, 1–12.
14. **Zve, E. S., E. Loukogeorgaki, D. C. Angelides** (2015), "Effect of zoning corrosion on the life-time structuralreliability of a jacket offshore structure. In The Twenty fifth International Ocean and Polar Engineering Conference", *International Society of Offshore and Polar Engineers.*
15. Carnarvon Fascine Wall Independent Review, K1488, Report R972 Rev 1.
16. IS: 9527 (PART 3) -1983 - Code of practice for design and construction of port and harbours structures.

FEASIBILITY STUDY OF FLYOVER AT CHAGANASSERY BYPASS

Joshua George Thomas[1], Nibin Thomas[1] , Remy p Rajan[1] , Samjos Chacko[1], Dr. Susan Rose[2]

[1] *UG Student, Department of Civil Engineering, Saintgits College of Engineering*

[2]*Associate Professor, Department of Civil Engineering, Saintgits College of Engineering*

Abstract: *Transportation is an essential feature in today's life and will continue to be the same in the future. Transportation, is the movement of humans, animals, and goods from one location to another. It makes manifold contribution to the economic industrial, social and cultural development of any country. The adequacy of transportation system indicates the economic and social development. Changanassery is a municipal town in Kottayam district in the state of Kerala, India. Changanassery is the gateway to the Western Ghats and Kuttanad. The roads meeting at the selected location are bypass road connecting Thiruvalla, Kottayam, Changanassery and Thengana. Due to movement of vehicles from major cities and town, there is increase in traffic congestion which leads to traffic delay. This lead to the demand in proper planning which will eliminate road traffic congestion. High volume of traffic during peak hours, inadequate signal facilities, pedestrian facilities, careless driving etc, worsen the situation. In order to solve the traffic congestion, PWD had come up with the idea of flyover starting from Palathra junction and end at old railway station. But the local people come up with an allegation that, due to insufficient width of road at the exit and entry point of the flyover, there may be a chance of occurrence of jam pack at the end locations. In this study, an attempt was made to study the existing traffic conditions and road geometry. The present traffic volume was analysed and the sufficiency of existing facilities were checked. Attempts are made to suggest few solutions for decreasing the traffic condition in the location and improving the traffic flow. For this traffic studies were carried out and the data was analysed. Based on the analysis there is a need for grade separation for the proper functioning of the junction and the width of the road has to be increased to reduce the congestion. Pedestrian facilities like footpath, guard rails, markings and road signs were recommended.*

Introduction:

Transportation is an essential feature in today's life and will continue to be the same in the future. Transportation, is the movement of humans, animals, and goods from one location to another. It makes manifold contribution to the economic industrial, social and cultural development of any country. The adequacy of transportation system indicates the economic and social development.

The spectacular growth of automobiles as one of the most convenient modes of travel has brought in its make frustrating problems of parking accidents, delay, congestion, and environmental degradation The increasing vehicle population necessitates a safe efficient and comfortable traffic system along with structural strength of the road. In India the problems faced by urban

centers of traffic and transportation are increasing.

The composition of traffic on Indian roads is heterogeneous in nature. It consists of various modes of vehicles like buses, cars, scooter, truck, etc of the fast moving category and cycles, cycle rickshaws bullock carts in slow moving category. This mix creates a common situation in understanding the behaviour of traffic.

Since an intersection involves conflict between traffic in different directions, its scientific design can control accidents and delay and can lead to orderly movement of traffic. Optimization of traffic light with countdown along with widened roads can help in managing the traffic. In fact, in urban areas evidencing exciting roads or the scope of improvement of intersection at- grade is very limited. So, due to the unavailability of land and to achieve fast and safe movement of vehicle at at-grade separator is one of the solution i.e. flyover. It minimizes the risk of accident as head to head and tail to tail. Now a day's city is developing to mega and metro and as a result, flyover is a better solution for the traffic problem. Monitoring of road conditions and traffic flow using CCTV can help in reducing the traffic congestion. Prevention measures should be taken in order to reduce close car parking in the road so as to reduce traffic blocks.

Literature Review:

Patel et al. (2021) observed that the number of accident occur due to high speed of vehicle , traffic delay, risk of pedestrian life, lack of proper facility like symbol, signals and markings. Fly over suggest for the traffic flow at this intersection and during the construction of flyover minimize traffic delay by the road safety audit and using the rapid construction of the fly over at intersection. The aim of the study is to minimize the accident at the selected intersection by improving it. Suggesting techniques of rapid construction of flyover to minimum traffic delay during the construction of the flyover and make the viewof flyover aesthetic.

Parthkumar et al. (2018) tries to evaluate over bridge performance at the IIM-A intersection in context to traffic congestion reduction as well as economic benefits. For this purpose variety of surveys werecarried out at intersection like CVC survey, stopped delay survey and spot speed calculation survey. Fromthe analysis of data, impact of an OB on traffic condition and economic benefit generated by presence an OB is calculated. Calculation is also carried out based on the assumption that if over bridge was provided parallel to 132 feet ring, what would be

its effect on traffic flow condition and how much economical advantage would be generated.They conducted the research to briefly study on the IIM-A cross road (andhajan mandal cross road) before and after the construction of the flyover, to check the present ground condition and to evaluate the fly over performance and impact on traffic condition. Various surveys are carried out and finallyconclude that the total number of vehicle benefitted by an over bridge, average delay time and saving in travel time and fuel consumption.

Chhatbar et al. (2019) research in extensive studies that was undertaken to determine effects of fly over construction to the way of life of the motorists and commuters and general travelling public. In addition, this is to make them aware of the advantages and dis-advantages that it may bring to their everyday life of activity. To reduce traffic congestion at an at-grade intersection near a big city, one method is construction a flyover bridge. The flyover facilitates the traffic flow in the directions of the bridge, but the infrastructure cannot fully solve all of the problems especially on the secondary road. Under the bridge, although it relieves the traffic congestion at the intersection, traffic signal can be considered as one of the solution.

Singh et al. (2017) tells that aim of traffic surveys is to capture data that accurately reflects the real-world traffic situation in the area. It may be counting the number of vehicles using a road or collecting traffic volume information, but there aremany other types of data that traffic surveys collect. In the past this has involved having people standing by the side of roads and recording their observations on paper pads. In recent years this approach has been largely replaced by recording traffic using video cameras, and then analyzing the video footage later in the office. Traffic surveys are generally required to transportation engineers for planning and designing traffic facilities, diagnosing given situations and finding appropriate solutions, studying the effectiveness of introduced schemes etc**.** Only because of this traffic volume survey we got to know the road condition. It helps our engineers to construct the road plan and the need of highways etc. That's the traffic volume is a basic necessity for any design, planning and construction of road, bridges, highways etc. The traffic volume study plays a very important role in improving safety at signalized and un-signalized intersections in both rural and urban areas.

Hazarika et al. (2019) conducted a study on a traffic survey done to know the current traffic scenario in Tezpur town of Assam, India. Four manual studies-Traffic volume study, on-street parking study, off-street parking study and spot

speed study have been done at five junctions of the town to know the existing condition of vehicular traffic and several recommendations are put forward to sort out the problem faced by the public daily and make a smooth flow of traffic as far as possible. From the studies conducted on the locations, it is evident that traffic in the Tezpur town area is heterogeneous in nature. Due to the narrow width of all approaching roads leading to the town and day to day increasing concentration of different vehicles and commercial establishment the town seems to be expanding in a haphazard manner with least concern among the civic authorities and the general public. This is evident from the traffic volume and parking studies so far conducted in this survey. The vehicles are parked here and there beside the main road and the collector streets along with the presence of temporary vendors occupying a side portion of the carriageway which make it inconvenient to different vehicle owners to smoothly drive on the road.

Prajapati et al. (2017) conducted a research to identify Level of service and locations of delays to determine the significant factors causing these delays by using Floating car method, license plate method and GPS method to make recommendations for improving the flow of traffic. Travel time data was collected by license plate method and by GPS during morning and evening peak hours on each stretches simultaneously. From the interpretation of the data collected Flow- Delay Model was generated. The Level of Service (LOS) concept proposed in Highway Capacity Manual 2000 was used to determine the level of congestion. From the theoretical studies, it can be inferred that the travel time delays are largely depends on traffic flow, on street parking, haphazard movement of vehicle.

Perumal et al. (2018) attempts to analyze the crossing behavior of pedestrians like crossing speed, compliance with signal, and pedestrian-vehicular interaction under mixed traffic conditions and to identify the influencing factors based on statistical tests. 775 pedestrian samples were observed from three signalized intersections in Mumbai, India for analyzing crossing behaviors and the significant factors affecting traffic signal compliance by pedestrians were identified. Pedestrian-vehicular interaction and the influencing factors were analyzed in this paper and could provide some valualble insights for improving pedestrian safety at signalized intersections. This work can further be extended by taking a much larger sample thereby giving better statistics results. Analyzing the pedestrian crossing behavior including pedestrian arrival pattern with

influencing parameters would increase the robustness of this work in future.

Objective:

The main objectives of the study are

i. To study the traffic characteristicsof the intersection
ii. To identify the problems of the selected intersection
iii. To suggest improvements for theintersection

The photographs of the junction is shownin Fig. 1.

Fig. 1 Changanassery Bypass junction

Methodology:

The flowchart for the methodology of the work is shown in Fig. 2.

Volume Count:

In order to find out the vehicles in the location and to find out the peak hour, volume count was done. The count wastaken from 7:00 am to 6:00 pm at 5 min interval. Classified volume count was done and the count was taken in 12 directions. From the volume study conducted, the peakhour was identified. The number of vehicles were converted into PCU and the volume data for five minutes interval was summed up to obtain volume count for each one hour. The hour with maximum PCU value was identified as the peak hour for both morning and evening sessions. Table. 1 shows the PCU values of each type of vehicles.

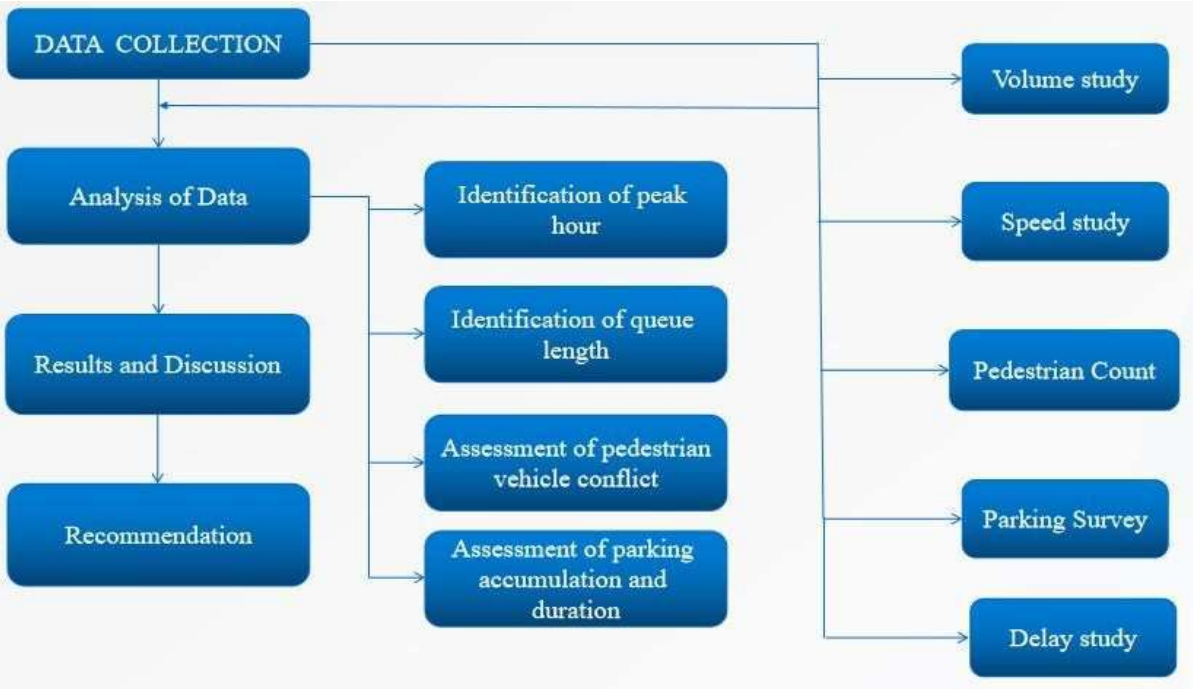

Fig. 2 Flow chart of methodology

Table. 1 PCU Values for Different Types of Vehicles

TYPE OF VEHICLE	CONVERSION FACTOR
CAR	1
BUS	3
TWO WHEELER	0.5
JEEP	1
AUTO	1
LORRY	4
TRUCK	4.5
OTHERS	6

From the data, peak hours in each direction is listed in Table. 2. Hour with highest PCU value is taken as peak hour and that with lowest PCU value is denoted as off- peak hour. The peak hours and corresponding volume are shown below.

Table. 2 Peak Hours in Each Direction

Direction	Time
Kottyam - Changanassery	09:00 am – 10:00 am
Changanassery - Kottayam	04:10 pm – 5:10 pm
Thengana - Changanassery	08:50 am – 9:50 am
Changanassery - Thengana	10:10 am – 11:10 am
Thiruvalla - Thengana	04:15 pm – 5:15 pm
Thengana - Thiruvalla	08:40 am – 9:40 am
Thengana - Kottayam	04:00 pm – 5:00 pm
Kottayam - Thengana	09:50 am – 10:50 am
Thiruvalla - Thengana	04:15 pm – 5:15 pm
Thengana - Thiruvalla	08:40 am – 9:40 am
Thiruvalla - Changanassery	08:35 am – 9:35 am
Changanassery - Thiruvalla	04:05 pm – 5:05 pm

The morning peak hour was found to be 9:20 am – 10:20 am and the evening peak hour was found to be 4:20 pm – 5:20 pm. PCU rate is 5156 at the intersection in morning peak hour which is greater than 3000 [Source : IRC 106-1990 (Table 2)]. So their arises a need for grade separation and widening of road is required. The width of the road is about 7m. Traffic flow directions is shown in Fig.3.

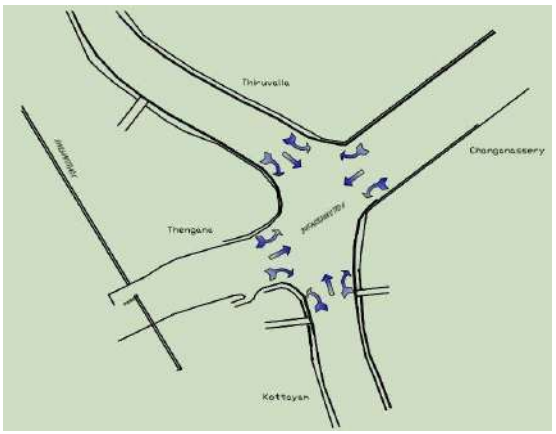

Fig. 3 Traffic Flow Directions

Speed Study:

Average speed of each type of vehicle during the peak hour was found out. Cumulative frequency curve for different roads are shown in Fig. 4, 5, 6 and Fig.7, were x-axis represents speed and y-axis represents cumulative frequency. A curve that represents the cumulative frequency distribution of grouped data on a graph is called a Cumulative frequency curve or an Ogive. Representing cumulative frequency data on a graph is the most efficient way to understand the data and derive results. Here the 98th percentile for the Thengana road was found to be 47.5 km/hr, in Changanassery road it was 26 km/hr, in Kottayam road it was 55 km/hr and in Thiruvalla road it was found to be 43 km/hr.

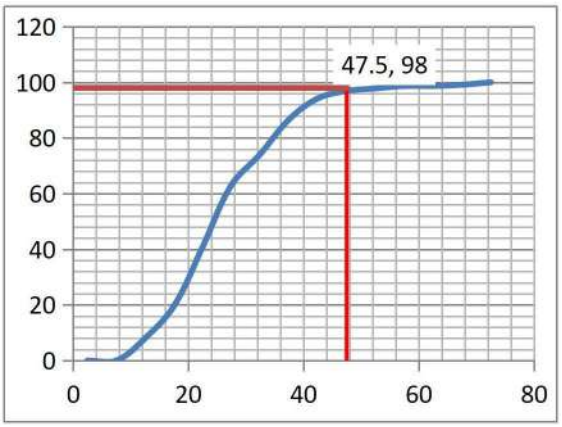

Fig. 4 Cumulative Frequency Curve for Thengana Road

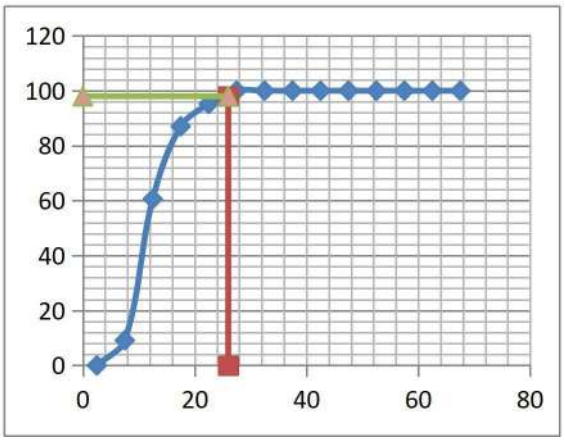

Fig. 5 Cumulative Frequency Curve for Changanassery Road

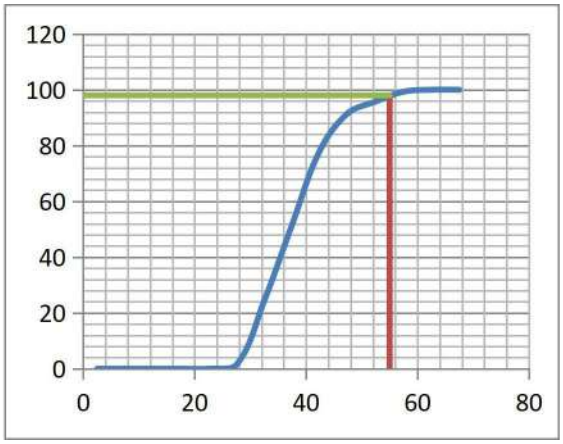

Fig. 6 Cumulative Frequency Curve for Kottayam Road

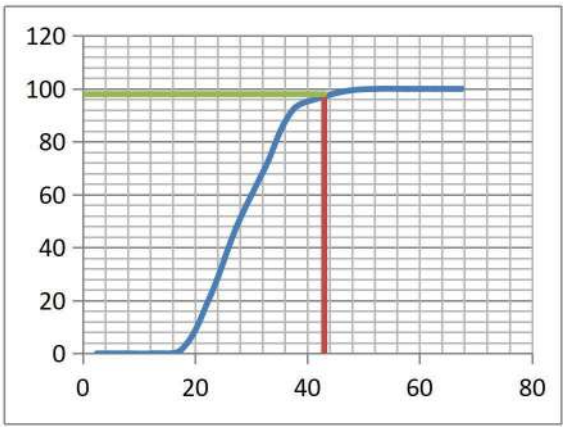

Fig.7 Cumulative Frequency Curve for Thiruvalla Road

Parking Study:

Parking survey data was analyzed to find out the maximum parking accumulation and duration. For this the number of each type of vehicle parked in a particular half hour duration was tabulated and the maximum number of each type of vehicle was found out.

In order to find out the duration of parking, each type of vehicle and their number was tabulated below duration. This was done by comparing registration number of vehicles parked in each 30 minute interval. Parking accumulation and duration of different roads are shown in Table. 3, 4, 5, 6, 7, 8, 9 and 10.

Table. 3 Parking Accumulation in Thengana

TIME	CAR	BIKE	TRUCK	AUTO	BUS
09:00-09:30	3	3	3	4	1
09:30-10:00	2	4	3	5	0
10:00-10:30	6	3	2	9	0
10:30-11:00	3	2	2	3	0
11:00-11:30	3	5	4	4	2
11:30-12:00	4	5	1	2	1
03:00-03:30	3	6	2	6	0
03:30-04:00	2	4	1	2	0
04:00-04:30	5	6	2	4	2
04:30-05:00	6	8	2	9	0
05:00-05:30	3	4	1	5	0

Table. 4 Parking Accumulation in Changanassery

TIME	CAR	BIKE	TRUCK	AUTO	BUS
09:00-09:30	1	2	0	4	0
09:30-10:00	2	4	0	1	0
10:00-10:30	1	2	0	7	0
10:30-11:00	2	4	0	6	0
11:00-11:30	2	6	0	5	0
11:30-12:00	2	8	0	3	0
03:00-03:30	5	6	0	5	0
03:30-04:00	4	4	0	4	0
04:00-04:30	6	2	0	3	0
04:30-05:00	5	3	0	7	0
05:00-05:30	3	2	0	3	0

Table. 5 Parking Accumulation in Kottayam

TIME	CAR	BIKE	TRUCK	AUTO	BUS
09:00-09:30	1	3	5	4	0
09:30-10:00	2	3	3	5	0
10:00-10:30	1	3	2	1	0
10:30-11:00	2	2	2	3	0
11:00-11:30	2	4	4	4	0
11:30-12:00	5	6	1	2	0
03:00-03:30	5	6	2	3	0
03:30-04:00	6	4	2	1	0
04:00-04:30	7	6	1	0	0
04:30-05:00	8	7	0	3	0
05:00-05:30	7	6	1	1	0

Table. 6 Parking Accumulation i n Thiruvalla

TIME	CAR	BIKE	TRUCK	AUTO	BUS
09:00-09:30	1	3	2	3	0
09:30-10:00	2	3	3	2	0
10:00-10:30	1	3	2	1	0
10:30-11:00	2	2	2	0	0
11:00-11:30	2	2	1	0	0
11:30-12:00	2	4	1	1	0
03:00-03:30	3	3	2	1	0
03:30-04:00	4	1	0	1	0
04:00-04:30	3	3	0	3	0
04:30-05:00	2	2	1	3	0
05:00-05:30	1	3	2	1	0

Table. 7 Parking Duration in Thengana

PARKING DURATION					
THENGANA ROAD					
DURATION IN MINUTES					
TYPE	<30	30-60	60-90	90-120	>120
CAR	8	1	0	0	0
BIKE	10	3	1	0	0
AUTO	11	0	0	0	0
TRUCK	0	0	0	0	0

Table. 8 Parking Duration in Thiruvalla

PARKING DURATION					
THIRUVALLA ROAD					
DURATION IN MINUTES					
TYPE	<30	30-60	60-90	90-120	>120
CAR	5	1	0	0	0
BIKE	2	2	0	0	0
AUTO	0	0	0	0	0
TRUCK	1	0	0	0	0

Table. 9 Parking Duration in Kottayam

PARKING DURATION					
KOTTAYAM ROAD					
DURATION IN MINUTES					
TYPE	<30	30-60	60-90	90-120	>120
CAR	4	2	0	0	0
BIKE	2	1	0	0	0
AUTO	0	0	0	0	0
TRUCK	1	1	0	0	0

Table. 10 Parking Duration in Changanassery

PARKING DURATION					
CHAGANASSERY ROAD					
DURATION IN MINUTES					
TYPE	<30	30-60	60-90	90-120	>120
CAR	10	3	0	0	0
BIKE	13	3	1	0	0
AUTO	3	0	0	0	0
TRUCK	6	3	1	0	0

From the parking accumulation table it is understood that two-wheelers contribute the most. From the parking duration table it was understood that most of the vehicles were parked for less than 30 minutes, in

that two-wheelers was the highest. Only few vehicles have been parked for more than two hours. From this we concluded that parking does not much affect the traffic flow.

Pedestrian Survey:

Up and down movements of pedestrians were counted and tabulated for each roads. An influence area of 75 meter was considered for study and the pedestrians crossing inside this influence area was counted. From the data collected, morning and evening peak hour was found out which is given in table. 11.

Table. 11 Peak Hours

	MORNING PEAK HOUR	EVENING PEAK HOUR
Thiruvalla Road	11:00-12:00	3:15-4:15
Kottayam Road	8:30-9:30	3:30-4:30
Thengana Road	8:15-9:15	3:30-4:30
Chaganassery Road	11:00-12:00	3:15-4:15

Pedestrian vehicle conflict:

Analysis was done to find out the pedestrian vehicle conflict at the intersection. This was done to find out whether pedestrian facilities are to be provided. For this PV^2 was calculated. Where P is the peak hour pedestrian which was found out earlier and V is the volume of vehicles at particular peak hour. The value of V is taken from volume count.

If PV^2 is greater than 2×10^8 pedestrian facilities must be provided. If PV^2 is greater than 10^{10} a pedestrian subway should be provided [Source : IRC:103, 2012].

In the bypass road,

P = 636

V = 3691 PCU/hr

$PV^2 = 8.6 \times 10^9$ which is greater than 2×10^8. Hence pedestrian facilities should be provided.

Delay Study:

A delay study determines the average time required and also the amount of delay caused on a given route. Delay is the extra time spent by drivers against their expectation. Data obtained from travel time and delay studies give a good indication of the level of service on the study section. Interval between the time at which the vehicle stops and goes at the intersection is taken and tabulated. It is found that PCU rate is 1414 in Kottayam-Thiruvalla road before the completion of flyover during peak hour. Also it was found that PCU rate is 512.5 after the completion of flyover. Average delay in Kottayam-Thiruvalla road was found out to be 120 seconds before completion of flyover during peak hour. As PCU rate is reduced after the completion of flyover,

the delay time also reduces about 3/4th of the present value.

Queue length:

Queue lengths are important parameters in traffic engineering for determining the capacity and traffic quality of traffic control equipment. Total length of vehicles at the traffic signal when its red is taken as queue length. At signalized intersections, queue lengths at the end of red time (red-end) are of greatest importance for dimensioning the lengths of lane. Queue length along 4 directions were observed which is shown in Table. 12. From the data queue length is seemed to be higher in value. After the completion of flyover the queue length in Kottayam road reduces upto a certain value, thus reducing the congestion and also the delay time.

Table. 12 Queue Lengths

	QUEUE LENGTH
Thiruvalla road	246.4 m
Cheganassery road	175 m
Thengana road	240 m
Kottayam road	125 m

Level Of Service (LOS):

Level of service (LOS) is a qualitative measure used to relate the quality of motor vehicle traffic service. LOS is used to analyze roadways and intersections by categorizing traffic flow and assigning quality levels of traffic based on performance measure like vehicle speed, density, congestion, etc. Analysis was done to find out the level of service of Kottayam- Thiruvalla road ranging from A to F . For this V/C ratio was found out, where V is the volume and C is the capacity. Graph b/w Operating Speed and V/C Ratio is shown in Fig.8. Table. 13 shows LOS of a Mid Block Section.

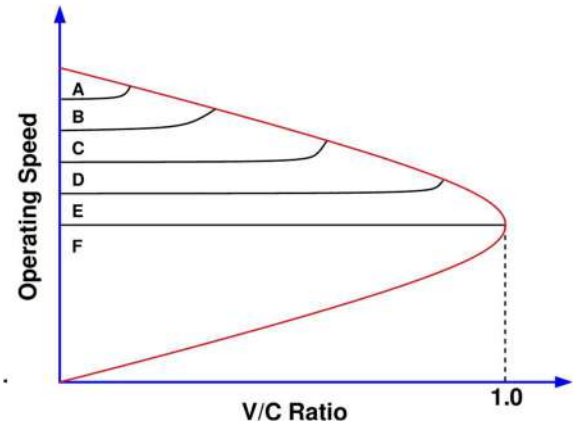

Fig. 8 Graph b/w Operating Speed and V/C Ratio

For Thiruvalla road,

V = 2721.5

C = 1500 [Source : IRC 106-1990 (Table 2)]

=> V/C = 1.81 > 1, which is of LOS –F

For Kottayam Road,

V = 2239.5

C = 1500 [Source : IRC 106-1990 (Table 2)]

=> V/C = 1.49>1, which is of LOS –F

From the result obtained, it is observed that

the flow is congested and thus grade separation is required.

Table. 13 LOS of a Mid Block Section

LOS	Quality	Speed (kmph)	V/C	Descripition
A	Free – flow	80	0.6	High level of physical and psychological comfort
B	Reasonable free- flow	70	0.7	Reasonable level of physical and psychological comfort
C	Near free - flow	60	0.8	Local deterioration possible with blockages
D	Medium flow	50	0.85	Non recoverable local disruptions
E	At capacity flow	40	0.9	Minor distrubances resulting break down
F	Congested flow	15	1	Break down of flow capacity drops

Summary and conclusion:

Summary:

Traffic studies like pedestrian count, volume count, parking study, speed study, delay study, etc were conducted. In order to reduce the congestion in traffic, PWD has proposed a flyover design which starts at a point away from the palathra junction and ends at a point before SH school junction. But from studies conducted, further increase in the traffic volume will occur which will cause for increase in traffic congestion. The data collected was analysed and necessary facilities were provided.

Conclusion:

- Widening of roads to 4 lane below the direction of flyover can ensure smooth flow of traffic.
- Due to increase in traffic volume count, separate grade separation is provided.

- As the traffic increases at the end of flyover, the length of flyover has to be increased to a distance of 0.8 km from SH school junction along Thiruvalla road so that the flyover ends at a place which causes less traffic.
- After the construction of flyover, the traffic volume count will reduce to a value less than the permissible limit.
- Reduction in the traffic volume will increase the speed of the vehicles.
- Delay of vehicle in the junction can be obtained from the delay study, construction of flyover and widening of road will resolve this problem.
- Since the number of vehicles parked on the roadside is less and doesn't cause any traffic congestion, no separate area is required for the parking facility.
- As per the result obtained from the pedestrian survey whose value is greater than the permissible limit, provision of footpath is made for the pedestrian with adequate crossing signals.

References:

1. **T. Patel and K. Dave** (2021) "Feasibility Study and Rapid Construction of Flyover at Sahakari Zin Intersection on NH-8, Himmatnagar", *International Journal of Engineering and Technology*, Pages:1-30.

2. **K. Parthkumar and M. Jain** (2018) "Before and After Study of an Flyover–A Case Study Of IIM-A Intersection", *International Journal for Scientific Research and Development*, Pages: 20-90.

3. **N. Chhatbar and P. Shinkar** (2019) "Economic Assessment of Flyover - A case study of Rajkot city", *GRD Journal*, Pages: 1-20.

4. **S. Singh and S. K. Singh** (2017) "Traffic Volume Survey Analysis of the Road Connecting Career Point University", *International Journal For Innovative Research In Multidisciplinary Field,* Vol 2, Pages: 112-117.

5. **M. Hazarika, B. Das and G. Kalita** (2019) "A Study On Traffic Survey at Tezpur Town of Assam, India",*Journal of Engineering Research and Application*, Vol 9, Pages: 20-28.

6. **N. Prajapati and H. Varia** (2017) "Travel Time and Delay Study of

Selected Links of Kalupur Area - Ahmedabad", *International Journal of Engineering Research & Technology (IJERT),* Vol 6, Pages:701-711.

7. **U. Gupta, G. Tiwari** (2018) " Case Study of Pedestrian Risk Behaviour and Survival Analysis", *Journal of the Eastern Asia Society for Transportation Studies*, Vol 8, Pages: 2123-2139.

DETERMINATION OF SOIL PROPERTIES, FLOOD HEIGHT AND PREPARATION OF FLOOD INUNDATION MAP USING GIS

Jincy K Jose[1], Sindhu A R[2]

[1] *PG Student, Department of Civil Engineering, Saintgits College of Engineering*

[2] *Assistant Professor, Department of Civil Engineering, Saintgits College of Engineering*

Abstract: *Flooding is one of the most frequent and devastating natural disasters and can oftenresult in severe damage to agricultural products, commercial infrastructure, personal property and loss of human lives. Accurate delineation of flooded waters is an important research issuein determining both economic and personal risk. Flood inundation mapping (FIM) is requiredto understand the effect of flooding in a particular area. By taking Pathanamthitta municipality, Kerala as study area we have designed a methodology for calculating the flood inundated areausing Arc GIS software. Flood depth was surveyed directly with help of local people and wardmembers. The elevation data is extracted using SRTM DEM and thus the flood level above sealevel is obtained. From this method, we find the areas with high flood level to zero flood leveland it is denoted using different colour. Among the 32 wards in Pathanamthitta municipality, 11 wards are affected by the flood. The resultant map shows highest range of flood level lies between 3 to 4 m, that is around 6.43% of the total area is highly affected by the flood whereas52.3% of the total area is zero flooded*

Keywords*: Binary Large Object, Digital Elevation Model, Ground Control Point, Open DataKit, Geographic Information System*

Introduction:

Flooding, as a major natural disaster, affects many parts of the world. Floods can be explained as excess flows exceeding the transporting capacity of river channel, lakes, ponds, reservoirs, drainage system, dam and any other water bodies, whereby water inundates outside water bodies areas. Due to this natural disaster, millions of infrastructure and property damages and hundreds of human lives are lost. On 16 August 2018, severe floods affected the south Indian state Kerala, due to unusually high rainfall during the monsoon season. It was the worst flood in Kerala in nearly a century. Over 483 people died, and 140 are missing. About a million people were evacuated. All 14 districts of the state were placed on red alert, one-sixth of the total population of Kerala had been directly affected by the floods and related incidents. Flood inundation maps are very essential for municipal planning, emergency action plans, flood insurance rates, and ecological studies. Geographic Information Systems (GIS) are successfully used to visualize the extent of flooding and also to analyze the flood maps to produce flood damage estimation maps and flood risk map. Floodis an overflow of a large amount of water beyond its normal limits. Flooding is one ofthe most significant

hazard occurred in Pathanamthitta in terms of number of affected population, agriculture andeconomic damage. The peak spell of rains that created the extreme floods in Kerala occurred between 8th to 17th of August2018. It was the worst flood in Kerala in nearly a century. Life of people in these areas has turned hell, about 74 camps were opened there. It was estimated that these flood events affected more than 10,53,143 population, 3338.651 Ha cultivated land, Rs. 1041.44609 L crop loss, 4366 number of damaged houses and 19 no's of casualty. Spatial technologies and infrastructure can play an important role in helping to acquire reliable, accurate and repeatedly obtained spatial information on flood events. Moreover, spatial technology like GIS not only provide a way of visualizing the spatial distribution of flood events, but also allows the potential to further analyse and estimate likely damages caused by flooding

Literature Review:

Jean Joy et.al (2019) studied about the "Kerala Flood 2018: Flood Mapping by Participatory GIS approach, Meloor Panchayat (2019)". This study formulates a new method for flood mapping, while remote sensing technology and flood modeling methods are irrelevant due to unavailability of data. In Kerala, a major flood occurred was on 1924, which is almost 100 years back and we cannot predict the future events also so that a flood map is essential for the future references. By taking Meloor Panchayat as study area, they designed a methodology for calculating the flood inundated area using GIS and PGIS technologies. By this method, we found that the flood height of some regions was up to 7.6 m, which is more than a double storied building and 53% of the study area was flood inundated.

Emin Tas et.al (2016) In this study “Flood inundation mapping by GIS and HECRAS”it is aimed to constitute flood inundation maps for Akarcay Bolvadin Subbasin.Topographic data of study area is defined for hydraulic model by sectioning along the river on Digital Elevation Model(DEM) which is created by ArcGIS, a Geographical Information System (GIS) software. It is used HEC RAS software as hydraulic model. Data migration between ArcGIS and HEC RAS is provided by using anintermediate module, HEC GeoRAS.After required geometrical and hydraulic structure data are constituted, flood inundation maps are obtained by inputting flow data into the model. Flow data is calculated by Fuller Method for various recurrence intervals.

PawarAmol et.al (2016) studied the "Application of GIS for flood Mapping of the Pune city, Maharashtra. Data used in the present study was SOI toposheets, DEM,

DGPS, GCP for ground truth, discharge data from Water Resources Department Maharashtra Government. For analysis, DEM of the city was processed for the fill for the using Arc Hydro tool. From the analysis it was found that the probable discharge for the different years from the Khadakwasala Reservoir was found to be 283593.06 Cumecs and submergence of the area was calculated. From the work, it gives the area which are more vulnerable for the flooding.

Methodology

There is a great deal of geographic data available in formats that cannot be immediately integrated with other GIS data. In order to use these types of data in GIS it is necessary to align it with existing geographically referenced data, this process is a new model called as georeferencing. Georeferencing is also a necessary step in the digitizing process. Digitizing in GIS is the process of tracing the information from images/maps, in a geographically correct way. The process of georeferencing relies on the coordination of points on the scanned image (data to be georeferenced) with points on a geographically referenced data (data to which the image will be georeferenced) In order to extract the elevation data, SRTM DEM was projected using the "Project Raster" tool in ArcGIS and Survey Point feature class projected using "Project (Data management)" tool. Small imperfections and sinks are removed using the "Fill" tool in the "Hydrology" toolset. This will remove the error pixels in DEM. The Flood depth collected is from ground level and for Finding out the inundated area, Flood level above sea levelis needed .In that case, SRTM DEM was used; the elevation values in SRTM DEM are above sea level.The Ground elevation is added with surveyed flood depth to get the flood height above sealevel. The DEM extraction process requires a stereo pair of images containing rational polynomial coefficients (RPC) positioning from aerial photography or pushbroom sensors.RPCs are used to generate tie points and to calculate the stereo image pair relationship. The field survey data is made into an excel sheet. This Table contains the Latitude (Y) and Longitude (X) collected using mobile GPS. This table is added tothe"ArcCatalog" GIS software. Using create feature class from "X-Y table" tool, the pointfeature class with entire survey details were created. In "X-Y table" tool dialogue box,the X Field is selected as Longitude column and Y field is selected as Latitude value. The coordinate system is set as Geographic coordinate system "WGS1984" because the GPS collects coordinates in "WGS1984". This Point has the survey results in its attribute table, which is useful in using for further analysis. Project Geo-database was created and DEMand Survey point feature class was

imported to it. For analysis and manipulation, the data must be in a projected coordinate system. According to the standards, the UTM Projection was chosen and for the study area the UTM zone is “UTM 43 North zone” Interpolation is the process of using points with known values or sample points to estimate values at other unknown points. It can be used to predict unknown values for any geographic point data, such as elevation, rainfall, chemical concentrations, noise levels, and so on. Here we use Kriging interpolation method. For the purpose of converting the raster to polygon feature, it was reclassified into 4 class using the “Reclassify” tool which is from spatial analytic tool from that Reclass and select reclassify. For example, Pixel values in cost distance raster range from 0 to 6300, which was reclassified to one class and value was given as “1”. Inundated area polygon was created using “Raster to Polygon” tool, thus reclassified raster was converted into polygon feature class. Then calculate the area using “calculate area” tool from spatial static s tool

Janerio, Brazil (2012) stabilized with basal geogrids and geosythetic encasement Hosseinpour et.al (2019). The 3D numerical analyses were carried out by considering a strip under the embankment and the 2D analysis was done using unit cell approach. He concluded that 3D analyses were better since they can stimulate field conditions better.

Experimental Investigation

Pathanamthitta municipality is the studyarea selected, which lies in the area of Pathanamthitta district, Kerala state. Total geographical area of Pathanamthitta municipality is 23.5 km^2. Population density of the city is 1597 persons per km^2

. There are 32 wards in the city, among them Pathanamthitta ward no 11 is the most populous ward with population of 1654 and Pathanamthitta ward no 09 is the least populous ward with population of 845.

Nearest railway station is Chengannurwhich is 26 km far fromhere. Kozhenchery isthe sub district head quarter and the distance from the city is 13 km. The flood height of certain points on the study area is taken directly by field survey. The collection has 2 stages; primary and secondary. In primary stage, the data's are collected with the help of local people and ward members. In secondary stage, the datawere verified by Deputy Town Planning Officer Pathanamthitta. The GPS location of the field points are also noted. More than one point is taken in areas where there is fluctuation in the flood level due to geographic characteristics. There are areas which are not affected by flood and also points where there is aflood height of about

four meters. These data are converted into anexcel sheet and export it as a shape file to input the data to ArcGIS. The covering of a land area by water brought about by natural causes (overflowing of rivers, heavy precipitation, or tides) or artificial causes (construction of reservoirs or ponds). Inundation may be long-term, in which case it is usually impossible to use the land (for example, land occupied by the basin of a reservoir), short-term, when use of the land is easy and feasible (for example, land flooded by high waters the spring), intermittent (caused by tides or by overflowing of rivers in the spring), which can be forecast fairly accurately, or sudden (an elemental disaster caused, for example, by a flood), for which the likelihood of an early warning is very small.

Result and Discussion

The method used was very effective in mapping the flood inundated area. Byground truthing, it was observed that the area was inundated during the flood event

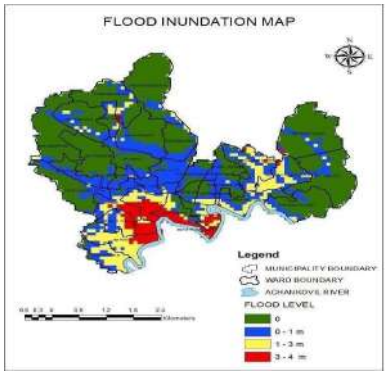

Fig 1: Flood Inundation Map

The above map shows the variation in flood height on different wards of the Pathanamthitta municipality. The highest range of flood level (3 to 4 meter) is depicted in red colour. The non-flooded area is in green colour. The intermediate flood levels ranging from 0 to 1 meter is shown in blue colour and 1 to 3 meter is shown in yellow colour. The percentage of area where flood affected is, in red zone 6.43 %, yellow zone 14.68 %, blue zone 26.85 % and 52.3 % of total area is zero flooded in green zone. Almost 25 % of total area is highly flooded. There are 32 wards in Pathanamthitta municipality. 11 wards were affected by flood ie, Town Ward, College War Kallarakadavu, Valamchuzhy, Azhoor West, Azhoor, Kodumthara, Kumbazha South, Kumbazha North, Chuttipara East, Myladumpara Thazham. Almost all portion of town ward are under flood. Highest flood level was reported at Valamchuzhy, Azhoor west, kallarakadavu, College Ward, Azhoor and Town ward (Red Wards like Poovanpara, Mundukootakal, Vanchipoika are situated away from theriver, so there is no flooding except on paddy fields and low-lying area that the pathanamthitta town is under flood.

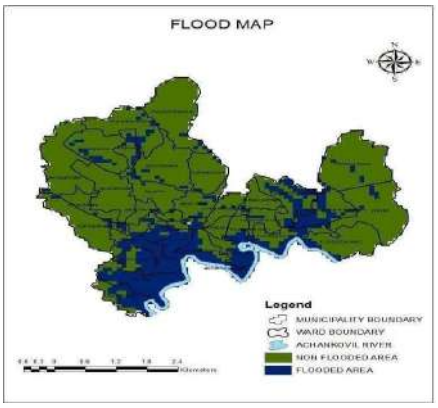

Fig 2: Flood Map

Green colour shows the non-flooded area and dark blue colour shows the flooded area. Water from streams and canals of the river entered directly to the water shed areas, it was observed that low lying land like paddy fields and agricultural lands were severely affected by flood. Also observed that Pathanamthitta town area is under flood, newly build settlements in town were more affected during the flood. City was liable to constructed in the low-lying area.

Flood map of the study area gives the details of passive areas affected by floodingPathanamthitta municipality region. Achenkovil river is one of the large waters. Maximum temperature here reaches up to 30°C and minimum temperature goes downto 23°C. Portion of Achenkovil river is pass through Pathanamthitta municipality. The river enters from the ward Kumbazha east (76.815700E, 9.255270N) and leaves at Kodumthara and there is low lying area which is always located there.

Flood map of the study area gives the details of passive areas affected by floodin Pathanamthitta municipality region. Achenkovil river is one of the large water body in Kerala that passes through Pathanamthitta

ArcGIS is a platform for organizations to create, manage, share, and analyze spatial data. It consists of server components, mobile and desktop applications, and developer tools. This platform can be deployed on-premises or in the cloud.

Conclusions:

1. This research paved the way to find the flood inundated area and the preparation of the map. The validation of software produced a difference of maximum 5%.
2. This map will facilitate future uses in disaster awareness and land use planningfor the effective use of flood plain. The flood which occurred on August 2018 in Kerala wasa major one and it affected many places including Pathanamthittadistrict..
3. A maximum flood height was noted as less than 4m whereas, there wereplaces with no flooding showed in green colour. We can identify the high flooded area in red colour.

4. From the flood map we can observethat high level of flooding occurred onlow lying areas like Town ward, Kumbazha south and places which are near to Achankovil River like Azhoor, Valamchuzhi, Kallarakada.
5. Zero level of flooding occurred on high elevated areas like Plaveli, Myladumpara, Thycavu, Mundukottackal etc.
6. The paddy fields of low lying areas were filled for development purpose which ledto the occurrence of floodin that areas.
7. These flood maps shows the flooded areas and non-flooded areas which can be used as a reference and management tool for furtherdevelopment planning.
8. It was observed that several landfilling occurred in low lying paddy fields and agricultural lands for the construction of houses, religious buildings and commercial establishments.
9. Further constructions or development on low lying and flood prone areas can be avoided. The unscientific way of landfill will increase the destructions in future flood

References:

1. Jean Joy, Shruti Kanga , and Suraj Kumar Singh (2019) Kerala Flood 2018: **Flood Mapping by Participatory GIS approach, Meloor Panchayat**, IJERT, 10, 197-205 .
2. Pawar Amol D, Jyoti Sarup, SushilKumar Mittal (2016) **Application of GIS for flood Mapping of the Pune city,** Research Gate, 4, 474-478.
3. Sandhya Kiran, N. Vijay Kumar (2017**) Flood Mapping Analysis of Chennai around City using Geomatics** JRTER, 7, 369-381.
4. Vahdettin Demir and Ozgur Kisi (2016**) Flood Hazard Mapping by Using Geographic Information System and Hydraulic Model: Mert River, Samsun, Turkey**, Advanced In Meterology, 10, 1155-116.
5. Emin Tas and Reynold Mes (2016), **Flood Inundation Mapping by GIS and a Hydraulic model (HECRAS):A case study in Turkey"** , Research Publisher ,1-5.
6. Sofia and Mathew (2016) **Flood Inundation Mapping in an Ungauged Basin**" Research Gate, 448-455.
7. Muthuswamy, Karthik Nelsind, Rangaswamy (2015) **Study and Analysis of Chennai Flood Using GIS**", Journal of Research Publication,1147-1160
8. Vinayak N., Mangrule and Umesh J.Kahalekar (2013) **Watershedplanning and development plan by using remote sensing and geographical information system of**

khultabad taluka of Aurangabad district, IJIC,3, 1093-1100

9. Harijith ,Mrineva (2012) **Study of wetland and preparation of flood inundation using Hec GIS**,Journel of Research Publication ,1247-1255.

STUDY ON THE UTILIZATION OF SHAPE MEMORY ALLOY IN CIVIL STRUCTURES

Vidyakrishna P Vidhyadharan[1], Er. Krupa Mary Varghese[2]

[1] *PG Student, Department of Civil Engineering, Saintgits College of Engineering*

[2] *Assistant Professor, Department of Civil Engineering, Saintgits College of Engineering*

Abstract: *A very common building material is cement concrete reinforced with steel bars, yet many masonry and concrete structures decay or become dangerous as a result of changes in environmental conditions, loading, layout, or use. The removal and transportation of significant quantities of concrete results in weight concentrations, excessive noise, dust, and extended recovery times, making repairs to major structures challenging and expensive. This prompted the development of intelligent materials, including SMA, which can lessen earthquake and environmental damage when combined with civil structures. The current work comprises of an analytical analysis of a 4.6-meter-long SMA-enhanced RC beam with a width of 250 millimeters and a depth of 300 millimeters. Investigations into SMA-based RC beam strengthening were conducted. The effects of materials, specifically CFRP and SMA introduced via the NSM technology, as well as the influence of the position and diameter of the NSM-SMA rod, were compared. According to the findings, using NSM-SMA resulted in a greater deformation reduction than using NSM-CFRP.*

Keywords: *ANSYS, CFRP, near surface mounted technique (NSM), Shape memory alloy (SMA)*

Introduction:

In seismically active areas, it is customary to design buildings and other engineering structures using seismic codes that enable for the structures to have a notable resistance to ground vibrations that could result from seismic activity. These buildings are made to absorb seismic energy by causing localized damage to the structural parts that sustain them, hence minimizing total building damage. In some circumstances, such as when expanding load capacity, eliminating fractures, or changing existing facilities, RC structures should be strengthened. Strength and serviceability standards must be met when designing reinforced concrete structures. However, the design for serviceability is not simple since time- dependent deformations caused by the creep and shrinkage of concrete make it difficult to predict behavior under prolonged service loads. As concrete structures age, SMAs show stresses and have a significant impact on their performance, leading to deflection and changing the way load is distributed. Under the impact of sustained

loading, it alsoresults in dimensional change in the material.

The differences in the quality and mix composition of the materials used to make concrete, as well as the internal reinforcing, are internal factors, and variations in ambient circumstances, such as humidity, temperature, etc., are external factors. The creep and shrinkage-related time-dependent effects in RC structures.

Therefore, creating a smart system for reinforced concrete constructions is crucial. Modern materials, such as super elastic (SE) Shape Memory Alloy (SMA) bars, have been created recently to address the issue of permanent deformation. These materials may experience significant inelastic deformations during loading and revert to its original shape when stressors are removed. Super elastic Shape Memory Alloy bars used structurally as reinforcement in reinforced concrete sections may have a substantial impact on how concrete structures behave. SMA bars can be used in conjunction with steel reinforcements to improve economy while increasing the section's load carrying capacity.

Shape memory alloys (SMAs) are metals that display the shape memory phenomenon as well as pseudo-elasticity, both of which are incredibly rare. Arne Olander first observed these un- usual properties in 1938 (Oksuta and Wayman 1998), but not until the 1960's were any serious research advances made in the field of shape memory alloys. The most effective and widely used alloys include NiTi (Nickel - Titanium), CuZnAl, and CuAlNi. Aconsiderable amount of energy is lost without permanent distortion when a SMA specimen experiences cyclic axial deformation within its superelastic strain range. This happenswhen austenite phase transitions to martensite during loading and martensite phase transitions back during unloading, releasing net energy. The following variables describe the temperatures at which each of these phases starts to develop and ends: Mf, As, Af, Ms. The shape memory effect during phase transition is depicted in Fig. 1.

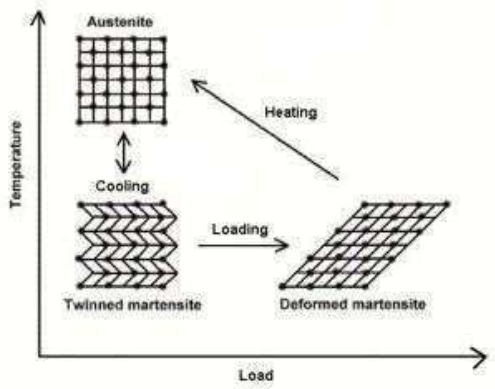

Fig. 1 Microscopic Diagram of the Shape Memory Effect (Google image)

Near surface mounted (NSM) technique is a newest class of strengthening technique. It involves cutting grooves, filling material such as mortar, epoxy resin. Fig. 2 shows the

Fig. 2 near surface mounted technique [Hong, K. (2018)]

Literatur Review:

Torra, V., et al. (2007) developed SMA models and included in a finite element simulation environment (ANSYS). These development tools were used to define a comprehensive damping strategy for a family home. The design and optimization approach for the dampers was described in the paper along with performance analysis and quantification of pertinent physical effects based on experimental data. The simulation outcomes demonstrate that the SMA dampers are able to dissipate half of the energy delivered to the structure and can reduce the maximum oscillation amplitude by a factor of 2. A passive, unattended damping solution suitable for family homesis provided by SMA dampers. Paul, N. K., et al. (2011) evaluated the structural behavior of the longitudinally reinforced concrete Tee-beam bridge girder, reinforcing with steel and shape memory alloy bars respectively, a three-dimensional finite element model was created and tested under a two point loading system. In the investigation, superelastic Shape Memory Alloy bars were used in place of 25% of the steel bars. Concluded that partial use of shape memory alloy bars combined with steel reinforcement in the longitudinal girder of RC bridges greatly increases their load carrying capacity and reduces the need for repairs caused by the structure's deterioration over time or other changes in loading. Ingalkar, R. S (2014) presented a review of rehabilitation techniques of building and bridges by using shape memory alloy. SMA Devices have been proposed as having a significant function in earthquake prevention for these buildings. Many historical structures and monuments in India, including the Taj Mahal, the Victoria Memorial, the Kutub-Minar, the Lal-Kella, the Nizam-Palace, etc., were built during various historical periods. Therefore, future earthquakes can be avoided by retrofitting such buildings with SMA devices. By using time history analysis, Shaji, G. S., et al. (2015) compared the behavior of steel braced frames with SMA braced frames. Analysis and

discussion of the impact on displacement and stress distribution were conducted. Due to low ductility and energy dissipation, failure of the connection between the braces and the frame, and asymmetric brace behavior in tension and compression, damage sustained during previous earthquakes suggests that braced systems may perform poorly. Utilizing cutting-edge materials in the bracing system is one technique to enhance CBF systems' effectiveness in terms of limiting interstory drifts. They have found that for various types of conventional braced frames, the inter-storey drift of SMA braces is lower than that of steel braces. Hamid, N. A., et al. (2018) investigated on the superelastic behavior of shape memory alloy, NiTi when used as reinforcement in concrete beams. Investigations were done into NiTi's potential to recover from and lessen permanent deformations of concrete beams. Experimental research was done on the behavior of simply supported reinforced concrete (RC) beams hybridized with NiTi rebars and the control beam subjected to monotonic loads. Conclusion: The SMA beam demonstrated improved performance in terms of better fracture recovery and deformation as a result of the contribution of the SMA bar in combination with high-strength steel to the conventional reinforcement. Alaneme, K. K., et al. (2019) studied the use of Cu and Fe based SMAs by exploratory examination of the extent of their use in buildings and civil structures as vibration control devices/systems. Based on the findings from the literatures analyzed, it was concluded that Cu and Fe based SMAs are technically useful, simply implementable and sustainable SMAs for consideration as structural vibration control systems/devices in buildings and civil structures. Saraswat, Yatendra et al. (2019) performed a static analysis of the effect of shape memory alloy on composite beam using finite element analysis on ANSYS software. The volume proportion of the shape memory alloy wires employed in the entire carbon/epoxy beam was 10%. As a result of using shape memory alloy wires in the beam, the deformation was decreased by nearly 50%, the stress by more than twice as much, and the strain was reduced by 1.25 times in the carbon/epoxy beam using SMAs wires. Huang, H., et al. (2020) developed a TMD with shape memory alloy (SMA) to reduce the vibration caused by off-tuning under seismic excitations. SMA was utilized to retune the TMD utilizing temperature control, which reduced the vibration brought on by the out of tune TMD.

A single SMA-based TMD was examined at various temperatures before being applied to buildings. According to the findings, as temperature rises from 40 °C to 65 °C, stiffness increases and the corresponding damping ratio drops. The TMD's dynamic properties can thus be changed. This study came to the conclusion that the damping ratio of the SMA-based TMD can be optimized by combining numerous SMAs and raising the phase transformation temperatures of SMA. Saraswat, Y. et al. (2021) analyzed two cases, in the first simple carbon/epoxy plate was analyzed and then the shape memory wire embedded in the plate which is about 1 percent of the volume of the plate and studied the buckling response effect on the plate. In the second case Shape Memory Alloy plate and loading but with a circular cutout at the middle of the plate, for this case analysis was done with both shape memory alloy and without the use of shape memory.It was observed that the shape memory alloy increases the strength of the plate in both cases. Tomar, R. (2021) studied the effect of shape memory alloy in carbon/epoxy laminated beam. A cantilevered beam that was separated into three layers of 10mm each and with dimensions of 1000mm long, 100mm wide, and 30mm high was taken into consideration. The analysis involved three cases. All three layers of the beam in the first instance were laminated using epoxy/carbon. In the second instance, the intermediate layer was laminated with shapememory alloy while the top and bottom layers were made of carbon/epoxy. In the third instance, the middle layer is made of carbon/epoxy, while the top and bottom layers are bonded with shape memory alloy.The findings showed that using shape memory alloy boosted the strength.

Objectives:

1. To study about Shape memory alloy
2. To study the effect of SMA on Reinforced Concrete Beam
3. To study the effect of diameter, position of rod in strengthening RC beam with NSM-SMA
4. To compare the deformation and equivalent stress of NSM-SMA and NSM-CFRP strengthened RC beam

Methodology:

Initially validation was carried out and the journal selected was Ortes, F., et al., (2015) “Numerical simulation of structural behavior of NSM CFRP strengthened RC beams using finite element analysis”. Fibre Reinforced Polymers

for Reinforced Concrete Structures. The next step involved designingan RC beam with a 4.5 m span and dimensions of 300 mm in depth and 250 mm in diameter. The reinforcement details was depicted in Fig. 3.

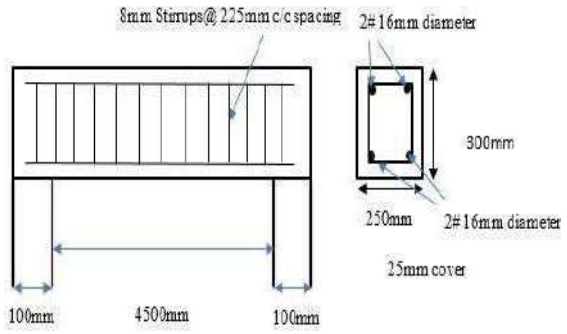

Fig. 3 Reinforcement detailing

Modeling

Three cases are considered for themodelling which are as follows:

Case 1:

(a) 12mm diameter CFRP rod at bottom center

(b) 12mm diameter SMA rod at bottom center

Case 2: 6mm diameter SMA rod at bothcorner below stirrup

Case3: 18mm diameter CFRP rod at bottomcenter

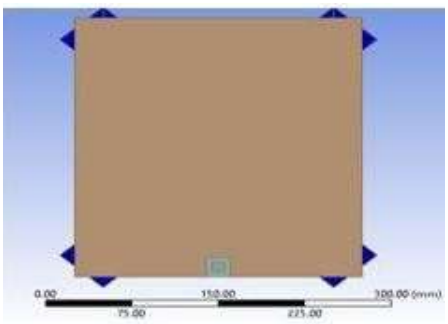

Fig. 4 Geometry of the model with 12mm rod at bottom

Geometry

The geometry of the beam with 12mm rod modeled is shown in Fig. 4 and the isometric view in Fig. 5.

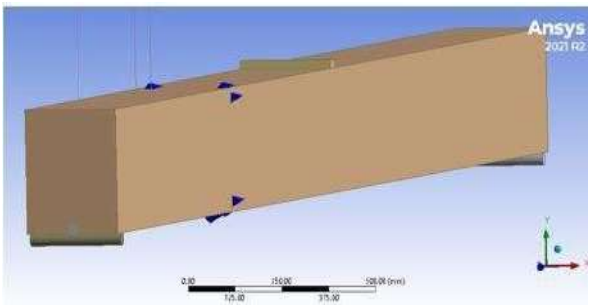

Fig. 5 Isometric view

Loading and Boundary conditions

The loading and boundary conditions used for all 3 cases are given as below:

- In static analysis a concentrated loadof 20.813 KN at the mid of the beam is considered.
- The beam is simply supported.
- Impactor and roller supports are provided, the material assigned issteel as deformation is less.
- Earth gravity is considered along –Y direction.

Loading Condition is shown in Fig. 6.

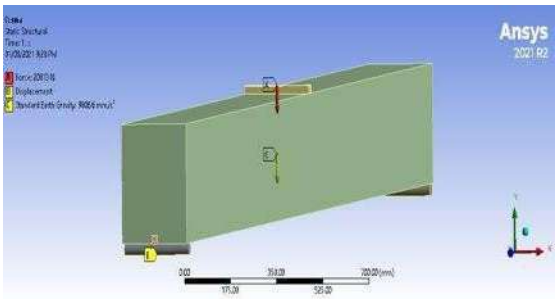

Fig. 6 Boundary condition

Discretization

In this section grid independence study and meshing was done. From the grid independence study, the element size was taken as 50mm, which results in 32626 elements in the domain and 142419 nodes. The quality of mesh is measured using the factor called skewness. Skewness is definedas the deviation of the cell structure from theprimitive shape.

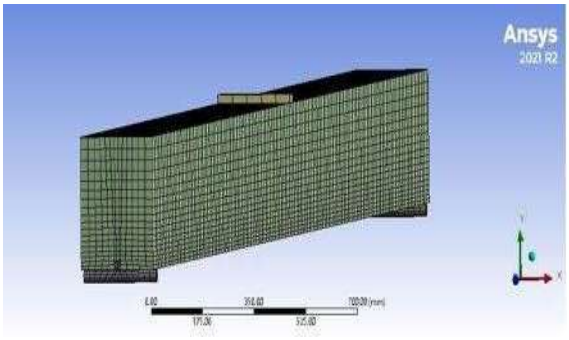

Fig. 7 Meshing

In meshing, the size of the mesh is a measure of accuracy of the result and the time required for the computation of results. Coarse mesh gives less accuracy and lower time for computation. As the mesh becomesmore and finer, the accuracy increases so as the time. A grid independence study is carried out and a reasonable mesh with acceptable deviation in result is selected. Thefinest mesh is taken as the reference for all mesh. The percentage deviation in the specified criteria in each mesh is compared with the reference mesh. The selected mesh size is mentioned and is used for the simulation in this study. Fig. 7 shows the meshing of the beam.

Results and discussions:

Result of deflection and stress on beams

In this section, the results of analysis of control beam, NSM-SMA 12mm rod, NSM-CFRP 12mm rod beam are presented. The results are shown in Fig. 8 to Fig. 13.

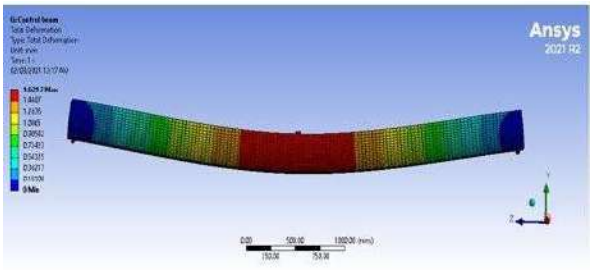

Fig. 8 Total deformation of RC Beam

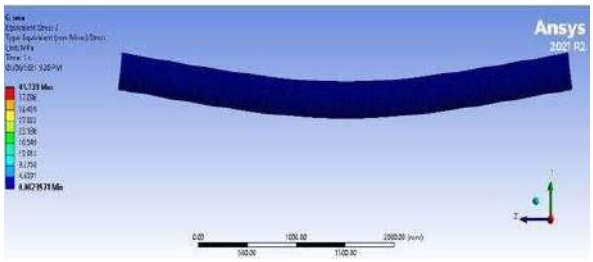

Fig. 9 Equivalent stress of RC beam

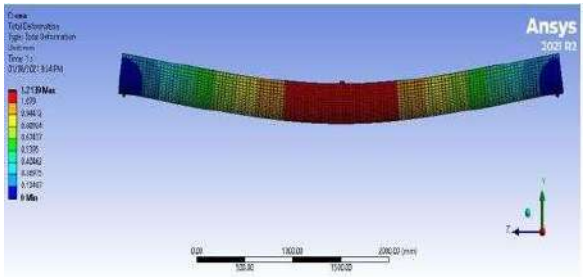

Fig. 10 NSM-SMA rod 12mm at bottom center total deformation

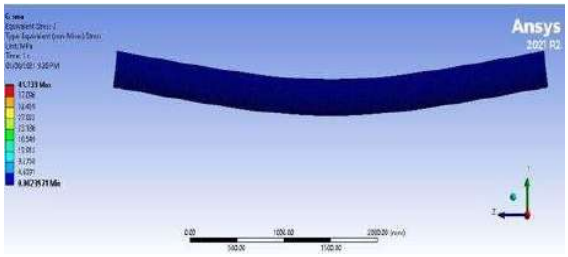

Fig. 11 NSM-SMA rod 12mm at bottom center Equivalent stress

Fig. 12 NSM-CFRP rod 12mm at bottom

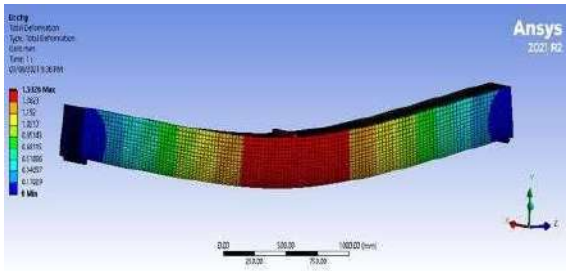

centertotal deformation

Fig. 13 NSM-CFRP rod 12mm at bottom

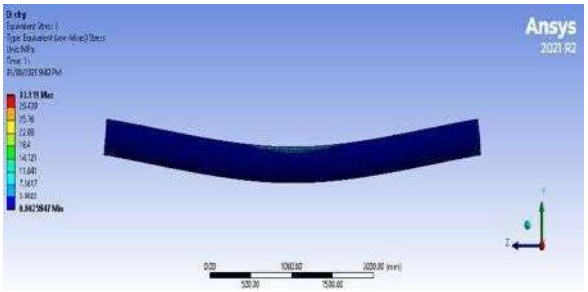

centerEquivalent stress

Result of comparison of RC beam, CFRP and SMA

In Fig. 14, the comparison of effect of materials used is shown, were the values of deformation is along Y axis and materials along X axis.

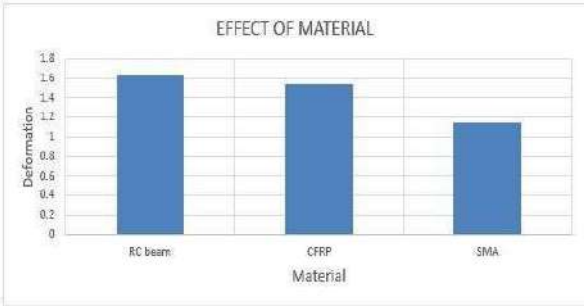

Fig. 14 Comparison of RC BEAM, CFRP andSMA

Result on the effect of diameter of the rod

For analyzing the effect of rod diameter, NSM-SMA with 12 mm rod at bottom center, NSM-SMA rod 18mm at bottom center and two NSM-SMA rod 6mm below stirrup corner were considered and the

valuesobtained are shown in Fig. 15 to Fig. 17.In Fig. 18, the comparison of diameter and deformation of NSM-SMA beam is shown.

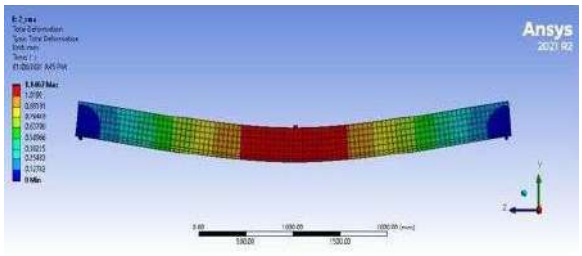

Fig. 15 NSM-SMA rod 6mm at bottom of stirrup corners total deformation

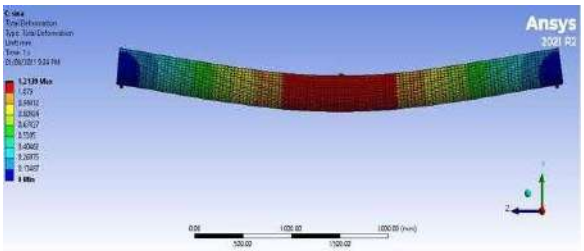

Fig. 16 Total deformation of NSM-SMArod 12mm at bottom center

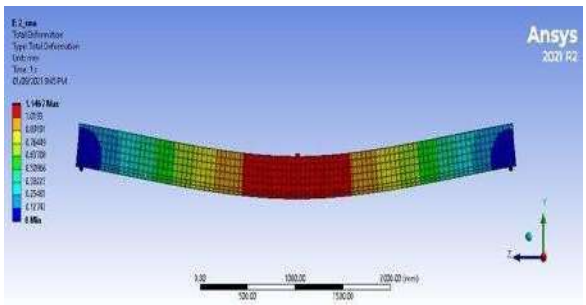

Fig. 17 Total deformation NSM-SMA rod 18mm at bottom

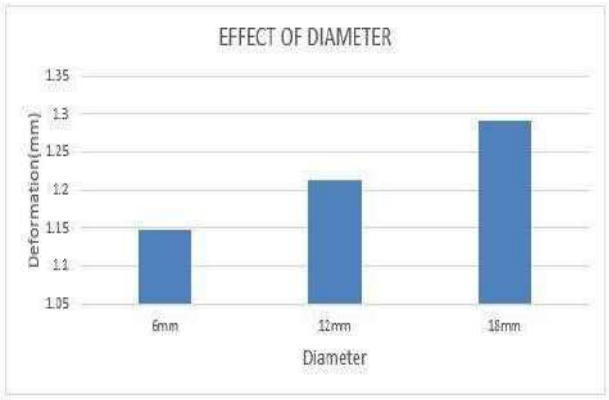

Fig. 18 Comparison of diameter and totaldeformation for NSM-SMA beam

Result on the effect of location of the NSMrod

In this section, two cases were considered, beam with two 6mm NSM-SMA rods at the bottom of both stirrup corners and another beam with NSM-SMA rod 12mm at bottom center. The effect of location of NSM SMA rods are shown in Fig. 19 and 20 respectively. Fig. 21 and 22 shows the values obtained for total deformation and equivalent stress when the location of the rod was analyzed by placing at the center and at the corners. The stress strain behavior of SMA is shown Fig.23.

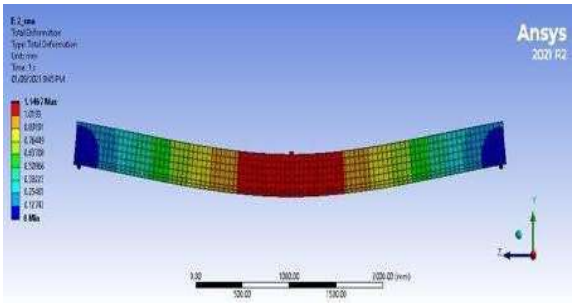

Fig. 19 NSM-SMA rod 6mm at bottom of stirrup corners total deformation

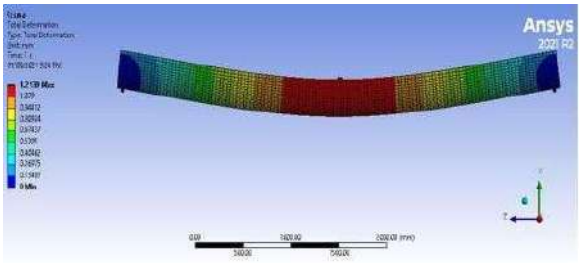

Fig. 20 Total deformation of NSM-SMArod 12mm at bottom center

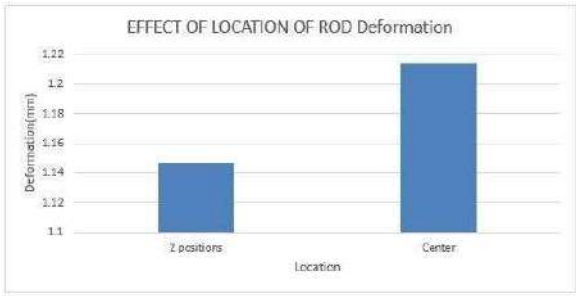

Fig. 21 Deformation based on location ofthe rod

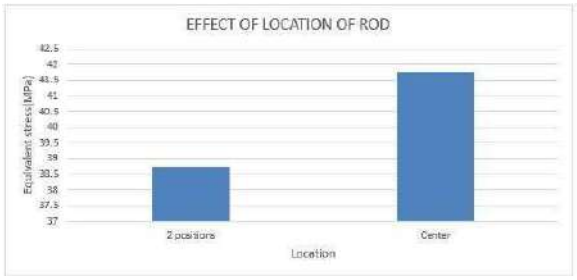

Fig. 22 Equivalent stress based on locationof the rod

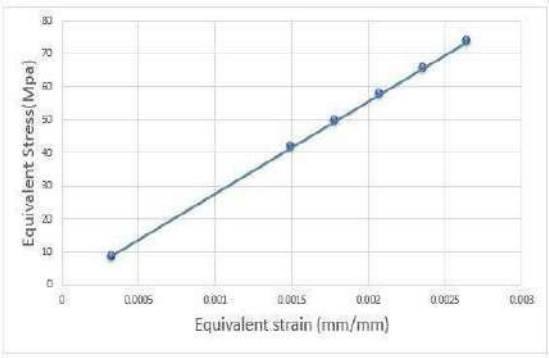

Fig. 23 Stress- Strain Graph

Discussions:

- For the control beam, the NSM-CFRP-fortified beam, and the NSM-SMA-fortified beam, respectively, the deformation results based on the impact of various materials employed in the study were 1.55mm, 1.53mm, and 1.2mm
- The result on the effect of 6mm, 12mm, and 18mm diameter of rod are 1.1467mm, 1.2139mm, and 1.2907mm respectively
- The stress- strain behavior depicted is in the elastic limit.

Conclusions:

The following are the conclusions drawn out from the analysis:

- It was discovered that the deformation reduction achieved with NSM-SMA is more than that of NSM-CFRP
- The effect of location analysis showed that when a rod is positioned in two spots as opposed to one in the center, there is less deformation
- The result on the effect diameter of rod revealed that lesser diameter rod has lesser deformation
- NSM-SMA strengthening of beam increases the load carrying capacity of RC beam
- With the use of SMA, structural repairs are made more easier and they can avoid the costs associated with removing and transporting huge pieces of concrete as well as the weight, dust, and noise concentrations that are brought on by doing so

References:

1. **Alaneme, K. K.**, **E. A. Okotete**, and **J. U. Anaele** (2019) Structural vibration mitigation–a concise review of the capabilities and applications of Cu and Fe based shape memory alloys in civil structures, *Journal of Building Engineering*, **22**, 22–32
2. **Gopika Shaji, M. P. M.** (2015) Seismic control of structures using shape memory alloys, *International Journal of Current Research*, **7**(11), 23613–23617
3. **Hamid, N. A.**, **A. Ibrahim**, **A. Adnan**, and **M. H. Ismail**, Behaviour of smart rein- forced concrete beam with super elastic shape memory alloy subjected to monotonic loading, *In AIP Conference Proceedings*, volume 1958. AIP Publishing LLC, 2018
4. **Huang, H.**, **K. M. Mosalam**, and **W.-S. Chang** (2020) Adaptive tuned mass damper with shape memory alloy for seismic application, *Engineering Structures*, **223**, 111171
5. **Ingalkar, R. S.** (2014) Rehabilitation of buildings and bridges by using shape memory alloys (SMA), *International Journal of Civil Engineering Research*, **5**(2), 163–168
6. **Paul, N.** and **S. Saha** (2011) Improvement of load carrying capacity of a RCC T-beam bridge longitudinal girder by replacing steel bars with SMA bars, *World Academy of Science Engineering and Technology*, **51**, 2011
7. **Saraswat, Y.** *et al.* (2021) Buckling strengths of composite plate using shape memory alloy under in-plane shear,

Turkish Journal of Computer and Mathematics Education (TURCOMAT),

12(2), 1729–1738

8. **Saraswat Yatendra, Y. S., parihar hemant** (2019) The effect of shape memory alloy in composite beam, *International Journal of Innovative Technology and Exploring Engineering*, **8**, 2278–3075
9. **Tomar, R.** *et al.* (2021) Static analysis of the effect of shape memory alloy in laminated beam, *Turkish Journal of Computer and Mathematics Education (TURCOMAT)*, **12**(2), 2114–2124
10. **Torra, V.**, **A. Isalgue**, **F. Martorell**, **P. Terriault**, and **F. Lovey** (2007) Built in dampers for family homes via sma: An ansys computation scheme based on mesoscopic and microscopic experimental analyses, *Engineering Structures*, **29**(8), 1889–1902